UNIVERSIDADE D
COIMBRA

João Carlos Pinho da Silva

HIGH FRUCTOSE FEEDING AND HEPATIC FATTY LIVER DISEASE INFLAMMATION: THE ROLE OF INTESTINAL MICROBIOTA

Tese no âmbito do Doutoramento em Biociências, especialização em Bioquímica orientada pelos Doutores John Griffith Jones e João Ramalho de Sousa Santos e apresentada ao Departamento de Ciências da Vida da Faculdade de Ciências e Tecnologia da Universidade de Coimbra.

Março de 2020

UNIVERSIDADE D
COIMBRA

João Carlos Pinho da Silva

HIGH FRUCTOSE FEEDING AND HEPATIC FATTY LIVER DISEASE INFLAMMATION: THE ROLE OF INTESTINAL MICROBIOTA

Tese no âmbito do Doutoramento em Biociências, especialização em Bioquímica orientada pelos Doutores John Griffith Jones e João Ramalho de Sousa Santos e apresentada ao Departamento de Ciências da Vida da Faculdade de Ciências e Tecnologia da Universidade de Coimbra.

Março de 2020

“It's on the strength of observation and reflection that one finds a way. So, we must dig and delve unceasingly.”

Claude Monet

Acknowledgments/Agradecimentos

Grateful! To the Portuguese Foundation for Science and Technology (FCT) for funding under the PhD fellowship SFRH/BD/90259/2012.

To Doctor John Jones (to “John”) for the intellectual freedom, wisdom sharing and perspective propulsion. To my colleagues and friends in the “Metabolic control” group, Getachew, Cátia, Cristiano, Ludgero, João Rito, Ivan, Mariana and Cristina for the goodwill support, good energy and companionship. To Professor Teresa Gonçalves, Doctor Célia Nogueira and Marta at the “Medical Microbiology” group for all the resilience, dedication and care. To Professor Ana Gil at CICECO, University of Aveiro and her team members Joana Pinto and João Rodrigues for key learnings and careful reception. To Professor Paula Macedo at “MEDIR” group on CEDOC, Nova Medical School, for the availability and resources. To Professor João Ramalho-Santos for the “words” in/and consideration.

À Fátima, pelos ensinamentos, companheirismo de aventura e amizade subjacente.

Ao Nuno pela virtude da presença e compleição da atitude.

Ao Alexandre pela sensibilidade, pelo erguer do brilho e “gargalhada cardiológica”. Ao Duarte pelo sorriso clarividente e coesão contagiante. Aos dois por lembrarem o que é impossível esquecer.

Aos meus Pais pela “banalização” do incondicional e exaltação de propósito. À minha Mãe pela Natureza entregue, ao meu Pai pela minúcia da profundidade.

Ao meu irmão pelo carisma, pelo carinho irreverente e rebate entreposto.

À Diana, por cada hipérbole, por cada gesto transbordante e pela melodia do horizonte.

Para a Bela.

Abstract

Chronic metabolic diseases related to obesity and lifestyle are imposing an ever-increasing burden on healthcare worldwide. Incidences of non-alcoholic fatty liver disease (NAFLD) and Type-2 diabetes (T2D) have been rising particularly rapidly in Western Societies, showing strong associations with sedentary lifestyle and excessive caloric intake in relation to daily expenditure. A significant fraction of this hypercaloric intake is accounted by sugar, in particular fructose, present in processed food and sweetened beverages. This diet promotes weight gain, insulin resistance and dyslipidemia thereby providing the foundations for NAFLD and T2D development. In addition to directly disrupting the control of systemic carbohydrate and lipid metabolism, such diets may also mediate these effects indirectly via the gut microbiome. The gut microbiome is a complex ecosystem that is normally in a symbiotic relationship with the host and having a key role in nutrient processing and energy harvest. In obesity-related diseases such as NAFLD and T2D, dysbiotic alterations in the microbiome composition, its metabolic endproducts, and its interactions with host tissues, are implicated in their pathogenesis.

The first part of this work aimed to study the effects of a diet high in simple sugars on the composition of the intestinal microbiome and its metabolite products in mouse models. It was hypothesized that dietary glucose and fructose have distinct effects on these parameters with focus on the relative abundance of Gram-negative species and alterations in SCFA levels. Three groups of mice were fed over 10 weeks with standard, high glucose or high fructose chow. Fecal samples were periodically collected and the microbiome was profiled by real-time quantitative polymerase chain reaction (qPCR). Fecal metabolites were analyzed by proton nuclear magnetic resonance (1H NMR).

On the metabolites content significant differences were also observed with a reduction in beneficial SCFA like butyrate, to be induced by fructose. For the mice fed the high fructose diet, unmetabolized fructose was found in the feces indicating that the intestinal absorption capacity had been saturated and that fructose was available to the entire intestinal microbiome. Mice fed the high fructose diets also showed a shift in microbiome species towards Gram-negative bacteria and decreased fecal levels of butyrate relative to acetate and propionate. An increased abundance of Gram-negative bacteria could promote visceral inflammation through increased abundance and leakage of endotoxin from the intestinal lumen into surrounding tissues. In addition, alterations in microbiome metabolic endproducts such as lactate and short-chain fatty acids (SCFA) can have an impact on intestinal as well as hepatic and peripheral metabolism through direct substrate effects as well as by activation of substrate-specific receptors such as the GPR family.

In the second part of the Thesis, the specific contributions of dietary glucose and fructose to hepatic and adipose tissue lipogenesis were determined by integrating ^{2}H-enrichment of triglyceride from deuterated water to provide estimates of de novo lipogenesis (DNL) and glycerol synthesis from all sources with ^{13}C-triglyceride (TG) enrichment from ^{13}C-glucose and fructose tracers to provide specific contributions of each exogenous sugar. In liver, exogenous fructose contributed significantly more to both DNL and glycerol synthesis compared to exogenous glucose. Moreover, fructose promoted the synthesis of saturated fatty acids to a greater degree than that of oleate whereas glucose did not. Fructose also contributed to mesenteric adipose tissue TG synthesis, albeit to a lesser degree than glucose while only glucose contributed to subcutaneous adipose tissue TG synthesis.

In conclusion, this dissertation provided new insights on the role of the intestine and visceral adipose tissue in the metabolism of dietary glucose and fructose and has opened two important new lines of research. First, the potential for overflow of fructose into the lower intestine: to what extent does this happen in humans in the Western diet setting and how does this influence microbiome composition and metabolism? In this context, there is evidence that fructose malabsorption in the human population may be more widespread than initially thought. Second, the lipogenic utilization of fructose carbons by mesenteric adipose tissue begs the question of how this sugar became available to these adipocytes. Was it via direct absorption or was it converted beforehand to glucose by intestinal gluconeogenesis? If it was by direct absorption, this implies that mesenteric adipocytes have a capacity for fructose uptake and metabolism. Also, it suggests that mesenteric adipose tissue has some degree of privileged access to nutrients that are absorbed by the intestine.

Resumo

As doenças metabólicas crónicas associadas a obesidade e estilo de vida representam um encargo significativamente crescente na saúde mundial. Nas sociedades ocidentais, as incidências de fígado gordo não alcoólico (NAFLD) e diabetes tipo 2 (T2D) têm aumentado consideravelmente correlacionando-se com sedentarismo e consumo excessivo de calorias perante o consumo diário. Nestas dietas hipercalóricas, o açúcar é maioritário em especial a frutose, presente em concentrações elevadas nos alimentos processados. Estas condições estimulam o aumento de peso, resistência à insulina e dislipidémia, que estão na base do desenvolvimento de NAFLD e T2D. Para além destas dietas promoverem distúrbios diretos no metabolismo de lípidos e hidratos de carbono, podem derivar indiretamente os mesmos efeitos, através do microbioma intestinal. Este é um ecossistema complexo que normalmente se encontra em simbiose com o hospedeiro, o que é fundamental para o processamento de nutrientes e extração de energia. Alterações às populações microbianas e perda de simbiose, produtos metabólicos dessas espécies e a respetiva interação com vários tecidos do hospedeiro estão na origem das patologias referidas.

A primeira parte deste trabalho visou estudar, em modelos de ratinho, o efeito de dietas ricas em açúcares simples, na composição do microbioma intestinal e dos seus produtos metabólicos. A hipótese propunha que a glicose e frutose produzem efeitos distintos, com foco para alterações na abundância relativa de espécies Gram-negativas e nos níveis de ácidos gordos de cadeia curta (SCFA). Três grupos foram alimentados por um período de 10 semanas com 3 tipos de dieta: standard, rica em glucose ou rica em frutose. Periodicamente, recolheram-se amostras fecais e o perfil microbiológico

analisado por real-time quantitative polymerase chain reaction (qPCR). Os metabolitos fecais foram analisados por ressonância magnética nuclear de protão (^{1}H NMR).

Observaram-se diferenças significativas no conteúdo em metabolitos com uma redução, induzida por frutose, em SCFA benéficos como o butirato. Nos animais alimentados com elevados níveis de frutose, moléculas não metabolizadas deste açúcar foram encontradas nas fezes, indicando uma saturação da absorção intestinal que resulta em maior disponibilidade de frutose para o microbioma. No mesmo grupo de ratinhos verificou-se uma alteração na composição microbiana com maior tendência para espécies Gram-negativas e um decréscimo nas concentrações de butirato em relação a acetato e propionato. A prevalência destas bactérias pode promover inflamação visceral pelo seu crescimento e libertação de endotoxinas do lúmen intestinal para os tecidos circundantes. Adicionalmente, variações nos metabolitos bacterianos como lactato e SCFA podem alterar o metabolismo intestinal, hepático e periférico através de modificações diretas por substratos, como ativação específica de recetores sensíveis a esses, tais como os da família GPR.

Na segunda parte desta Tese, foram determinadas as contribuições específicas da glucose e frutose nas dietas, para a lipogénese no fígado e tecido adiposo, através da integração do enriquecimento nos triglicerídeos (TG) em ^{2}H proveniente de água deuterada para quantificação da lipogénese *de novo* (DNL) e síntese de glicerol gerais, com o enriquecimento nos mesmos TG em ^{13}C proveniente de marcadores ^{13}C-glucose e ^{13}C-frutose para analisar as contribuições específicas destes açúcares exógenos.

No fígado, a frutose deteve um contributo significativamente superior para a DNL e síntese de glicerol quando comparada com glucose. Neste contexto, a frutose promoveu a produção de ácidos gordos saturados em maior escala, efeito não verificado com a

glucose. No tecido adiposo mesentérico a frutose contribuiu para a síntese de TG embora em menor porção que a glicose. No tecido adiposo subcutâneo apenas a glicose contribuiu para a lipogénese.

Em nota conclusiva, esta dissertação apresenta novas evidências no papel do intestino e tecido adiposo visceral no metabolismo da glicose e frutose e estabelece bases para duas novas linhas de investigação. A primeira reporta à saturação de frutose no intestino grosso: em que medida este fenómeno ocorre em humanos sob dietas ocidentais e a influência que terá na composição do microbioma e metabolismo? Existem evidências de que a malabsorção de frutose em humanos poderá ser transversal a um grupo maior de populações que inicialmente esperado. A segunda refere-se à utilização dos carbonos da frutose para lipogénese no tecido adiposo mesentérico em que se questiona por que processo este açúcar fica disponível aos adipócitos. Por via de absorção direta ou através de gluconeogénese intestinal por conversão prévia a glicose? Se se verificar a absorção direta, será demonstrado que os adipócitos mesentéricos são capazes de assimilar e metabolizar frutose inferindo que o tecido adiposo mesentérico possui, em alguma medida, um acesso privilegiado a nutrientes absorvidos pelo intestino.

Abbreviations

^2H_2O – Deuterated water

ACC – Acetyl coA carboxylase

ALT – Alanine-aminotransferase

AMP – Adenosine monophosphate

AST – Aspartate-aminotransferase

ATP – Adenosine triphosphate

AUC – Area under the curve

BCCA – Branched chain amino acids

BMI – Body mass index

ChREBP – Carbohydrate receptor element binding protein

CK-18 – Cytokeratin 18

CK18 – Cytokeratin-18

CVD – Cardiovascular Disease

DAG's – Diacylglycerols

DNL – De novo lipogenesis

F1P – Fructose-1-phosphate

FA – Fatty acid

FAS – Fatty acid synthase

FFA – Free fatty acids

FGF 21 – Fibroblast growth factor-21

FIAF – Fasting-induced adipose factor

FLI – Fatty liver index

GGT – Gamma-glutamyl transferase

GLP-1 – Glucagon-like peptide 1

GLY – Glycerol-3-phosphate

GPR – G-coupled protein receptor

HDAC – Histone deacetylases

HDL – High Density Lipoproteins

HFCS – High Fructose Corn Syrup

HMDB – Human metabolome database

IDF – International Diabetes Federation

IGT – Impaired Glucose Tolerance

IL-6 – Interleukin-6

IR – Insulin Resistance

ISA – Isotopomer spectral assay

KC – Kupfer Cells

KHK – Ketohexokinase

LDL – Low Density Lipoproteins

LPL – Lipoprotein lipase

LPS – Lipopolysaccharides

MAT – Mesenteric adipose tissue

MCP-1 – Monocyte chemoattractant protein-1

MUFA – Mono-unsaturated fatty acids

NAFLD – Non-alcoholic Fatty Liver Disease

NASH – Non-alcoholic Steatohepatitis

NEFA – Non-esterified fatty acids

NFS – NAFLD fibrosis score

NMR – Nuclear magnetic resonance

OGTT – Oral glucose tolerance test

PCA – Principal component analysis

PFK1 – Phosphofructokinase-1

PGN – Peptidoglycan

PLD – Phenyllactate dehydratase

PLS-DA – Partial least squares discriminant analysis

PNPLA3 – Patatin-like phospholipase domain containing protein 3

PPAR-γ - Proliferator-activated receptor γ coactivator

PQN – Probabilistic quotient normalization

qPCR – Real-time quantitative polymerase chain reaction

ROS – Reactive Oxygen Species

SCAT – Subcutaneous adipose tissue

SCD1 – stearoyl coA desaturase-1

SCFA – Short-chain fatty acid

SFA – Saturated fatty acids

snr – signal to noise ratios

SREBP-1c – Sterol receptor element binding protein-1c

STOCSY – Statistical total correlation spectroscopy

T2D – Type 2 Diabetes

TG – Triglyceride

TLR – Toll-like receptor

TM6SF2 – Transmembrane 6 superfamily member protein 2

TMA – Trimethylamine

Triose-P – Triose-phosphate

TSP – Sodium 3-([2,2,3-d_4]trimethylsilyl) propionate

TZD's – Thiazolidinediones

VAT – Visceral Adipose Tissue

VIP – Variable importance to the projection

VLDL – Very Low-Density Lipoproteins

Table of Contents

Chapter A

General Concepts

Metabolism is presently defined as “all the chemical processes in your body, especially those linked with the conversion of nutrients for energy and growth”. On its first recorded use, in 1878, the word metabolism was proposed at the time as “the sum of the chemical changes within the body by which the protoplasm is renewed, changed, or prepared for excretion”. The study of metabolic phenomena dates further back, with *Sanctorius* identified as the pioneer of scientific investigation into metabolic processes in 1561 [1].

The defective perspective of these processes functioning is the basis for the turnover to a metabolic disease profile. On this dynamic the concept of metabolic flexibility has emerged as an important paradigm to explain the transition from healthy to disease state. Metabolic flexibility is the capacity of an organ or a whole organism to maintain its metabolic functions when faced with different nutrient composition and quantities. For example, the heart will oxidize glucose for energy if glucose is abundant, but if it becomes scarce it can switch instead to fatty acids or ketone bodies. This adaptability depends to a significant degree on the correct functioning of regulatory components that include insulin and glucagon-mediated actions as well as neuroendocrine signalling, among others [2].

A.1 Metabolic Syndrome

Eskil Kylin, a Swedish physician, was the first to introduce the term “Metabolic syndrome” into the clinical setting in 1923, using it to describe the co-occurrence of hypertension, hyperglycaemia and gout [3, 4]. Later, in 1947, Jean Vague described the link of cardiovascular disease (CVD) and diabetes with metabolic syndrome [5, 6]. Specifically, he described the associations between atherosclerosis, renal calculi and upper body adiposity. The association between general adiposity and fat accumulation in the liver began to be established in 1970’s [7-9]. In 1988, Gerald Reaven proposed that insulin resistance (IR) was a common factor linking the key co-morbidities of the Metabolic syndrome, namely type 2 diabetes (T2D) dyslipidaemia and cardiovascular disease [10]. The central role of insulin resistance in the development of the Metabolic syndrome was further reinforced in subsequent studies with new designations proposed such as “the deadly quartet” [11] and “the insulin resistance syndrome” [12].

In 1998, the World Health Organization (WHO) provisionally defined Metabolic syndrome as insulin resistance (or its surrogates Type 2 diabetes or impaired glucose tolerance) in combination with any two of the following conditions: abdominal obesity, hypertriglyceridemia, high blood pressure or microalbuminuria [13]. However, there was a lack of consensus on this definition with regards to the co-morbidities that should be included [14-18]. In 2009, the International Diabetes Federation (IDF), the American Heart Association (AHA) and the National Heart, Lung, and Blood Institute (NHLBI) published a consensus definition [19].

Metabolic syndrome was indicated by abnormalities in any three of the following five conditions: 1) increased waist circumferences to threshold values varying according the different regional populations, genetics and dietary factors; 2) circulating triglyceride

levels higher than 150 mg/dL; 3) concentration of HDL-cholesterol lower than 40 mg/dL in men and 50 mg/dL in women; 4) Blood pressure levels higher than 130/85 mmHg; and 5) circulating fasting glucose concentration higher than 100 mg/dL. In a review of metabolic syndrome definitions conducted in 2005, the importance of visceral obesity – which was not in Reaven´s original definition, was emphasized [18] – but the role of non-alcoholic fatty liver disease (NAFLD) *per se* was not explicitly considered.

A.2 Non-alcoholic Fatty Liver Disease (NAFLD)

NAFLD was first described in 1980 [20] and is defined by elevated lipid accumulation in liver which is not related to excessive alcohol consumption. Affecting around 24% of global population [21] among which 30% of men and 20% women [22], NAFLD is now considered as a key component of the metabolic syndrome [23] given its strong associations with both obesity and IR. On diagnosis, fatty liver disease is designated as NAFLD when alcohol consumption is established to be less than 30 g/day for men and 20/g day for women [24].

The accumulation of triglycerides in the liver is initially benign, but when combined with the development of inflammation it leads to a more severe state known as non-alcoholic steatohepatitis (NASH). NASH can then proceed to cirrhosis and/or hepatocellular carcinoma. The two hits hypothesis, conceived by Day and James [25], has been proposed to explain NAFLD progression to NASH. Alongside triglyceride accumulation, the liver is also exposed to increased inflow of circulating FFA that are in part a consequence of peripheral IR. In response, there is an increase in hepatic β-oxidation of FFA resulting in high ROS levels that induce lipid peroxidation of

unsaturated fatty acids. This in turn promotes an inflammatory cascade leading to hepatocellular mitochondrial dysfunction, and stimulation of liver fibrosis by hepatic stellate cells. In addition, FFA directly mediate endoplasmic reticulum oxidative stress in hepatocytes leading to the activation of c-Jun-N-terminal kinases and NF-kB pathway which results in the production of cytokines and other pro-inflammatory molecules. Moreover, they promote the synthesis of Fas ligands that activate Fas receptors known to promote apoptosis through effector caspases in liver such as caspase 3 [26]. During this cell damage and death process, intracellular components from hepatocytes such the intermediate filament component cytokeratin 18 (CK-18), are detected at high levels in the circulation of NAFLD patients [27].

Following apoptosis, hepatic Kupffer cells (KC) are activated by apoptotic fragments thereby potentiating hepatic inflammation. This is mediated via Toll-like receptors (TLR's), particularly TLR-3 and TLR-4, and the scavenger phagocytosis receptors. This cellular response results in the production of cytokines such as TNF-α and several other interleukins [28] that perpetuate the vicious cycle of inflammation.

A.2.1 Role of adipose tissues in NAFLD/NASH pathogenesis

As the principal source of circulating FFA, adipose tissue plays a major role in NAFLD pathogenesis. Subcutaneous adipose tissue stores account for about 60% of total body triglyceride [29] while visceral adipose tissue (VAT) holds about 20% [30]. However, since VAT is entirely drained by the hepatic portal vein, it can account for a disproportionately large proportion of FFA reaching the liver. It is generally recognised that increased waist circumference, which reflects an expansion of VAT depots, is

strongly linked to NAFLD [31]. VAT expansion not only leads to potentially higher FFA release to the liver but is also associated with increased secretion of cytokines such as TNF-α that promote the progression of benign NAFLD to NASH. This is accompanied by a decreased secretion of adiponectin, a hormone that inhibits lipogenesis and promotes β-oxidation and is considered to play an important role in hepatic lipid homeostasis [32]. Thus, in addition to an increased inflammatory burden, NAFLD patients are also deficient in circulating adiponectin [33].

A.3 Intestinal microbiome and diet-induced metabolic diseases

The intestine is the principal site where dietary components are processed into nutrients that can be absorbed and utilized by the rest of the body. The large and diverse population of microorganisms that reside in the intestinal lumen normally play a key role in this process through a symbiotic relationship with the surrounding intestinal tissue. In essence, the microorganisms have access to dietary components that are otherwise undigestible and therefore provide no nutritional benefit to the host, and through their own metabolic activities they generate metabolic by-products that the host can utilize, and indeed have become somewhat reliant on them during evolution.

The best example of this is the microbial fermentation of complex carbohydrates to yield short chain fatty acid products. In return, the microorganisms are provided with a regular food supply in a protected environment at constant temperature. Since infection of the intestine or any other tissue by microorganisms is an existential threat to the host, this relationship can be threatened by an increased presence of pathogenic microbes

and/or increased contact between microbes and the intestinal epithelium or microbial passage through the intestinal barrier into the general circulation. Additionally, the microorganisms may generate metabolic by-products that are harmful to the organism, for example ethanol or trimethylamine *N*-oxide. This so-called state of dysbiosis between the intestinal microbiota and host can be triggered by diet, and/or may be predisposed by the genetic composition of the host – in particular regarding the function of the immune system. In diseases such as NAFLD and T2D, which are strongly associated with unbalanced hypercaloric diets, many of the symptoms can be linked to the effects of intestinal microbiota dysbiosis [34-37].

The gut microbiome is defined by the group of microbes and bacterial species inhabiting the intestinal lumen. It is an extremely diverse ecosystem that includes more than 160 different bacterial species [38] and almost 10,000,000 identified genes [39] – more than three times that of the human genome. The composition of gut microflora is dominated by two major phyla: Bacteroidetes and Firmicutes [38]. While these account for 90 % of the total microbial content, the remaining 10% is represented by a high diversity of bacteria as well as several yeast species. This intestinal microbiome is highly sensitive and responsive to factors such as the environment, genetics and diet [40]. While the species/abundance profile of the gut microbome is unique for each individual it is nevertheless highly influenced by both lifestyle and diet [41].

Both the species composition of the intestinal microbiome and its metabolic products can be categorized as being beneficial or harmful to the host (see Table A.1 and Table A.2) Ultimately, it is the integrated effects of all these parameters on intestinal function, neuroendocrine energy sensing, and inflammatory status that determines whether the microbiome is acting symbiotically or dysbiotically.

The development of obesity is associated with shifts in the abundance of different bacterial species. For example, a group of obese subjects were reported to have an increased ratio of Firmicutes to Bacteroidetes compared to lean controls [42]. Moreover, transferring the microbiome of obese subjects to germ-free mice induced obesity in these animals [43]. In addition, germ-free mice show resistance for obesity development even under the typical western diets largely enriched in fat and carbohydrates and under similar intake levels [44-46].

Table A.1 – Major groups of microorganisms considered to be beneficial or harmful to the host

Beneficial Species	**Harmful Species**
Firmicutes to *Bacteroides* ratio [47, 48]	
Lactobacillus [49, 50]	*Proteobacteria* [51-53]
Roseburia [54-56]	*Ruminococcus* [57-59]
Faecalibacterium [54, 60, 61]	*Bacteroides* [50, 55, 56]
Bifidobacterium [50, 57]	*Enterococcus* [50, 55]
Lachnospiraceae [55]	*Streptococcus* [55]

The ratio of Gram-negative to Gram positive bacteria may also be a determinant of dysbiosis [35]. Gram-negative species release lipopolysaccharides (LPS) that are potent activators of the innate immune system [62]. LPS is recognized by toll-like receptors (TLR) leading to inflammation, particularly in adipocytes [63] with macrophage infiltration.

Gut microbiota changes are also associated with Type 2 diabetes. It was observed that diabetics present a typical reduction of butyrate-producing bacteria and higher levels of Lactobacillus spp. which is associated to fructose metabolism. Indeed, there are types of

Lactobacillus specifically designated as fructophilic [56]. In obese humans, a decrease in Gram-positive bacteria, which include butyrate-producing species, was found to be associated with reduced insulin sensitivity [64]. When these subjects were transplanted with faeces from lean healthy subjects, insulin sensitivity was restored in association with an increased abundance of butyrate producers in their gut microbiome [64].

Table A.2 – Gut microbial products that are considered to be beneficial or harmful to the host

Beneficial products	**Harmful products**
Bile Acids [65, 66]	LPS [67-71]
Short Chain Fatty Acids (SCFA) [72-76]	Peptidoglycan (PGN) [77-79]
Tryptophan/Indole [80-83]	Bacterial DNA [84-87]
Carotenoids and Phenolic compounds [88-90]	Trimethylamine (TMA) [91-93]

A.3.1 Short Chain Fatty Acids – bacterial fermentation products with key functions

Short-chain fatty acids (SCFA) are produced by the bacterial fermentation of complex carbohydrates [94] and account for up to 10% of daily energy requirements [95], [96]. Acetate, propionate and butyrate are the principal SCFA, and are normally generated in the molar proportion of 60:20:20, respectively [97]. Acetate and propionate are mainly produced by Bacteroidetes while butyrate is generated by Firmicutes [98]. Different tissues of the host have different SCFA preferences. Butyrate is a highly preferred energy source for colonocytes and much of it is therefore immediately utilized as soon as it is generated in the luminal space. Butyrate that is not utilized by the intestine enters the portal vein blood and is captured and metabolized by the liver. Butyrate has shown to

improve insulin sensitivity and attenuate adiposity [99]. Propionate may be utilized for intestinal gluconeogenesis [100] with the balance being efficiently extracted by the liver and utilized for hepatic gluconeogenesis [101]. While the majority of butyrate and propionate are metabolized by splanchnic tissues and are therefore not usually available to peripheral tissues, net extraction of acetate by the intestine and liver is much lower. Hence, a significant fraction of endogenously generated acetate enters the general circulation where it is metabolized by a wide range of tissues, including heart, skeletal muscle and brain astrocytes.

In addition to being oxidizable substrates, SCFA also trigger signalling actions via specific G-coupled protein receptors, namely GPR41 and GPR43. Through these signalling actions SCFA mediate the effects of the microbiome on many physiological processes in the host, including inflammation and obesity progression, by yet unclear mechanisms [102]. Butyrate and acetate also modulate acetylation/deacetylation of histones, through histone deacetylase inhibition [103]. Short chain fatty acids have been shown to promote fatty acid oxidation preventing obesity and reducing insulin resistance and an anti-tumorigenic effect which can prevent fibrosis in NAFLD [99, 104].

Microbiota harvesting causes a significant decrease of angiopoietin-like protein 4 [105], also designated as fasting-induced adipose factor (FIAF), which is an inhibitor of LPL. This bacterial effect thus increases LPL activity resulting in increased adiposity through higher lipoprotein absorption.

Gut bacterial species also have an active role in the modulation and recirculation of bile acids. This mediation occurs via farnesoid X receptors on the intestinal border which are responsible for bile acids absorption [106]. Microbiota mediate the formation of secondary bile acids such as lithocholic and deoxycholic acids. Among other things,

secondary bile acids act as agonists for the G-protein coupled receptors TGR5 which promote increased secretion of glucagon-like peptide 1 (GLP-1), especially in liver Kupffer cells, which improve glucose sensitivity [107]. Certain metabolites derived by microbial metabolism and even bacterial DNA have been implicated as potential pro-inflammatory components [108].

A.3.2 Microbiome dysbiosis and intestinal barrier integrity

Among the most important outcomes of intestinal microbiome dysbiosis is the loss of intestinal barrier integrity, which among other things results in the leakage of LPS and other potent pro-inflammatory agents into the host circulation. Indeed, an increase in intestinal permeability is implicated in the pathology of obesity-related diseases such as NAFLD and Type 2 diabetes [109].

Having a surface of about 400 m^2 in humans, the intestinal barrier is the main site of nutrient absorption, a process that requires around 35% of the resting energy expenditure of the human body [110]. The gut wall is composed of 4 layers starting from the side of the lumen: the mucosa, submucosa, muscularis and serosa (Figure A.1). The major part of the physical barrier is constituted by the epithelial cells that divide the lumen and mucosal tissues.

For maintaining integrity there are proteins designated as tight junctions that allow paracellular passage of water, ions and small molecules (< 0.4 nm) but are impermeable to larger macromolecules such as endotoxins and dietary antigens. These proteins also bind the endothelial cells together in the layer structure [111]. Important for structure stability and cell-cell signalling, adherence junctions are also localized below tight

junctions. Two types of proteins are involved in these complexes, occludins and claudins. They interact and form connections with adjacent cells through the actin cytoskeleton and as well for the bridging of pores for water and ion exchange.

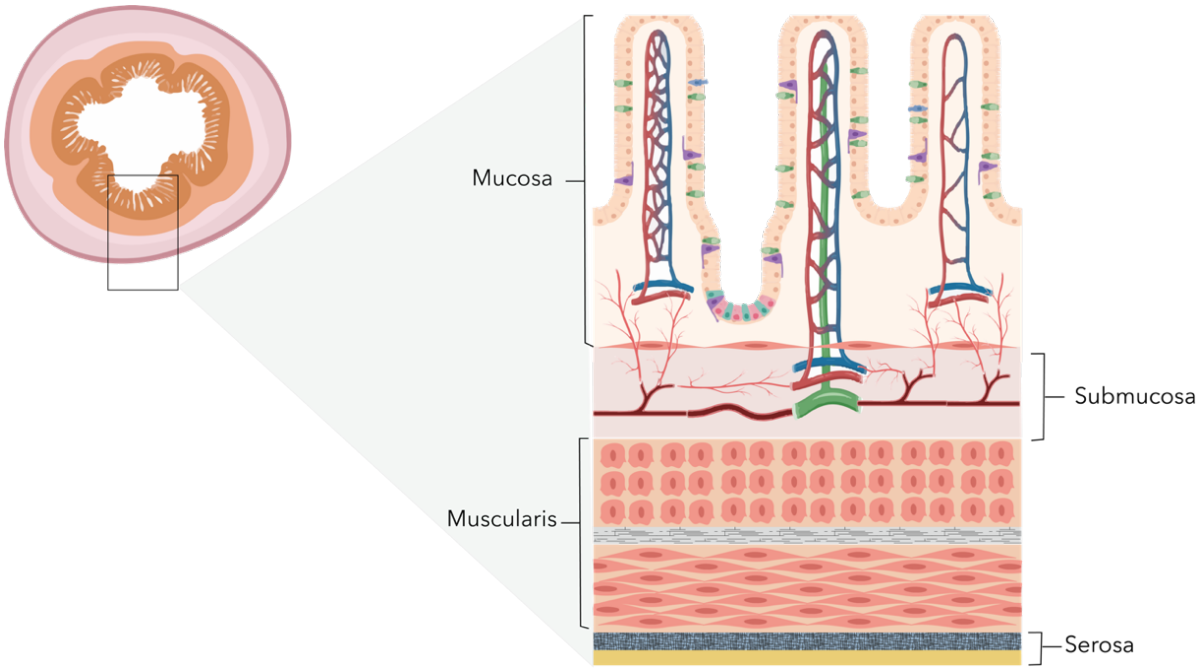

Figure A.1 – Cross section of the intestinal layer – The lumen of the intestine is enclosed by a complex and highly functional barrier. This is composed of four distinct layers: the serosa that constitutes the outer structure of the intestine; the muscularis, a thick section composed essentially by muscle – long and circular cells; the submucosa that holds vasculature that connects to epithelium; the mucosa where there are the villus and the epithelial cell lining linked together by tight junctions and incorporating all the functional cells for producing mucus and to perform phagocytoic functions.

Within the cells there are zonula occludens proteins, that link the cytoskeleton to other proteins. Deficiencies in the expression of any of these proteins can compromise the intestinal barrier [112]. In addition, enterocyte tight junction structure and intestinal barrier function can be disrupted by zonulin, a protein involved in tissue morphogenesis, fluid movement, and innate immunity of the intestinal lumen. This endogenously-secreted protein is a homolog of the Zot enterotoxin that causes actin polymerization and tight junction detachment [113]. Like its homolog, zonulin increases the permeability

of the jejunum and ileum regions [114]. Its mode of action involves the activation of the protease receptor PAR-2 and protein kinase-C, inducing an increase in endothelial growth factors that modulate the actin cytoskeleton [115, 116]. Subsequently, this cellular stress leads to occludin and zoluna occludens ZO-1 being displaced from the intestinal layer [117] causing intestinal permeability to increase. Increased levels of zonulin have been found to be associated with an excess of Gram-negative bacteria, small intestine bacterial overgrowth and circulating endotoxin levels, that in turn are also linked with obesity, type 2 diabetes and NAFLD [118-121].

A.4 Dietary fructose and metabolic disease

In Western societies, the increased consumption of simple carbohydrates is implicated in the high rates of obesity, metabolic syndrome and NAFLD. It is estimated that in the USA, 15 – 25 % of total food calories come from refined sugars [122]. In North America, the majority of refined sugar is in the form of High Fructose Corn Syrup (HFCS). HFCS consists of a mixture of glucose and fructose, and has largely replaced sucrose [123]. HFCS-55, which is the most highly used formulation for soft drinks and processed foods, is nominally composed of 45% glucose and 55% fructose although the true proportions of fructose/glucose may be somewhat higher [124].

Introduction of HFCS in the 1970s has augmented the steep rise in fructose consumption in the US. In 1900, fructose consumption was estimated at 15 g/day; by 1977 it had risen to 37 g/day and in 2004 it stood at 55 g/day [125]. This increased HCFS consumption is associated with a 20% higher prevalence of diabetes [126] while the increased consumption of fructose *per se* has been associated with rises in rates of

obesity, NAFLD and type 2 diabetes [127-129]. High fructose consumption is considered as one of the major predictors for NAFLD [130-132].

Fructose absorption occurs via GLUT5: a transporter with a passive diffusion centralized mechanism and with high specificity for fructose. The intestinal luminal side has a high abundance of this transporter. On the basolateral side, fructose can pass via GLUT2, which also transports glucose [133, 134]. As with other absorbed nutrients, fructose is transported from the intestine via blood draining the portal vein where it then enters the liver. The liver has high levels of GLUT5 as well as lesser amounts of other transporters that can take up fructose such as GLUT2 and GLUT8 [135]. As a result, any fructose that is present in portal vein blood is almost quantitatively absorbed by the liver during first passage [136, 137] hence its concentration in peripheral blood is typically low. Despite this absorptive capacity, intestinal fructose uptake may be saturated during high fructose feeding. In mice fed a diet where the carbohydrate component was 100% fructose, un-metabolized fructose was detected in the faeces indicating that its absorption had not been complete [138].

Fructose metabolism is shown in Figure A.2. Recent studies indicate that it can be metabolized by enterocytes and adipocytes as well as hepatocytes [139-142]. In fact, the intestine has been recently proposed as the primary site for fructose metabolism under conditions of low or moderate fructose loads, with the liver only participating following dietary fructose loads that exceed the intestinal metabolic capacity [143]. After uptake, fructose is phosphorylated by ketohexokinase (KHK), also known as fructokinase, to form fructose-1-phosphate (F1P). F1P is then cleaved to dihydroxyacetone phosphate and glyceraldehyde by aldolase B. Triokinase converts glyceraldehyde to glyceraldehyde-3-phosphate. Unlike glucose, whose conversion to triose-P is highly

regulated by glucokinase and phosphofructokinase (see Figure A.2), none of the steps involved in fructose conversion to triose-P are under insulin control but are instead only limited by fructose and ATP levels.

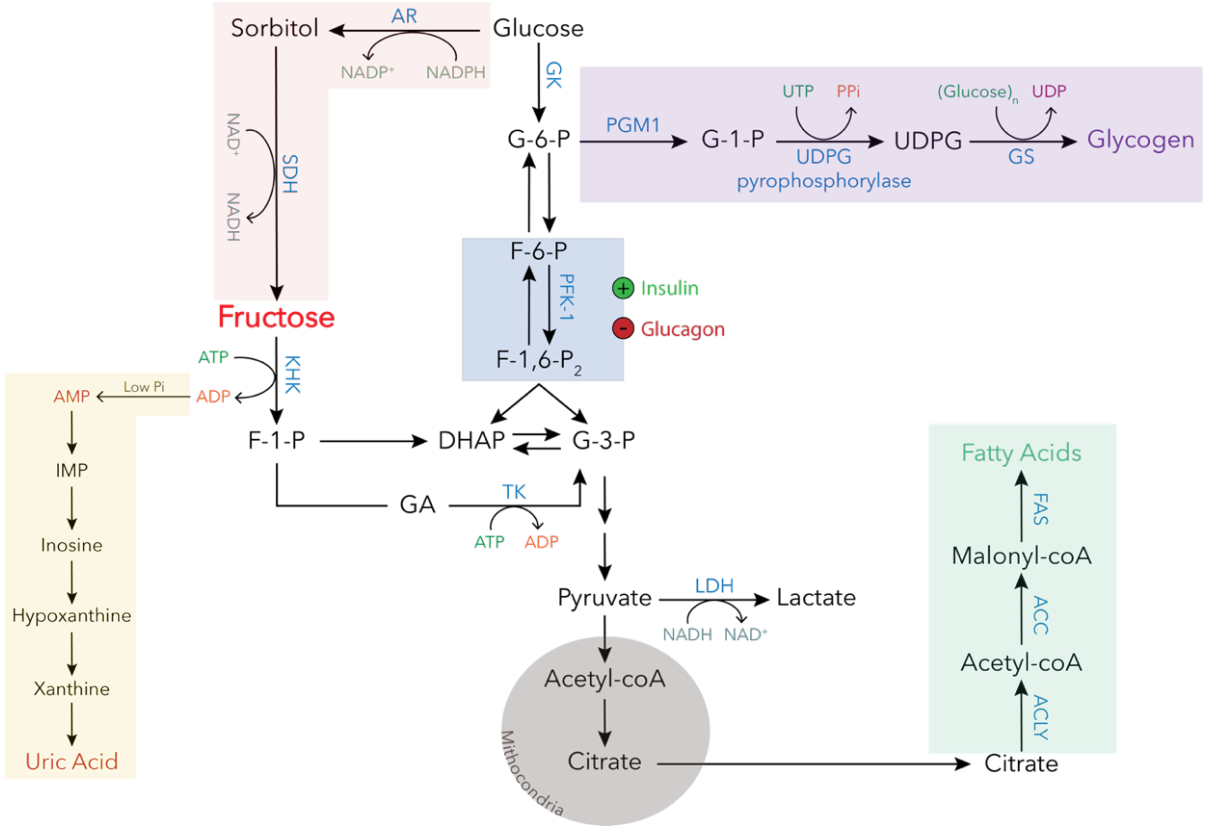

Figure A.2 – Metabolic pathways associated with fructose, including its catabolism into glycolytic triose phosphates, its endogenous production from glucose and formation of uric acid secondary to ATP and inorganic phosphate depletion – Code: KHK – Ketohexokinase; F-1-P – Fructose-1-phosphate; GA – Glyceraldehyde; DHAP – Dihydroxyacetone phosphate; G-3-P – Glyceraldehyde-3-phosphate; AR – Aldose reductase; SDH – Sorbitol dehydrogenase; GK – Glucokinase; G-6-P – Glucose-6-phosphate; F-6-P – Fructose-6-phosphate; PFK-1 – Phosphofructokinase-1; F-1,6-P2 – Fructose-1,6-bisphosphate; LDH – Lactate dehydrogenase; ACLY – ATP Citrate lyase; ACC – Acetyl-CoA carboxylase; FAS – Fatty acid synthase; PGM1 – Phosphoglucomutase 1; G-1-P – Glucose-1-phosphate; UTP – Uridine triphosphate; PPi – Pyrophosphate; UDPG – Uridine diphosphate glucose; UDP – Uridine diphosphate; GS – Glycogen synthase.

The immediate triose-phosphate products can feed several pathways including fatty acid synthesis via *de novo* lipogenesis (DNL), synthesis of glycerol-3-phosphate that then

undergoes esterification with fatty acids to form triglycerides [144], synthesis of glucose and glycogen via gluconeogenesis and the indirect pathway, and production of lactate following conversion to pyruvate. It has been proposed that fructose metabolism may cause extensive "futile cycling" at the level of F1,6-P_2 and F6P, possibly disrupting the reciprocal regulation of these pathways [145, 146]. More recently, a functional pathway for endogenous fructose production from glucose via sorbitol has been identified in mammals [147]. Recent studies also demonstrate that fructolytic enzymes are also highly expressed in intestinal tissues indicating that at least some dietary fructose may be metabolized as soon as it is absorbed [148].

Fructose metabolism promotes high rates of hepatic triglyceride synthesis by providing high inflows of glycolytic precursors as well as through the activation of transcription factors ChREBP and SREBP-1c, both of which upregulate the expression of DNL-pathway enzymes. These transcription factors appear to be activated through a number of parallel mechanisms. Recent studies indicate that ChREBP is activated by increased levels of xylulose-5-phosphate and/or glucose-6-phosphate resulting from fructose catabolism [146]. These metabolites in turn stimulate phosphatase 2A [149] that itself increases the production of one of ChREBP isoforms, ChREBP-α that subsequently promotes the generation of the other isoform, ChREBP-β. ChREBP-β is more potent in activating lipogenic genes independently of insulin action [150] (Figure A.3). Fructose has also been shown to promote a rise in SREBP-1c levels [151] that potentiates expression of DNL enzymes. This may be mediated in part by peroxisome proliferator-activated receptor γ coactivator (PPAR-γ) activation [152] (Figure A.3). Acetyl-coA carboxylase (ACC), and fatty acid synthase (FAS) were shown to be increased in expression and activity in more than 60% in response to high fructose diets [153]. Additionally, fructose

has been shown to activate transcription factor XBP-1, that in turn increases ACC 1 and 2 isoforms, FAS and stearoyl-coA desaturase 1 (SCD1) [154].

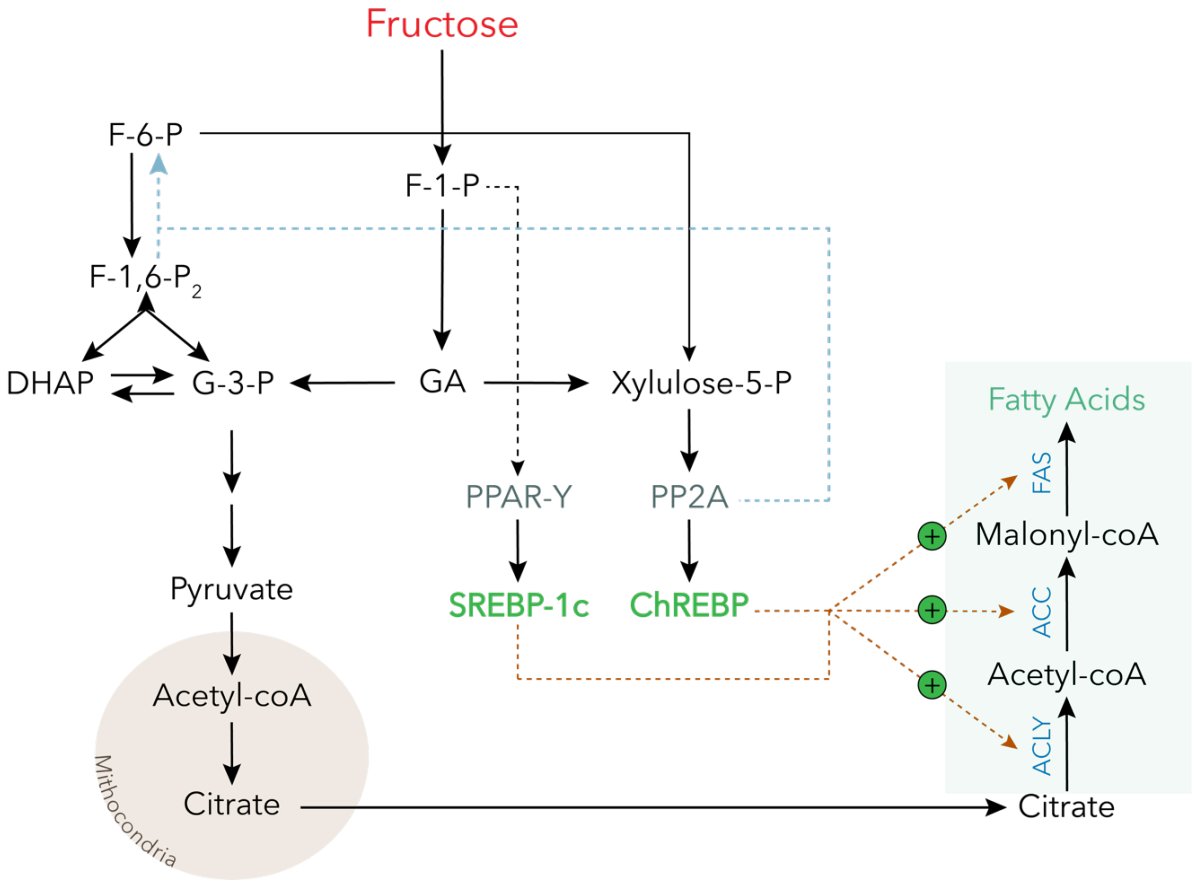

Figure A.3 – Fructose induction of lipogenesis transcription factors ChREBP and SREBP-1c – Metabolites resultant from fructolysis, namely F-6-P, F-1-P and xylulose-5-P lead to the activation of transcription factors that stimulate directly the expression of lipid synthesis enzymes. Code: F-6-P: Fructose-6-phosphate; F-1,6-P_2: Fructose-1-6-bis-phosphate; DHAP: Dihydroxyacetone phosphate; G-3-P: Glyceraldehyde-3-phosphate; F-1-P: Fructose-1-phosphate; GA: Glyceraldehyde; PPAR-γ: Peroxisome proliferator activated receptor; SREBP-1c: Sterol receptor element binding protein 1c; Xylulose-5-P: Xylulose-5-phosphate; ChREBP: Carbohydrate receptor element binding protein; ACLY: ATP Citrate lyase; ACC: Acetyl-coA carboxylase; FAS: Fatty acid synthase

Concomitantly, it is observed that high fructose does not cause a postprandial peak in insulin levels thereby attenuating systemic triglyceride clearance and adding to hepatic fat storage [155]. While triglycerides *per se* do not seem to be involved in metabolic regulation or signalling activities, incomplete products of fatty acid

esterification/lipolysis such as diacylglycerols directly interfere with insulin signalling [152].

In addition to lipogenesis, there are several aspects of fructose metabolism that promote tissue damage starting with its initial phosphorylation and resulting disruption of ATP/ADP/AMP balance, which in the case of the liver, leads to increased uric acid production. It is well established that high uric acid concentrations promote intracellular oxidative stress, in part via nitric oxide signalling [156, 157]. Compared to glucose, fructose metabolism is estimated to produce one hundred times more ROS [125] which among other things contributes to intracellular stress and ubiquitin-driven apoptosis. Additionally there is one product of fructose metabolism, methylglyoxal, that is a powerful glycating modifying agent leading to cell stress as well as modification of insulin signalling [158]. Finally, high fructose feeding has also been shown to be associated with alterations in microbiota species composition and increased intestinal permeability [159].

A.5 Bullet Summary

- A significant proportion of people in Western societies are overweight or obese.
- The majority of these have significant co-morbidities including NAFLD and Type 2 Diabetes.
- These conditions are closely linked to overnutrition in general and increased intake of refined sugars in particular.

- These dietary components promote NAFLD and Type 2 diabetes in part through disruption of a) the symbiotic relationship between the intestinal microbiome and surrounding tissues and b) hepatic control of glucose and lipid metabolism.

Chapter B

Intestinal microbial and metabolic profiling of mice fed with high-glucose and high-fructose diets

(Published [138])

B.1 Abstract

Increased sugar intake is implicated in Type-2 diabetes and fatty liver disease, however, the mechanisms through which glucose and fructose promote these conditions are unclear. We hypothesize that alterations in intestinal metabolite and microbiota profiles specific to each monosaccharide are involved. Two groups of six adult C57BL/6 mice were fed for 10-weeks with diets with glucose (G) or fructose (F) as sole carbohydrates, and a third group was fed with a normal chow carbohydrate mixture (N). Fecal metabolites were profiled by nuclear magnetic resonance (NMR) and microbial composition by real-time polymerase chain reaction (qPCR). Although N, G and F mice exhibited similar weight gains (with slight slower gains for F) and glucose tolerance, multivariate analysis of NMR data indicated that F mice were separated from N and G, with decreased butyrate and glutamate and increased fructose, succinate, taurine, tyrosine and xylose. The different sugar diets also resulted in distinct intestinal microbiota profiles. That associated with fructose seemed to hold more potential to

induce host metabolic disturbances compared to glucose, mainly by compromising intestinal barrier integrity. This may reflect the noted non-quantitative intestinal fructose absorption hence increasing its availability for microbial metabolism, a subject for further investigation.

B.2 Keywords

Fructose; absorption; short-chain fatty acids; metabolic profiling; metabolomics; intestinal microbiota

B.3 Introduction

In recent decades, Western societies have seen steep increases in obesity rates and a surge of associated complications such as non-alcoholic fatty liver disease (NAFLD) and Type 2 Diabetes (T2D) [160-162]. Over this same period, the average daily caloric intake has risen, driven in large part by a substantial increase in sugar consumption [155]. In European countries, sugar is consumed as sucrose, while in North America there has been an increased utilization of high fructose corn syrup (HFCS). Both formulations result in the delivery of approximately equivalent amounts of glucose and fructose to the gastrointestinal tract (sucrose being rapidly hydrolysed to fructose and glucose in the upper small intestine) followed by absorption of glucose and fructose by specific transporters: SGLT1 for glucose and GLUT5 and GLUT2 for fructose. Therefore, when sugar intake is low, these monosaccharides are rapidly and quantitatively absorbed becoming unavailable for intestinal microbiota metabolism, particularly those residing

in the lower intestine. However, with high sugar intake, these transporters, particularly those involved with fructose uptake, may become saturated thereby increasing the residence time of monosaccharides in the intestinal lumen and providing an increased opportunity for microbial metabolism.

There is now extensive evidence that interactions between gut microbiota and diet promote obesity per se as well as obesity-related complications such as NAFLD and T2D [163]. In animal models, high fat feeding resulted in impaired intestinal integrity and leakage of pro-inflammatory endotoxins into portal vein blood that in turn provoked hepatic inflammation. This process was associated with a shift in intestinal bacterial species distribution [164, 165]. Diet composition has also been shown to alter intestinal metabolites, including those generated by microbial activity such as short-chain fatty acids. These changes can be noninvasively followed by metabolomic analysis of feces [166-168].

Of the monosaccharide components of dietary sucrose or high-fructose corn syrup (HFCS), fructose is more pro-inflammatory and lipogenic to liver than glucose [169-172]. To date, the search for possible mechanisms has focused on liver, since this organ is responsible for the majority of systemic fructose metabolism. We hypothesized that, in addition to hepatic mechanisms, part of the deleterious effects of high fructose feeding are mediated through intestinal metabolism of fructose by resident microbiota. To examine if fructose and glucose have different effects on the intestinal metabolome we fed mice with diets in which carbohydrate components were solely comprised of fructose or glucose and periodically compared their fecal metabolite and microbial profiles over a 10-week period. To determine the effects of replacing the standard dietary

mixture of simple and complex carbohydrates by either of these simple sugars on these parameters, a third group of animals fed on normal chow was also included in the study.

B.4 Experimental section

B.4.1 Animal model

All animal studies were approved by the University of Coimbra Ethics Committee on Animal Studies (ORBEA) and the Portuguese National Authority for Animal Health (DGAV), approval code 0421/000/000/2013. Eighteen adult male C57BL/6 mice (8 weeks of age at start of study) were obtained from Charles River Labs, Barcelona, Spain, and housed at the Faculty of Medicine Bioterium, University of Coimbra. The study was limited to mice of a single gender because of space constraints. Power analyses and sample size calculations were based on circulating metabolites and hepatic metabolic parameters measured in our previous studies of fat and sucrose metabolism in rats [173, 174]. Animals were housed 3 to a cage, 2 cages per group (or diet, see below), and were maintained in a well-ventilated environment, and a 12h light/12h dark cycle. Upon delivery to the Bioterium, mice were given a two-week interval for acclimation, with free access to food (standard chow, see composition below) and water. After this period animals were randomly assigned to three synthetic diets supplied by Special Diets Services, Argenteuil, France over a 10-week period. These were standard chow (60% carbohydrate, 16% protein and 3% lipid by weight); high glucose (60% glucose, 16% protein and 3% lipid by weight); high fructose (60% fructose, 16% protein and 3% lipid by weight). The carbohydrate component of the normal diet was composed of

cornstarch (63%), maltodextrin (21%) and sucrose (16%); the total fiber composition was 17% by weight for each diet. These synthetic diets were formulated on an AIN-93G background and packaged in coarse powder form (the high glucose and fructose formulations could not be pelletized). For this reason, the mice were provided with the powdered standard chow placed in small open Petri dishes during the initial 2-week adjustment period and this method of feed delivery was used in the subsequent studies. Hereafter, the three diets will be referred to as normal (N), glucose (G), and fructose chow (F).

B.4.2 Sample Collection

Fecal samples were collected every two weeks for analysis by ^{1}H NMR spectroscopy and qPCR. Collections were performed on three consecutive days (one day for each of the diets) and six mice at a time in a clean and sterile flow chamber to minimize sample contamination (Figure B.1). One-half of each fecal sample was used for NMR studies and the other half for qPCR analysis. Samples were placed in Eppendorf tubes and immediately frozen in liquid nitrogen followed by storage at -80 ºC until further processing and analysis.

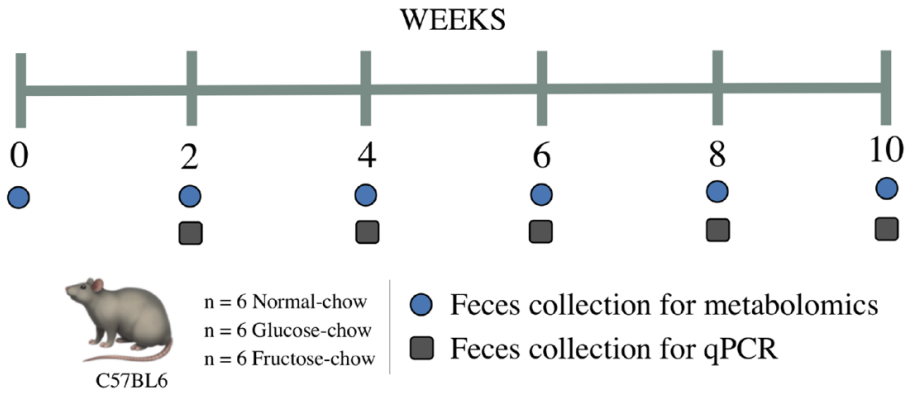

Figure B.1 – Scheme of sample collection

B.4.3 Oral glucose tolerance test

Mice were fasted throughout the dark period and through the initial 4 h of the light period for a total time of 16 h. Mice were then gavaged with a solution of 10% glucose prepared in sterilized drinking water whose volume corresponded to 2 mg glucose/g body weight. Blood glucose levels were monitored from tail tip samples at 0, 15, 30, 60 and 120 min after gavage using a OneTouch Vita (LifeScan) glucometer.

B.4.4 Metabolite extraction

Processing of samples to obtain fecal extracts was performed according to previously published methods [175, 176]. Briefly, 70 mg of thawed stool samples were homogenized by vortex mixing in 700 µl phosphate buffer (0,1M K_2HPO_4/NaH_2PO_4, pH 7.4) containing 10% D_2O, 0.01% (w/v) of NaN_3 and 0.5 mM of sodium 3-([2,2,3,3-d_4]trimethylsilyl) propionate (TSP). After mixing, samples were submitted to 3 rapid freeze-thaw cycles using liquid nitrogen. Homogenization was next performed for 10 cycles as follows: ultrasonication – vortex – break. In the end, slurries were centrifuged (16,000 g, 10 min) and the supernatants collected. The remaining residues were subjected once again to homogenization and centrifugation and their supernatants were combined with those from first pass extractions. Extracts were stored at -80ºC until analysis.

B.4.5 NMR spectroscopy

Fecal extracts were thawed at room temperature and 225 µl transferred to a 5 mm NMR tube. The same volume of 99% D_2O containing 0.002% TSP was added [175].

Unidimensional standard ^{1}H NMR spectra of fecal extracts were obtained at 298 K on a Bruker Avance III spectrometer operating at 500.13 MHz for ^{1}H, using a noesy 1D pulse sequence (Bruker library) with 100 ms mixing time, a 3 μs t1 delay, and water suppression during relaxation delay and mixing time. 256 transients were acquired into 32 k complex data points, with 7 KHz spectral width, 4 s relaxation delay and 2.34 s acquisition time. Each free-induction-decay was multiplied by a 0.3 Hz exponential line-broadening function prior to Fourier transformation. Spectra were manually phased and baseline corrected. Chemical shifts were referenced internally to TSP at δ=0.0 ppm. Peak assignments were carried out based on 2D NMR of selected samples, existing literature [176-178] and spectral databases, mainly the Bruker Biorefcode database and the human metabolome database (HMDB) [179]. Statistical total correlation spectroscopy (STOCSY) was performed to aid assignment.

B.4.6 Univariate and multivariate statistical analysis

Two-Way analysis of variance (ANOVA) was used to assess differences in body weight and OGTT values. Multivariate analysis was applied to the ^{1}H NMR spectra of fecal extracts, after exclusion of the water (4.60-5.05 ppm) region. Spectra were aligned using recursive segment-wise peak alignment [180] and normalized through probabilistic quotient normalization (PQN) [181], to account for sample differences impacting significantly on total spectral area and profile. Principal component analysis (PCA) and partial least squares discriminant analysis (PLS-DA) were performed after unit variance scaling (SIMCA-P 11.5, Umetrics, Sweden). PLS-DA loading weights were obtained by multiplying each variable by its standard deviation and were coloured according to each

variable importance to the projection (VIP). In addition, the relevant peaks were selected and integrated (Amix 3.9.14, BrukerBioSpin, Rheinstetten, Germany), normalized and variations assessed using the non-parametric t-test (Wilcoxon test). Effect sizes [182] were computed for all relevant resonances ($p<0.05$) and corrected for multiple comparisons using the Benjamini and Hochberg method [183]. Statistical tests, boxplots and loadings plots were carried out using R-statistical software (version 3.2.0, R Project) and MATLAB (version 8.3.0, MathWorks Inc.).

B.4.7 DNA extraction and quantitative polymerase chain reaction (PCR)

Frozen fecal samples were weighed immediately after collection. Upon thawing, 300 μL of sterile phosphate buffer (PBS 1x) was added and the mixture was submitted to ultrasonication for 20 min. 270 μL of lysis buffer (MagNa Pure Bacteria Lysis Buffer, Roche, Basel, Switzerland) were added to the fecal slurry, followed by 30 μL of proteinase K (Qiagen, Netherlands). This mix was incubated at 65°C for 10 min, vortexed and incubated for 10 min at 95°C. Samples were filtered in a filter tube (Becton DiKinson Biosciences) to remove the debris and the filtrate was centrifuged (8,787 g, 15 min, 4°C) and the supernatant collected. DNA was extracted using a kit (MagNa Pure Nucleic Acid Isolation Kit I, Roche, Basel, Switzerland) and performed on a MagNa Pure Compact Instrument (Roche, Basel, Switzerland). Fecal DNA samples were then stored at -80°C.

Real-time quantitative PCR (qPCR) was used to quantify populations of total bacteria, *Enterobacteria* and *Lactobacilli*. Specific reactions for each different type of bacteria were performed with specific primers [184]. For total bacteria, the following 16S rRNA primer

was used: F (forward) 5' AACGCGAAGAACCTTAC 3', R (reverse) 5' CGGTGTGTACAAGACCC 3' [185]. For *Enterobacteria*: F (forward) 5' ATGGCTGTCGTCAGCTCGT 3', R (reverse) 5' CCTACTTCTTTTGCAACCCACTC 3', and for *Lactobacilli*: F (forward) 5' GCAGCAGTAGGGAATCTTCCA 3', R (reverse) 5' GCATTYCACCGCTACACAT 3' were used. The specificity of the primers was tested by sequencing of the amplicon resulting from the PCR reaction of one sample of fecal DNA. Standard curves were established prior to sample analysis using plated cultures of *Escherichia Coli* (*E. coli)* and *Lactobacillus fermentum*. DNA was extracted, PCR products were purified, and concentrations were measured by spectrophotometry at 260 nm (Eppendorf Biophotometer ®). DNA from *E.coli* was used for the total bacteria standard curve. For *E. coli*, 10^4-10^{10} gene copies were used to establish the linearity of standard curves while for *Lactobacillus*, 10^5-10^{10} copies were used. Real time PCR reactions for bacteria quantification were carried out on a LightCycler ® (Roche, Basel, Switzerland). PCR reactions were prepared on a total volume of 20 µL containing 2 µL of LightCycler FastStart DNA MasterPLUS SYBR Green I (Roche, Basel, Switzerland), 0.3 µM of each specific primer and 2 µL of DNA sample, diluted 1/100. To exclude carryover contamination, a negative control was included in each PCR experiment.

B.5 Results

B.5.1 Weight gain and glucose tolerance

Mice fed with either glucose or fructose carbohydrate diets had overall similar weight gains to those fed with standard chow (consisting of a mixture of cornstarch, maltodextrin and sucrose in proportions of 4.0:1.3:1.0) over the 10-week period, as shown in (Figure B.2a). At weeks 4 and 6 of feeding schedule, the group of fructose-fed mice had less weight gain compared to either glucose- or normal chow-fed mice, but by week 10, growth rates from the three groups had converged. Glucose tolerance, as assessed by the area under the curve (AUC) of plasma glucose levels from 0-120 minutes following an oral glucose load, showed no significant differences between the different diets nor were there any significant longitudinal changes in this parameter (Figure B.2b-e). However, by the end of the study, the group fed with fructose carbohydrate showed a tendency towards faster recovery from the glucose load and presented lower values of circulating glucose at 120 min post-load (Figure B.2e).

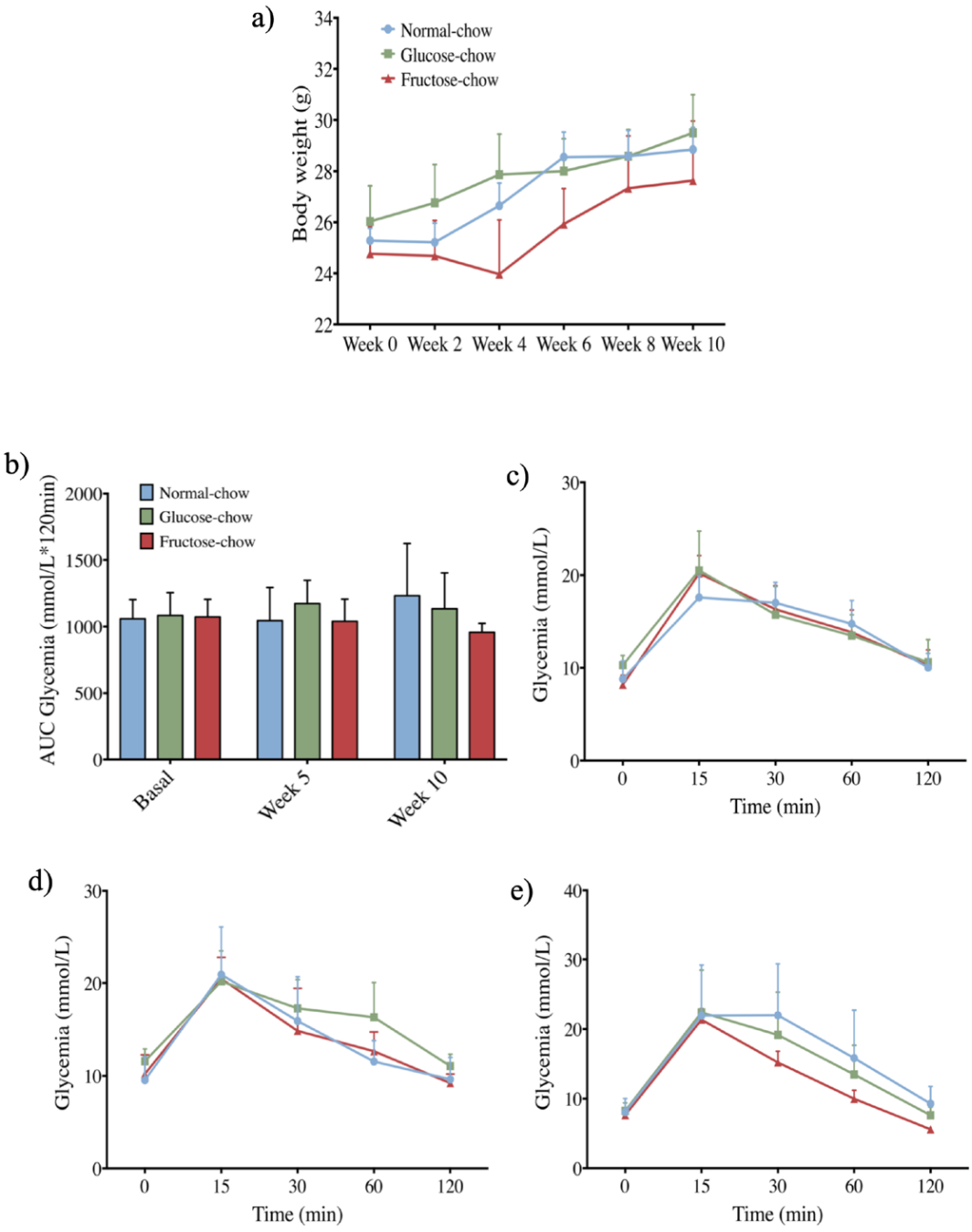

Figure B.2 – Body weight alteration along time and oral glucose tolerance tests (OGTT) performed at 3 time points (Week 0, Week 5, Week 10): a) Body weight curves monitored each two weeks of the three different diets; b) Area under the curve (AUC) of the different obtained profiles for OGTT tests on week 0, week 5 and week 10; c), d) and e) OGTT profiles for the three different diets groups performed at week 0, week 5 and week 10, respectively. 2-way-ANOVA's with time and diet as variables were performed on body weight and OGTT results and turned the following outcomes: Body Weight – Time ($P < 0.0001$; $F = 38.54$; $DF = 5$), Diet ($P = 0.0140$; $F = 5.745$; $DF = 2$); OGTT Basal – Time ($P < 0.0001$; $F = 142.8$; $DF = 4$), Diet ($P = 0.09004$; $F = 0.1056$; $DF = 2$); OGTT Week 5 – Time ($P < 0.0001$; $F = 82.69$; $DF = 4$), Diet ($P = 0.3784$; $F = 1.042$; $DF = 2$); OGTT Week 10 – Time ($P < 0.0001$; $F = 79$; $DF = 4$), Diet ($P = 0.2012$; $F = 1.788$; $DF = 2$).

B.5.2 Fecal Metabolite Profiles

A typical ^{1}H NMR spectrum of a fecal extract of a mouse before intervention (Figure B.3) shows the predominance of branched-chain amino acids (BCCA) and other amino acids (threonine, alanine, lysine, aspartate, taurine, tyrosine and phenylalanine), several organic acids (butyrate, propionate, lactate, acetate, pyruvate, succinate, fumarate, 4-hydroxyphenylacetate (4-HPA) and formate), trimethylamine (TMA), methanol, uracil and xylose. Table B.1 lists the full set of identified spin systems.

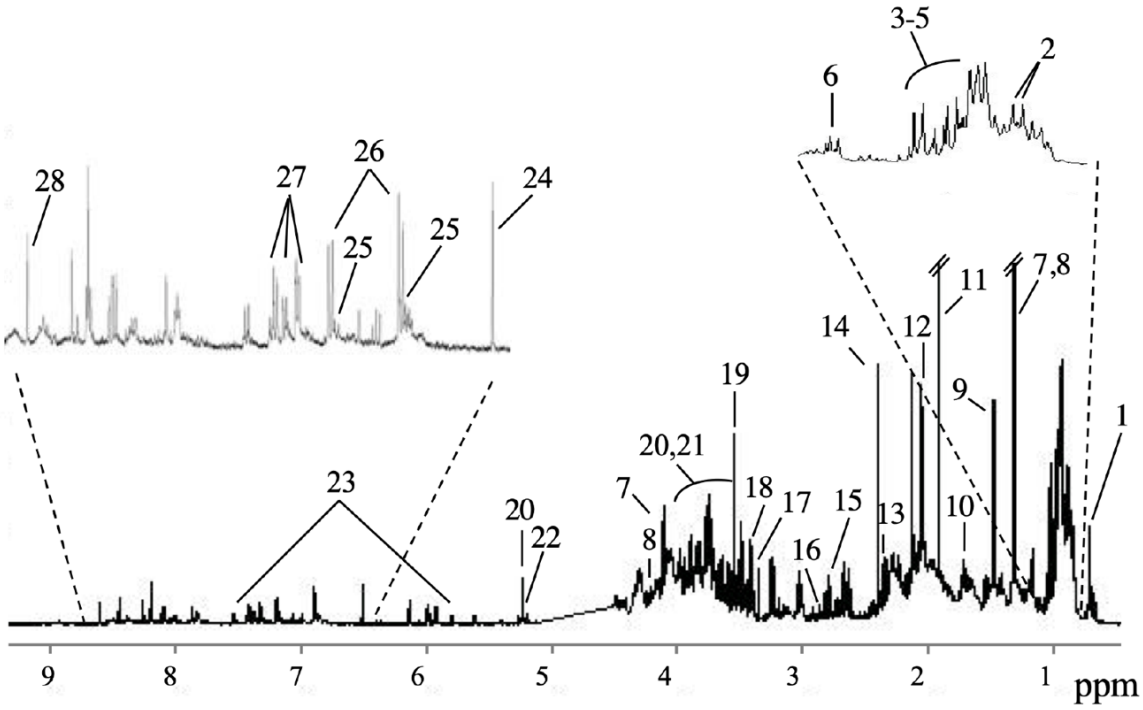

Figure B.3 – Typical ^{1}H NMR spectrum of a rat fecal extract at week 0 - Main assignments shown: 1, bile acids (tentative assignment), 2, butyrate; 3, leucine; 4, isoleucine; 5, valine; 6, propionate; 7, lactate; 8, threonine, 9, alanine; 10, lysine; 11, acetate; 12, N-acetylglycoproteins; 13, pyruvate; 14, succinate; 15, aspartate; 16, TMA (trimethylamine); 17, methanol; 18, taurine; 19, glycine; 20, xylose; 21, α-glucose; 22, β-glucose 23, uracil; 24, fumarate; 25, 4-HPA (4-hydroxyphenylacetate); 26, tyrosine; 27, phenylalanine; 28, formate.

Table B.1 – List of metabolites found in the ^{1}H NMR spectra (500 MHz) of fecal extracts. Ui: unassigned spin systems. s: singlet, dd: doublet of doublets, t: triplet, m: multiplet, br: broad resonance. a: tentative assignment; TMA: trimethylamine; TMAO: trimethylamine-*N*-oxide.

Metabolite	**δ_H /ppm (multiplicity)**
4-hydroxyphenylacetate	3.46 (s), 6.87 (dd), 7.16 (dd),
Acetate	1.92 (s)
Acetoacetate	2.27 (s), 3.46 (s)
Acetone	2.23 (s)
Alanine	1.48 (d), 3.78 (q)
Aspartate	2.69 (dd), 2.82 (dd), 3.91 (dd)
Bile acids [a]	0.68 (s), 0.70 (s), 0.72 (s)
Butyrate	0.90 (t), 1.57 (m), 2.17 (t)
Choline	3.20 (s), 3.52 (m), 4.08 (m)
Ethanol	1.19 (t), 3.65 (q)
Formate	8.46 (s)
Fructose	3.58 (m), 3.66 (dd), 3.70 (m), 3.81 (dd), 3.83 (m), 3.90 (dd), 3.95 (m), 4.01 (m), 4.04 (m), 4.06 (m), 4.12 (m)
Fumarate	6.53 (s)
Galactose	3.49 (dd), 3.64 (dd), 3.75 (m), 3.83 (m), 3.93 (d), 3.98 (d), 4.10 (t, C1H), 4.60 (d, CH2), 5.28 (d, C5H)
Glutamate	2.04 (m), 2.12 (m), 2.34 (m), 3.75 (dd)
Glutamine	2.15 (m), 2.47 (m), 3.79 (t)
α-Glucose	3.42 (t), 3.54 (dd), 3.71 (t), 3.77 (dd), 3.84 (m), 5.23 (d)
β-Glucose	3.23 (dd); 3.44 (m), 3.50 (t), 3.72 (dd), 3.90 (m), 4.65 (d)
Glycerol	3.55 (m), 3.65 (dd), 3.78 (m)
Glycine	3.56 (s)
Hypoxanthine	8.19 (s), 8.21 (s)
Isoleucine	0.94 (t), 1.01 (d), 1.26 (m), 1.47(m), 1.98 (m), 3.62 (d)
Lactate	1.34 (d), 4.11 (q)
Leucine	0.96 (t), 1.73 (m)
Lysine	1.48 (m), 1.73 (m), 1.92 (m), 3.03 (t), 3.77 (t)
Methanol	3.36 (s)
Phenylalanine	3.13(dd), 3,29(dd), 4.00(dd), 7.34(m), 7.38(m), 7.44(m)
N-acetyl residue [a]	2.05 (s)
Propionate	1.06 (t), 2.18 (q)
Pyruvate	2.38 (s)
Succinate	2.41 (s)
Sucrose	3.48 (t), 3.56 (dd), 3.63 (s), 3.77 (t), 3.83 (dd), 3.85 (m), 3.89 (m), 4.06 (t), 4.22 (d), 5.41 (d)
Taurine	3.26 (t), 3.43 (t)
TMA	2.88 (s)
TMAO	3.28 (s)
Threonine	1.33 (d), 3.61 (d), 4.26 (dd)
Tyrosine	6.98 (dd), 7.20 (dd), 3.95 (dd), 3.20 (dd), 3.06 (dd)
Uracil	5.78 (d), 7.54 (d)
Urea	5.80 (s,br)
Valine	0.99 (d), 1.04 (d), 2.27 (m), 3.61 (d)
Xylose	3.23 (dd), 3.33 (dd), 3.42 (t), 3.53 (dd), 3.63 (m), 3.93 (dd), 4.59 (d), 5.21 (d)
Unassigned spin systems varying significantly between groups	
U1	5.93 (d), 5.98 (d), 6.07 (d), 6.11 (d), 8.03 (s), 8.27 (s), 8.38 (s)
U2	8.63 (s)

PCA scores of all ^{1}H NMR spectra for the three groups of animals (Figure B.4a) showed that normal (blue) and high-glucose (green) diets had similar effects on fecal extracts

metabolic profile, with slightly higher dispersion for the latter (Figure B.4a,c). Conversely, high-fructose diet induced significant changes in about half of the samples and suggested two different directions in PCA space (Figure B.4a,b), although apparently not following a clear trend over the 10-week feeding trial.

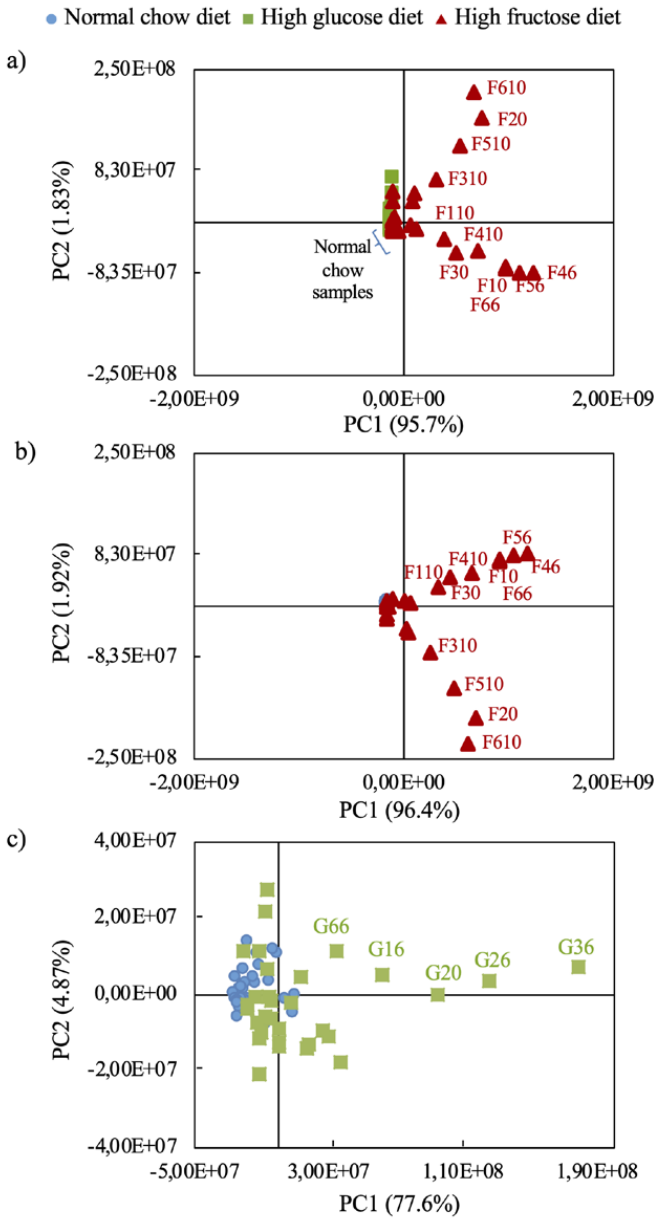

Figure B.4 – PCA scores scatter plots using ^{1}H NMR spectra of fecal extracts for a) all three diets, b) normal chow and high-fructose diets and c) normal chow and high-glucose diets (note the lower range in PC axis in c), in order to clarify the differences between these two diets). Outlier G12 was removed from dataset. Data points for fructose- and glucose-chow fed mice are identified by diet (F,G), mouse ID number (1-6 per diet) and the week of sampling. For example, G12 signifies glucose-fed mouse number 1 that was sampled at week 2.

Pairwise PLS-DA scores (Figure B.5, left) confirmed the separation of high-fructose diet from both normal and high-glucose diets (Figure B.5a, c) and indicated a small separation between animals on high-glucose and normal chow diets (Figure B.5b). It should be noted that model predictive power (Q^2) is, in this context, expected to be low (indeed Q^2=0.38-0.19), as time progression is observed to be an important source of variability within each group reflected in the partial overlap between groups. The basis for the sample separations noted were specified through inspection of PLS-DA loading weights (Figure B.5, right), peak integration and univariate analysis. Table B.2 lists all detected metabolite changes separating animal classes based on their diet, also represented in boxplot form in Figure B.6, Figure B.7, Figure B.8. Notably, two unassigned spin systems are also part of these changes: U1 singlets at δ 8.03 and 8.39 and U2 singlet at δ 8.62 (the latter tentatively assigned to nicotinate).

High-glucose diet induces significant changes in 8 fecal metabolites (Table B.2 and Figure B.6), namely acetate (↑), aspartate (↓), formate (↑), methanol (↑), propionate (↑), pyruvate (↑), taurine and unassigned singlet U2 at δ 8.62 (↓). All of these changes are also noted in high-fructose animals, with the exception of propionate levels which are close to controls (Table B.2 and Figure B.7) and with enhanced effect size and statistical relevance for formate (↑), methanol (↑) and taurine (↑), in fructose-fed mice. Direct comparison between the two sugar diets (Table B.2 and Figure B.8) unveils relevant changes specific of the fructose diet, namely: butyrate (↓), fructose (↑), glucose (↑), lactate/threonine (↑), phenylalanine (↑), propionate (↑), succinate (↑), tyrosine (↑), xylose (↑) and U1 at δ 8.03, 8.39 (↓). Notably, propionate levels seem to respond differently to high-glucose and high-fructose diets, increasing and decreasing, respectively.

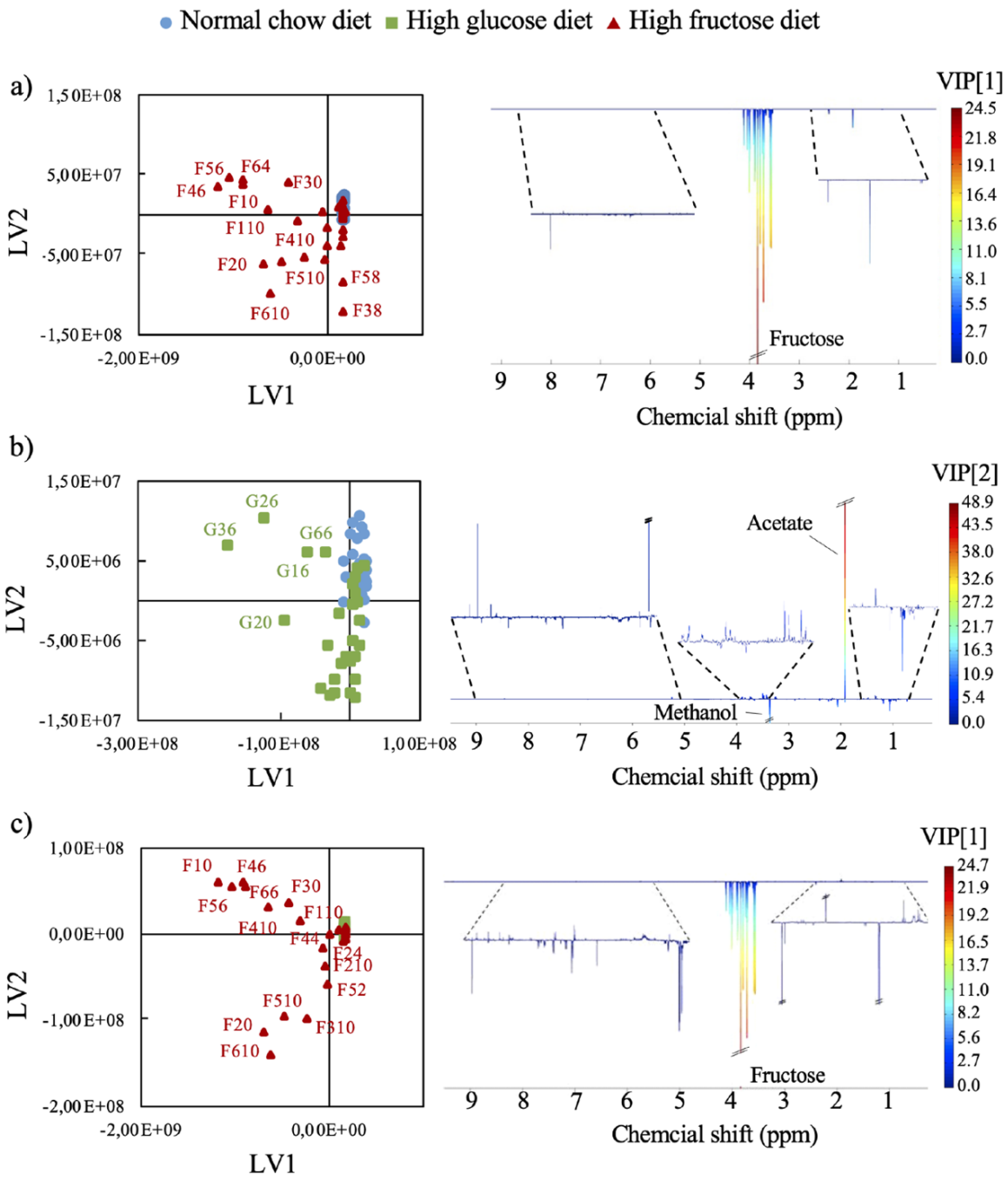

Figure B.5 – PLS-DA scores (left) and loadings weights (right) for animals fed with a) fructose- *vs* normal chow, Q^2 0.38, R^2X 0.96, R^2Y 0.40; b) glucose- *vs* normal chow, Q^2 0.36, R^2X 0.81, R^2Y 0.55; c) fructose *vs* glucose-chow, Q^2 0.19, R^2X 0.98, R^2Y 0.26. The outlier G12 was removed from the dataset.

Table B.2 – Statistically relevant (p-value < 0.05) metabolite changes separating animal classes based on their diet. The chemical shifts shown correspond to the integrated peaks (Table S1 lists the full set of metabolites). N, normal chow; F, fructose-chow; G, glucose-chow. Values correspond to changes in the first named group, compared to the second named group e.g. aspartate is decreased in G, compared to N. ES: effect size. Ui: unassigned resonances. s: singlet, dd: doublet of doublets, t: triplet, m: multiplet. [a]Metabolite with p-value > 0.05 after false discovery rate correction based on Benjamini and Hochberg method; b this resonance is tentatively assigned to nicotinate.

		G vs N		**F vs N**		**F vs G**	
Metabolite	**δ/ppm (multiplicity)**	**ES**	**p-value**	**ES**	**p-value**	**ES**	**p-value**
Acetate	1.92 (s)	0.96±0.53	1.4E-6	1.12±0.54	1.2E-7	-	-
Aspartate	2.82 (dd)	-1.38±0.56	6.6E-8	-1.38±0.56	4.9E-7	-	-
Butyrate	0.90 (t)	-	-	-0.86±0.52	2.9E-3	-1.06±0.53	1.6E-4
Formate	8.46 (s)	0.69±0.52	6.6E-5	1.36±0.55	5. 3E-8	-	-
Fructose	4.04 (m)	-	-	1.07±0.53	7.2E-8	1.07±0.53	1.0E-6
Glucose	5.23 (d)	-	-	-	-	0.77±0.51	9.7E-3
Glutamate	2.15 (m)	-	-	-0.79±0.52	2.1E-3	-	-
Methanol	3.36 (s)	0.58±0.51	1.1E-4	0.80±0.52	1.1E-5	-	-
Lactate/ threonine	1.33 (d)	-	-	-	-	0.61±0.51	8.2E-3
Phenylalanine	7.34 (m), 7.38 (m)	-	-	0.80±0.52	3.7E-3	0.55±0.50	1.3E-2
Propionate	2.18 (q)	0.92±0.53	7.6E-4	-	-	-0.55±0.50	1.1E-2
Pyruvate	2.38 (s)	0.69±0.52	3.7E-2 [a]	0.74±0.52	1.2E-3	-	-
Succinate	2.41 (s)	-	-	1.40±0.56	6.6E-9	0.99±0.52	6.6E-6
Taurine	3.43 (t)	0.75±0.52	6.1E-5	1.70±0.58	4.2E-9	1.02±0.53	9.4E-5
Tyrosine	7.20 (d)	-	-	0.66±0.51	2.7E-2	0.69±0.51	5.8E-3
Uracil	7.58 (d)	-	-	-0.56±0.50	3.7E-3	-	-
Xylose	5.21 (d)	-	-	1.53±0.57	5.7E-10	0.78±0.51	1.1E-3
U1	8.03 (s), 8.39 (s)	-	-	-	-	-0.72±0.51	6.3E-3
U2 [b]	8.62 (s)	-1.21±0.55	4.7E-6	-1.11±0.54	5.6E-5	-	-

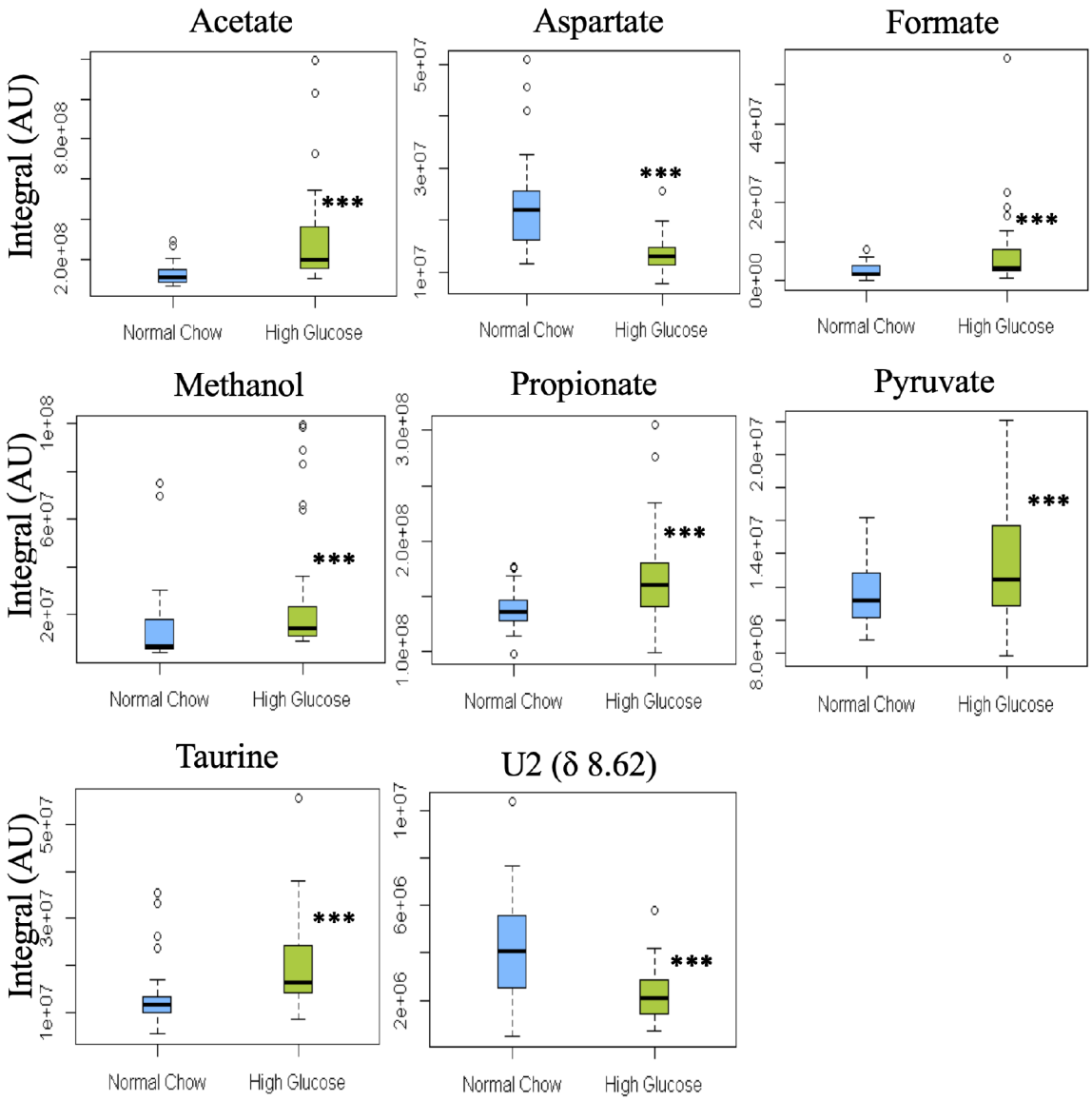

Figure B.6 – Boxplots of all statistically relevant (p-value < 0.05) metabolite changes between Normal Chow and High Glucose diets

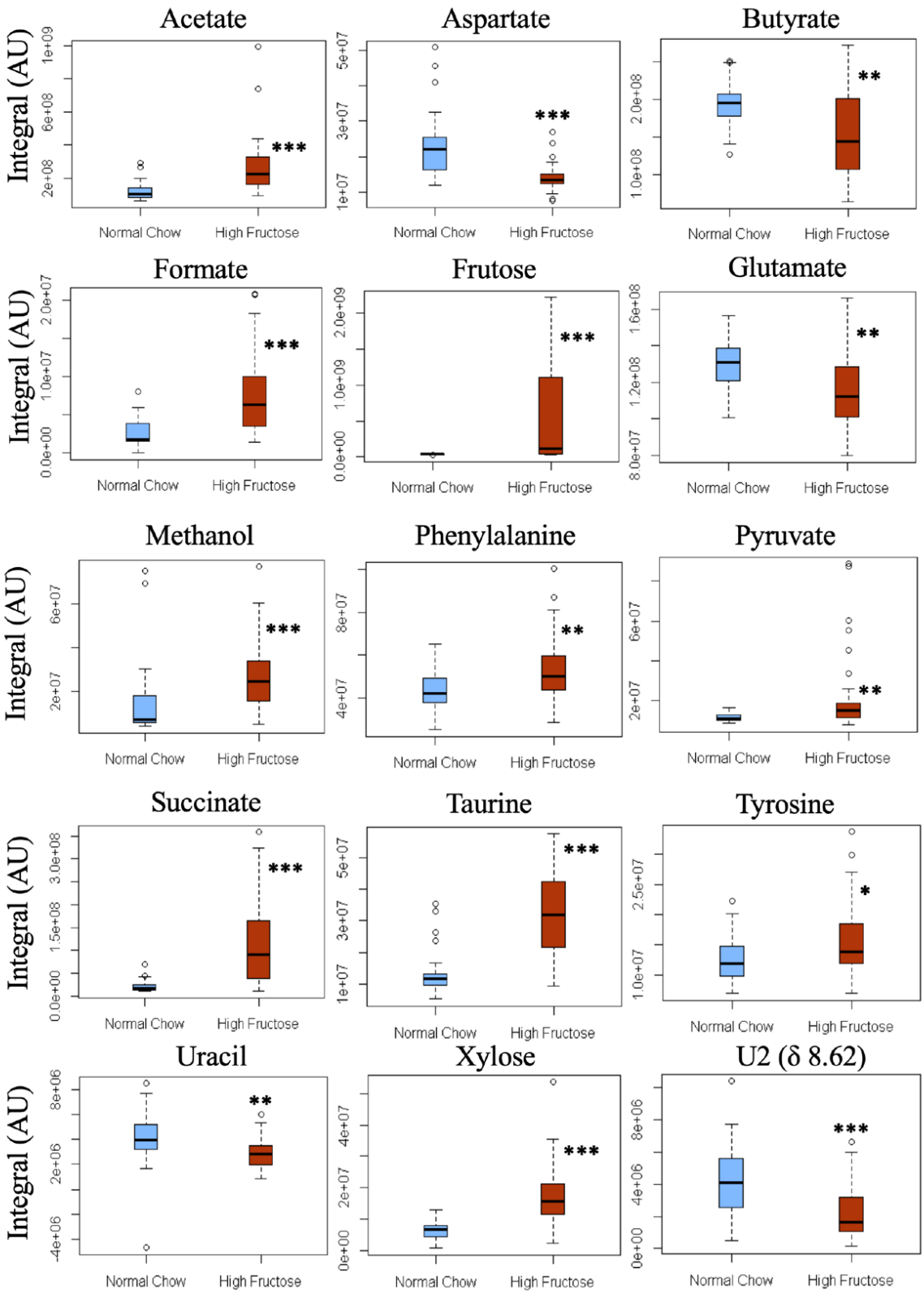

Figure B.7 – Boxplots of all statistically relevant (p-value < 0.05) metabolite changes between Normal Chow and High Fructose diets

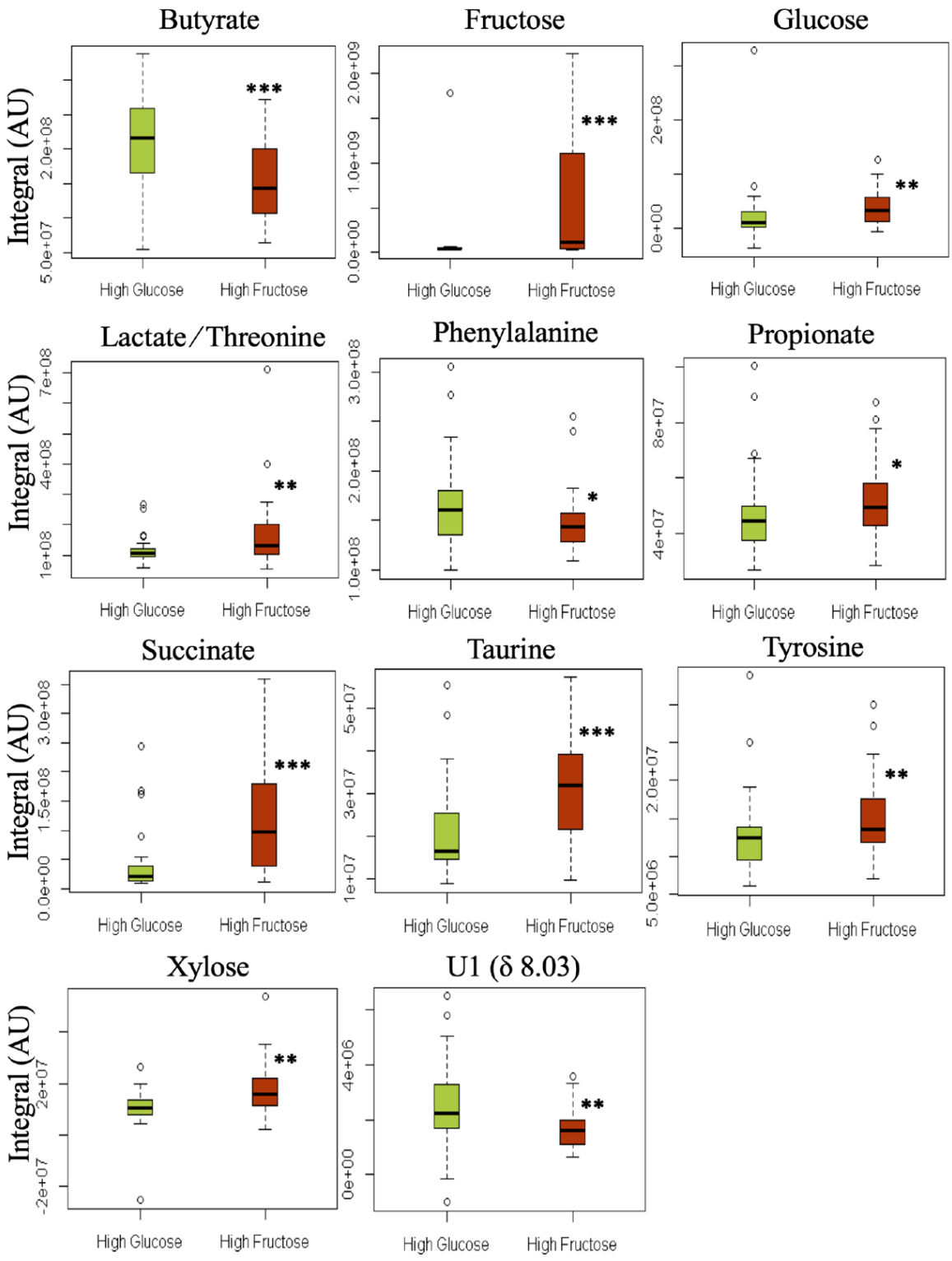

Figure B.8 - Boxplots of all statistically relevant (p-value < 0.05) metabolite changes between High Glucose and High Fructose diets

The average time trajectories of these differentiating metabolites for fructose-chow are shown in Figure B.9. Notably, butyrate levels were persistently lower (except for week 8) and propionate levels remained close to those of normal chow-fed mice (again with the exception of week 8). Fructose, succinate, phenylalanine, tyrosine and xylose all exhibited relatively higher levels in fructose-chow fed mice compared to mice fed with the other diets. As seen by the magnitude of the error bars, these metabolite levels showed high inter-animal variability, with the sole exception of fructose. Lactate overlaps with threonine and lactate/threonine levels increased at week 10, albeit with high variability. The unassigned spin system U1 exhibited consistently low levels in fructose-chow, compared to both normal- and glucose-chow groups, and therefore contributed to the metabolic signature of mice fed with fructose-chow. In addition, the interesting bidirectional behaviour of the animals fed with fructose-chow (Figure B.4 and Figure B.5) was further explored through PLS-DA of the deviant high-fructose samples (Figure B.10), revealing that separation of data points within the cohort fed with fructose-chow related to the extent of incomplete fructose absorption (expressed by high levels of fructose in fecal extracts). Correlation studies showed no correlation of fructose-chow sample composition to animal body weight.

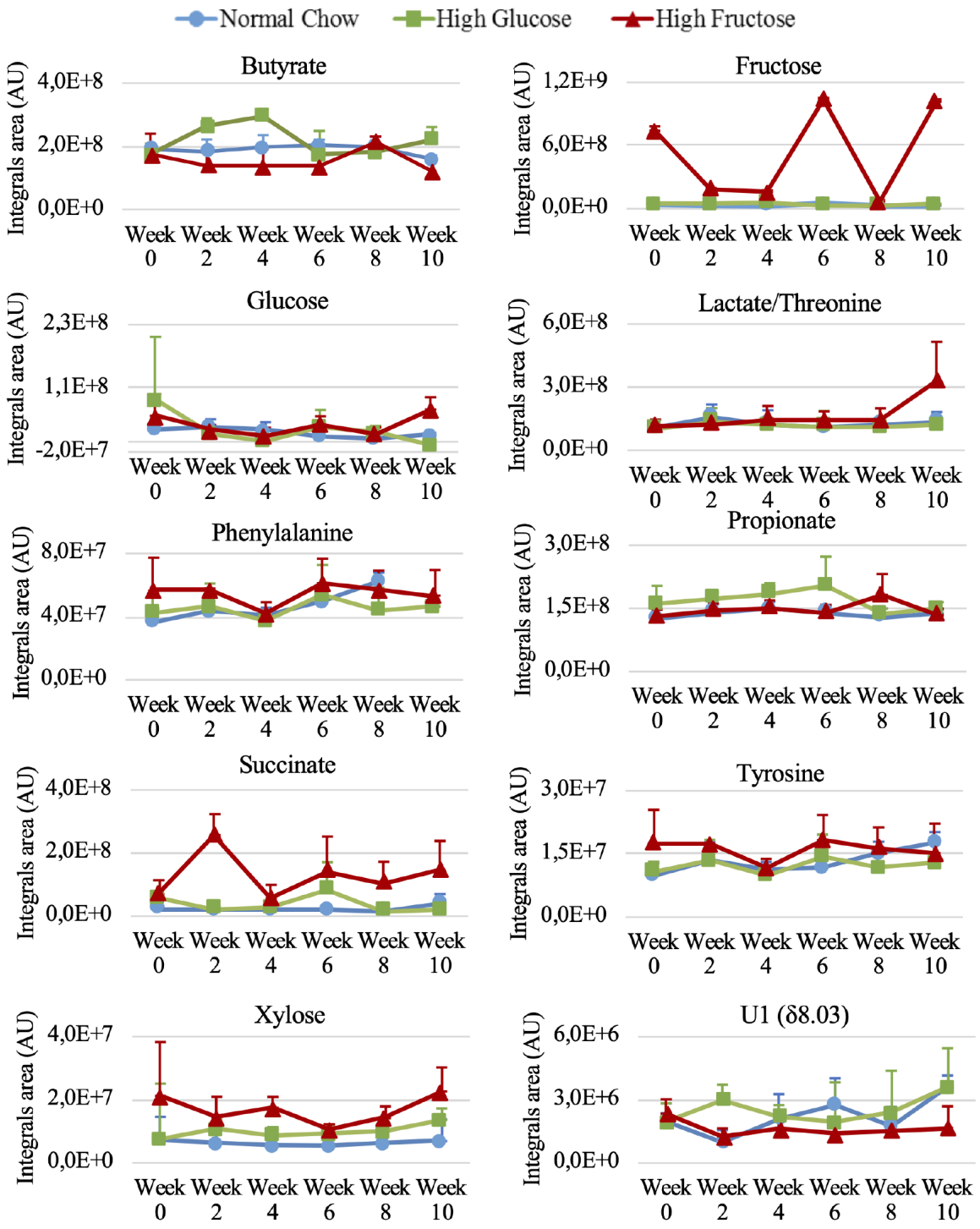

Figure B.9 – Time-course variations for main metabolites distinguishing animals fed with fructose-chow from those fed with normal chow or glucose-chow. These 12 metabolites have been selected from the data in Table 1. Normal chow: blue line, glucose-chow: green line, fructose chow: red line.

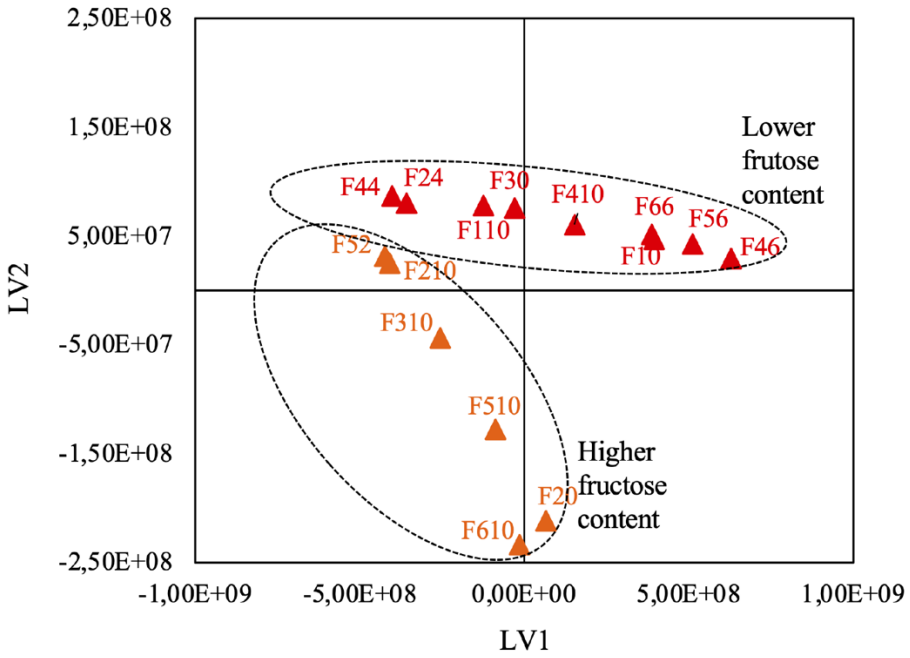

Figure B.10 - PLS-DA scores of the two subgroups of high-fructose fed animals

B.5.3 Fecal Microbial Profiles

Intestinal microbiota plays a significant role in dietary carbohydrate metabolism, in particular the fermentative breakdown of complex carbohydrates into simple absorbable metabolites such as short chain fatty acids (SCFA) [186]. Recent studies suggest that increased consumption of simple over complex carbohydrates promotes intestinal dysbiosis and wider metabolic disruption. Since dysbiosis is thought to be mediated in part by a shift in bacterial species distributions [187], we compared the effects of normal-chow, glucose-chow and fructose-chow feeding on the abundances of *Enterobacteria* and *Lactobacillus*, representing gram-negative and gram-positive bacterial groups, respectively. The total abundances of *Enterobacteria* and *Lactobacillus* showed high variability between individuals fed with the same diet, as shown in the supplemental data (Table B.3).

Table B.3 – Real-time qPCR quantification absolute values (copies/μg of DNA) of bacterial groups in animal faeces: intra and intervariability between animals.

	Week no.				
	2	4	6	8	10
Total Bacteria			Normal Chow		
	9,578E+12	2,013E+13	3,232E+12	9,017E+11	4,794E+10
	1,564E+13	9,107E+11	1,066E+13	5,386E+11	----------
	1,046E+12	5,561E+12	9,437E+11	1,201E+12	2,537E+10
	9,911E+11	----------	8,022E+11	5,726E+11	8,240E+10
	2,178E+13	4,592E+11	1,091E+12	1,411E+12	3,429E+10
	2,066E+13	3,345E+12	6,329E+11	5,379E+11	----------
			High Glucose		
	2,02E+12	1,862E+12	1,938E+12	----------	----------
	1,23E+12	2,032E+12	1,388E+12	5,429E+12	2,847E+10
	----------	1,130E+12	1,521E+12	4,414E+12	2,240E+10
	----------	6,671E+12	2,936E+12	2,655E+13	1,136E+10
	5,17E+12	9,965E+11	5,311E+11	----------	1,151E+10
	----------	1,432E+13	1,049E+13	5E+11	7,577E+10
			High Fructose		
	2,265E+12	1,438E+13	6,697E+11	1,966E+12	1,018E+10
	1,776E+12	5,571E+12	6,577E+11	1,494E+12	6,598E+09
	7,296E+11	1,327E+12	1,023E+12	1,729E+12	1,303E+10
	6,654E+11	1,696E+13	2,352E+13	9,208E+11	9,933E+09
	9,116E+12	7,614E+11	1,359E+13	2,320E+12	9,268E+09
	----------	6,654E+11	1,112E+12	7,707E+11	7,161E+09
% *Enterobacteria*			Normal Chow		
	2,121E-04	2,418E-04	7,250E-05	3,286E-03	2,323E-04
	6,572E-05	1,264E-01	9,670E-05	2,004E-04	----------
	4,479E-04	7,659E-04	8,015E-02	2,332E-04	6,861E-03
	1,426E-03	----------	4,373E-02	7,614E-03	5,133E-01
	1,474E-04	4,146E-02	7,069E-03	3,717E-03	2,165E-02
	1,448E-04	4,994E-04	9,021E-03	9,285E-03	----------
			High Glucose		
	2,300E-04	1,592E-02	2,667E-02	----------	----------
	6,193E-03	6,805E-04	3,813E-05	6,220E-03	2,358E-03
	----------	2,509E-04	7,515E-03	5,095E-04	6,226E-04
	----------	1,714E-04	1,128E-03	1,248E-04	1,893E-01
	5,906E-03	1,928E-02	8,743E-04	----------	3,044E-02
	----------	3,860E-04	6,588E-06	2,571E-01	1,481E-02
	----------	----------	----------	----------	----------
			High Fructose		
	6,555E-04	3,568E-04	6,524E-02	3,009E-03	1,741E-01
	3,072E-02	1,487E-04	7,537E-01	1,125E-03	1,844E-02
	5,624E-05	3,509E-03	2,682E-02	4,017E-03	1,287E-01
	3,645E-03	1,533E-05	1,024E-04	2,613E-03	4,126E-02
	1,913E-04	5,059E-03	1,878E-04	2,239E-04	9,725E-02
	----------	6,919E-03	1,437E-02	5,731E-03	1,168E-01
% *Lactobacillus*			Normal Chow		
	3,153E-03	1,484E-03	1,256E-01	1,628E-01	2,771E-02
	7,965E-03	2,789E-02	2,256E-02	2,512E-01	----------
	4,826E-02	1,300E-02	2,084E-01	1,015E-01	5,432E-02
	6,226E-01	----------	2,272E-01	8,595E-01	1,331E-03
	2,191E-02	1,729E-02	2,935E-01	4,321E-01	5,783E-03
	5,255E-02	5,411E-02	5,616E-01	1,087E-01	----------
			High Glucose		
	2,199E-02	1,102E-01	2,601E-02	----------	----------
	4,704E-01	1,153E+00	2,367E-02	2,761E-02	1,825E-02
	----------	3,171E-01	9,000E-02	9,793E-02	1,471E-02
	----------	1,046E-01	9,720E-03	6,342E-03	3,156E-02
	4,131E-01	5,453E+00	1,084E-01	----------	6,181E-02
	----------	2,388E-02	6,237E-05	6,565E-02	1,191E-01
			High Fructose		
	3,939E-03	1,770E-03	1,713E-01	5,976E-02	4,785E-01
	8,149E-02	6,061E-03	1,549E-02	7,070E-02	2,940E-02
	4,509E-01	2,862E-03	1,401E-02	1,986E-02	1,328E-01
	7,745E-02	1,614E-03	1,318E-02	8,862E-01	2,406E-01
	3,997E-03	1,485E-01	1,294E-02	9,392E-03	5,190E-01
	----------	2,673E-02	7,729E-02	1,309E-01	1,646E-01

To get a measure of the relative abundances of these bacteria classes, ratios of *Enterobacteria* to total and *Lactobacillus* to total were calculated (Table B.4). While the proportion of *Enterobacteria* generally increased over the 10-week period for all three diets, the rate of increase was slower for glucose- and fructose-chow compared to standard chow (Table B.4). The proportion of *Lactobacillus* showed a general decrease in mice fed with normal chow or glucose-chow over the 10-week interval. However, for mice fed with fructose-chow, the proportion of *Lactobacillus* increased over the same period (Table B.4). Given that the *Lactobacillus* genre encompasses fructophilic bacteria, and that our NMR data showed a carry-over of dietary fructose into feces, these results could reflect an intestinal substrate profile that promotes the growth of *Lactobacillus* over other species under conditions of high fructose feeding.

Table B.4 – Values of the variation of Enterobacteria and Lactobacillus bacteria, given as the count ratio of each bacteria type over total bacteria in feces, as a function of time, every two weeks, for 10 weeks. High biological variability is evident and can be further observed in Table B.3 for inter and intra-animal diversity.

			Week		
	2	**4**	**6**	**8**	**10**
% *Enterobacteria*			***Normal-chow***		
	4,07E-04 ± 5,16E-04	3,39E-02 ± 5,47E-02	2,34E-02 ± 3,22E-02	4,06E-03 ± 3,75E-03	1,35E-01 ± 2,52E-01
			Glucose-chow		
	4,11E-03 ± 3,36E-03	6,11E-03 ± 8,96E-03	6,04E-03 ± 1,05E-02	6,6E-02 ± 1,27E-01	4,75E-02 ± 8,02E-02
			Fructose-chow		
	7,05E-03 ± 1,33E-02	2,67E-03 ± 2,94E-03	1,43E-01 ± 3E-01	2,79E-03 ± 1,98E-03	9,61E-02 ± 5,77E-02
% *Lactobacillus*			***Normal-chow***		
	1,26E-01 ± 2,44E-01	2,28E-02 ± 1,99E-02	2,4E-01 ± 1,85E-01	3,19E-01 ± 2,92E-01	2,23E-02 ± 2,43E-02
			Glucose-chow		
	3,02E-01 ± 2,44E-01	1,19 ± 2,13	4,3E-02 ± 4,5E-02	4,94E-02 ± 4,06E-02	4,91E-02 ± 4,33E-02
			Fructose-chow		
	1,24E-01 ± 1,87E-01	3,13E-02 ± 5,82E-02	5,07E-02 ± 6,43E-02	1,96E-01 ± 3,41E-01	2,61E-01 ± 1,97E-01

B.6 Discussion

B.6.1 Replacement of normal chow carbohydrate with pure glucose or fructose for 10 weeks did not result in increased body weight or glucose intolerance

Our study showed that for C57BL/6 mice, substitution of normal chow carbohydrate constituents with pure glucose, over a period of 10 weeks, did not significantly alter overall weight gain, and were in fact gaining significantly less weight up until the sixth week of the study. Mice that received fructose-chow had noticeably slower weight gain compared to both glucose-chow and normal-chow groups, although converging at the end of the study period. These observations are consistent with those of Mellor et al., who found that either weaned or adult mice fed for 6 weeks with fructose-chow (of a similar composition as that used here) showed 11% and 18% less weight gain, respectively, compared to controls fed with standard chow [188]. We also did not see any significant differences in glucose tolerance between the three groups. In the study of Nunes et al. where mice were fed for 8 weeks with glucose- and fructose-chow formulations identical to those used in our study, no differences in glucose tolerance and insulin sensitivity were observed, while weight gain was significantly less for mice fed with fructose-chow [189]. Hence, in our study, the fecal metabolite and microbiota distributions observed for the three diets are not related to glucose tolerance status, although they may in part reflect the transitory slower weight gain of animals fed with the high-fructose diet.

B.6.2 Effects of fructose- and glucose-chow on fecal extract metabolite profiles

The intestinal microbiome is associated with a complex array of intra- and extracellular metabolites. Some of these are end-products of nutrient breakdown that are cleared into the surrounding medium, for example SCFA and lactate, while others represent intracellular metabolic pathway intermediates. Since feces contain a very high density of bacteria, the fraction of the total metabolite recovery contributed by intracellular sources is likely to be considerable, given that intracellular concentrations of certain metabolites such as glutamate and taurine can reach millimolar levels. Moreover, metabolic products of one bacterium species may be utilized for energy and/or converted to new metabolites by another species. Thus, the effects of different diets on the profile of metabolites that are predominantly intracellular, such as taurine, glutamate and aromatic amino acids, involve complex metabolic interactions both within and between different bacterial species. We will focus on those metabolites that are considered to have a significant influence on the host metabolic health.

Alterations in SCFA production, namely acetate, propionate and butyrate, *via* microbial fermentation are recognised as key links between intestinal microbiota activity and risks for metabolic diseases such as Type 2 diabetes and NAFLD [34, 187]. Butyrate is a preferred oxidative substrate for enterocyte (and specifically colonocytes) energy generation, and it also shows tumour suppression and anti-inflammatory effects [190, 191]. Our results indicate that mice fed with fructose-chow had lower levels of fecal butyrate compared to those fed glucose- or normal chow. If this was a limiting factor in enterocyte energy generation, it could compromise energy-intensive enterocyte functions such as tight-junction maintenance thereby increasing intestinal permeability

and leakage of pro-inflammatory endotoxin into portal vein blood, which provokes hepatic inflammation [163, 164]. Such a mechanism might contribute to the so-called "second hit"; a cellular insult that when superimposed on high lipid levels transforms benign NAFLD into more severe forms such as non-alcoholic steatohepatitis (NASH). Other animal studies have demonstrated a link between dietary fructose supplementation, increased intestinal permeability, and augmented NAFLD severity. In a study of C57BL/6 mice fed with either normal chow or a Western-style diet high in fat and sugar, the addition of fructose to the drinking water increased endotoxin translocation for both diets [159]. In normal-chow-fed mice that were supplemented with 30% fructose in drinking water, elevated hepatic lipid and plasma transaminase levels were associated with impaired intestinal barrier function and increased concentrations of portal plasma endotoxin [192]. Since these studies did not examine the effects of fructose supplementation on fecal SCFA levels, a direct link between the detrimental effects of high fructose feeding on intestinal integrity and a decreased abundance of fecal butyrate remains to be established. Interestingly, certain *Lactobacilli* counteract the inhibition of enterocyte butyrate uptake by enteropathogenic *E. coli* [193]. Thus, the increased abundance of *Lactobacilli* over *Enterobacteria* that we observed in fructose-chow fed mice over glucose- and normal-chow fed animals could mitigate the lower abundance of butyrate.

Acetate, which accounts for the majority (60-80%) of intestinal SCFA production, was elevated in mice fed with both glucose- and fructose-chow compared to normal-chow fed animals, while propionate levels were not different between fructose-chow and normal-chow fed animals but were significantly higher in the glucose-chow fed group. Whether increased intestinal acetate production is beneficial or detrimental remains

unclear. On the one hand it is an agonist of the intestinal GPR43/FFAR2 receptor that, among other effects, promotes intestinal secretion of incretins such as GLP-1, thereby contributing to better postprandial glycemic control [194]. On the other hand, in a cross-sectional study of lean and obese youths, elevated plasma acetate levels (as well as butyrate and propionate) and enhanced fermentation of fructose by fecal microbe cultures were found to be associated with increased body mass index, adiposity and *de novo* lipogenesis rates [195]. Fecal levels of propionate, the only gluconeogenic SCFA of the three and accounting for 10-15% of SCFA production, were similar between fructose- and normal-chow fed mice but were significantly elevated in glucose-chow fed mice. As for acetate, the effects of altered intestinal propionate levels on metabolic dysfunctions associated with obesity and ectopic lipid accumulation are also unclear. Increased levels of circulating propionate has been associated with obesity and steatosis [195], while other reports claim that increased intestinal propionate levels hasten the postprandial satiety response thereby protecting against obesity [196].

The elevated levels of fecal aromatic amino acids in mice fed fructose-chow compared to either glucose- or normal-chow fed mice may have also important implications on intestinal integrity and immune status. Both tyrosine and phenylalanine can be metabolized by bacteria to aryl propionates via the dehydration of phenyllactic acid, mediated by phenyllactate dehydratase (PLD) [197]. Tryptophan is also degraded by this pathway to form 3-indole-propionate, a potent antioxidant that also preserves intestinal barrier function. The higher levels of tyrosine and phenylalanine observed during fructose feeding may indicate a reduced PLD capacity, which would also result in less 3-indole propionate production from tryptophan and therefore less protection of intestinal barrier function. The higher dietary amounts of phenylalanine and tyrosine

(1.07% and 0.74%, respectively), over tryptophan (0.27%) could explain their higher visibility in the ^{1}H NMR spectrum.

B.6.3 Incomplete intestinal fructose absorption

In mice provided with fructose-chow, there were significant amounts of unabsorbed fructose in the feces indicating insufficient intestinal capacity for its absorption. There were no significant levels of hexose in the feces of either glucose-chow or normal-chow fed mice. Intestinal fructose absorption is largely mediated by the constitutive GLUT-5 transporter [133], whose expression is upregulated by high-fructose feeding [148]. Despite this, it appears that at least in humans, the intestinal capacity for fructose uptake is overwhelmed by high fructose intake resulting in malabsorption and discomfort from microbial fructose fermentation [198, 199]. While defective fructose absorption has been previously documented in GLUT5-knockout mice [133], to our knowledge our study is the first to report incomplete fructose absorption in wild-type mice. Given that fructose absorption is facilitated by the presence of dietary glucose [186], the absence of glucose in the high-fructose chow may have potentiated its incomplete absorption by mice that were fed on this diet.

B.6.4 Different Taurine fecal levels among diets

Fecal levels of taurine also showed significant differences between the diet groups, with the highest levels observed for fructose-chow fed mice. Taurine has a wide range of cytoprotective actions and inhibits the development of diet-related diseases such as diabetes and NAFLD [200, 201]. All three diets were formulated with the same AIN-93G

background, which does not contain taurine [202]. Therefore, intestinal taurine must have originated from endogenous sources. Under these conditions, the principal mechanism for taurine appearance in the intestine is secretion of taurine-conjugated bile acids from the gall bladder followed by microbial deconjugation and release of taurine. Re-absorption of this released taurine is low since taurine transporters are mostly located upstream in the small intestine. Lactobacillus species are effective at deconjugating bile acids, particularly those conjugated to taurine [203]. These species were more abundant in fructose-chow compared to glucose- and normal-chow groups. Moreover, bile acid deconjugation by Lactobacillus can be further stimulated by high glycolytic activity [204]. Since fructose can be efficiently utilized as a glycolytic substrate by these species [205] the presence of unabsorbed fructose in the lower intestine may further promote bile acid deconjugation and taurine release. Increased deconjugation of bile acids has several potentially adverse outcomes. Firstly, it promotes the elimination of taurine thereby depleting endogenous taurine pools. Among other things, this may reduce protection against complications of diabetes and NAFLD. Secondly, increased levels of hydrophobic unconjugated bile acids and/or their secondary products may directly compromise intestinal barrier function [206] or modify whole-body cholesterol and fatty acid homeostasis through altering bile acid signalling via farnesoid X receptors in the liver [207].

B.6.5 Variability in microbial and metabolite profiles

Our study revealed substantial variability in both faecal metabolite and microbial profiles between different animals fed with the same diet, as well as for individual

animals across the 10-week feeding interval. Such variability has been observed in rodent studies [208] and, in a study of repeated fecal sampling of humans, the intra-individual coefficient of variation was over 40% [209]. Our results highlight the importance of multiple feces sampling per individual, during a feeding trial or interval, to obtain representative levels of fecal metabolites and microbial populations.

B.7 Conclusions

In Western societies, increased intake of refined sugar, consisting of roughly equimolar amounts of glucose and fructose, is implicated in the surge of Type 2 Diabetes and NAFLD incidences. While glucose and fructose are isocaloric, they are metabolized quite differently by the tissues and organs of the body. Our study indicates that the intake of these sugars also results in different profiles of intestinal microbiota and their associated metabolites. The intestinal metabolite profile associated with fructose feeding seems to have more potential for inducing host metabolic disturbances compared to that of glucose, mainly through compromising intestinal barrier integrity. When taken in high amounts, intestinal fructose absorption is not quantitative hence its availability as a substrate for microbial metabolism is increased. It remains to be determined whether this characteristic explains the differences in intestinal microbiota and metabolite profiles between fructose and glucose. Our results show that in tandem metabolomics and microbial characterisation of animal fecal extracts are a particularly valuable strategy to study the role of sugar intake in relation to diabetes or fatty liver disease.

Chapter C

Determining Contributions of Exogenous Glucose and Fructose to de novo Fatty Acid and Glycerol Synthesis in Liver and Adipose Tissue

(Published [210])

C.1 Abstract

The *de novo* synthesis of triglyceride (TG) fatty acids (FA) and glycerol can be measured with stable isotope tracers. However, these methods typically do not inform the contribution of a given substrate to specific pathways on these synthetic processes. We integrated deuterated water ($^{2}H_2O$) measurement of *de novo* lipogenesis (DNL) and glycerol-3-phosphate (GLY) synthesis from all substrates with a ^{13}C nuclear magnetic resonance (NMR) method that quantifies TG FA and glycerol enrichment from a specific [U-^{13}C]precursor. This allowed the [U-^{13}C]precursor contribution to DNL and GLY to be estimated. We applied this method in mice to determine the contributions of fructose and glucose supplemented in the drinking water to DNL and GLY in liver, mesenteric adipose tissue (MAT) and subcutaneous adipose tissue (SCAT). In liver, fructose contributed significantly more to DNL of saturated fatty acids (SFA) and oleate as well as to GLY compared to glucose. Moreover, its contribution to SFA synthesis was significantly higher compared to that of oleate. MAT and SCAT had lower fractional rates

of total DNL and GLY compared to liver and glucose was utilized more predominantly than fructose for TG synthesis in these tissues. This novel $^{2}H_2O/^{13}C$ integrated method revealed for the first time, tissue specific selection of substrates for DNL, particularly fructose in regard to glucose in liver. Also, was able to discriminate the distribution of specific FAs into the TG *sn*2 and 1,3 sites.

This stable isotope integrated approach yielded information so far uncovered by other lipidomic tools and should powerfully assist in other nutritional, pathological or environmental contexts.

C.2 Keywords

Lipogenesis, deuterated water, fructose, NAFLD

C.3 Introduction

The increased consumption of glucose and fructose, either as sucrose or in the form of high-fructose corn syrup, is implicated in the surge of non-alcoholic fatty liver disease (NAFLD) and systemic dyslipidemia [211-213]. These sugars promote the accumulation of triglycerides (TG) by several interconnected mechanisms that include the activation of factors such as ChREBP and PGC-1β that induce the transcription of metabolic pathway enzymes and cofactors for the transformation of sugar to fat [152, 214], allosteric inhibition of fatty acid (FA) oxidation via metabolites such as malonyl-CoA [215], and increased availability of acetyl-CoA and triose phosphate (Triose-P) precursors for FA formation via *de novo* lipogenesis (DNL) and glycerol-3-phosphate (GLY) biosynthesis.

Although glucose and fructose are ingested in approximately equal quantities*, fructose is considered to be the more potent lipogenic substrate, particularly for the liver. However, to our knowledge, the contributions of exogenous glucose and fructose to the acetyl-CoA precursor pool of DNL and to GLY synthesis have not been directly measured in either humans or animal models.

In this report, we demonstrate that in mice provided with a mix of glucose and fructose where one or the other sugar was uniformly enriched with ^{13}C, the contribution of the ^{13}C-enriched sugar to DNL and GLY synthesis can be estimated from ^{13}C NMR analysis of hepatic TG ^{13}C-isotopomers. To account for dilution of the newly-synthesized FA ^{13}C-isotopomers by pre-existing unlabeled TG†, deuterated water (^2H_2O) was administered alongside the [U-^{13}C]sugars (Figure C.1). The positional ^2H-enrichment and ^{13}C-isotopomer distributions of TG can be resolved and quantified by sequential ^2H and ^{13}C nuclear magnetic resonance (NMR) spectroscopy which constitutes an innovative integration method developed during this study. Moreover, the ^{13}C NMR spectrum of TG yields a wealth of information on the identity and position of individual FAs [216-219]. In our experimental setting, this allowed the contribution of the ^{13}C-enriched sugar to the synthesis of specific FAs or FA classes to be resolved while at the same time providing a detailed compositional analysis of the TG sample.

* Even with high fructose corn syrup, the proportion of fructose to glucose is typically 55/45.

† This is typically unavoidable due to the relatively slow turnover rates of TG pools.

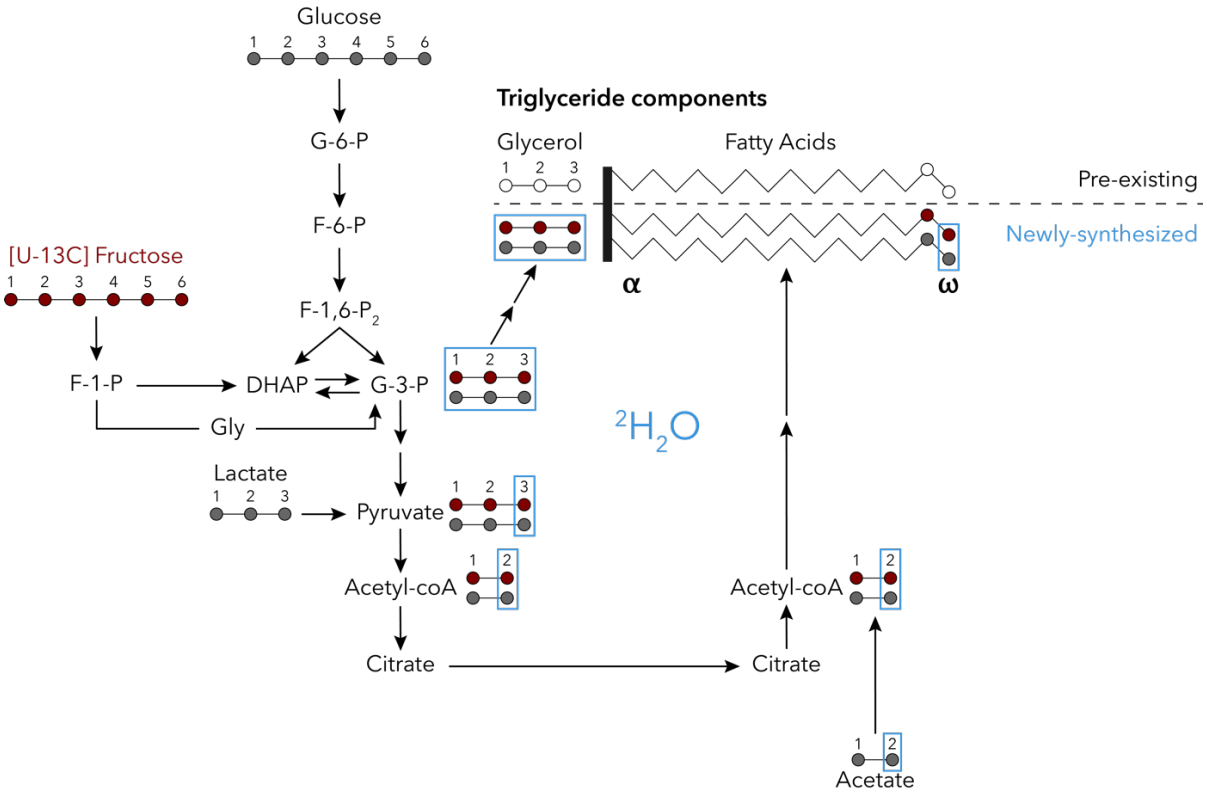

Figure C.1 - Integration of $^{2}H_2O$ and [U-^{13}C]fructose tracers to quantify the contribution of exogenous fructose as part of a glucose/fructose mixture to *de novo* synthesis of TG FA and glycerol moieties - The [U-^{13}C]fructose carbon skeleton and selected metabolic intermediates are represented as red filled circles while the carbon skeletons of unlabeled glucose and other endogenous metabolites (lactate and microbially-generated acetate) are represented by light gray circles. Pre-existing FA and glycerol carbons are represented by unfilled circles. ^{2}H-enrichment of triose-P and glycerol hydrogens, the methyl hydrogens of pyruvate, acetate, acetyl-CoA, and the terminal (**ω**) hydrogens of TG fatty acyls, are represented by blue boxes. Note that the combination of unlabeled fructose and [U-^{13}C]glucose generates the same set of triose-P and FA ^{13}C-isotopomers. Some metabolic intermediates were omitted for clarity.

C.4 Materials & Methods

C.4.1 Materials

Unless otherwise specified, non-deuterated chloroform ($CHCl_3$) used to prepare TG extracts for $^{1}H/^{2}H$ NMR spectroscopy had a purity of 99.8% and contained 100-200 ppm

amylenes as stabilizers (Sigma-Aldrich). 99% enriched [U-^{13}C]glucose and [U-^{13}C]fructose and 99.9% enriched $^{2}H_2O$ were manufactured by Cambridge Isotopes Limited, Cambridge, MA, USA and purchased though Tracertec, Madrid, Spain.

C.4.2 Animal studies

Forty 12-week-old C57BL/6 mice were used in this study (20 male and 20 female). Animals were fed with standard chow and maintained in a 12-hour light cycle as well as controlled humidity, ventilated air and temperature at the CEDOC-NOVA Medical School bioterium. At the beginning of the dark period, animals were injected intraperitoneally with 99.9% enriched $^{2}H_2O$ containing 0.9% NaCl (4 mL/100 g body weight). The drinking water was supplemented with 5% of $^{2}H_2O$ and glucose and fructose were added (17.5 g of each sugar to 100g water). For 10 of the male and 10 of the female mice, the glucose portion was enriched to 50% with [U-^{13}C]glucose. For the remaining 10 male and 10 females, the fructose portion was enriched to 20% with [U-^{13}C]fructose. Animals were allowed to feed and drink *ad libitum* during the entire 12-hour dark period and were euthanized by cervical dislocation the following morning. Livers and adipose tissue depots were freeze-clamped and stored at -80°C until further processing for TG extraction and purification. Urine was also collected overnight for analysis of body water ^{2}H-enrichment.

C.4.3 Liver TG extraction and purification

Liver TGs were extracted and purified as previously described [220, 221]. Briefly, livers were powdered under liquid nitrogen and then rapidly mixed with HPLC-grade

methanol (4.6 mL/g) followed by methyl-tert-butyl ether (MTBE) (15.4 mL/g). The mixture was placed in a shaker for 1 hour at room temperature then centrifuged at 13,000x *g* for 10 min. The liquid fraction was collected, and phase separation was induced by adding 4 mL of distilled water to the liquid fraction and letting it rest at room temperature for 10 min. The liquid was then centrifuged for 10 min. at 1,000x *g*. The upper organic phase containing the lipids was carefully separated and dried under nitrogen gas in an amber glass vial. TGs from the dried organic fraction were purified with a solid phase extraction (SPE) process. Discovery DSC-Si SPE cartridges (2g/12 mL) were washed with 8 mL of hexane/MTBE (96/4; v/v) followed by 24 mL of hexane. The dried lipids were re-suspended in 800 µL of hexane/MTBE (200/3; v/v) and loaded into the column after washing. The lipid vials were washed with a further 500 µL of solvent to quantitatively transfer the lipids to the column. TGs were eluted with 32 mL of hexane/MTBE (96/4; v/v), collected in 4 mL fractions. Fractions containing TGs were identified by thin-layer chromatography [222]. A few microliters of the eluted fractions were spotted on the TLC plate alongside TG standards and the plate was developed with petroleum ether/diethyl ether/acetic acid (7.0/1.0/0.1; v/v/v). After drying, lipid spots were visualized under iodine vapor. The TG-containing fractions were pooled and dried under nitrogen gas and stored at –20°C until NMR analysis. For analysis of adipose tissue TGs, 40-60 mg of frozen adipose tissue portions were placed for a few minutes in a 1 mL glass vial containing ~0.5 mL $CHCl_3$ and gently shaken. The supernatant was pipetted away from the solid tissue and prepared for NMR analysis without any further purification.

C.4.4 NMR Analysis

Purified TGs were dissolved in ~0.4 mL $CHCl_3$. To these, as well as to the adipose tissue $CHCl_3$ fractions, 25 μL of a pyrazine standard enriched to 1% with pyrazine-d_4 and dissolved in $CHCl_3$ (0.07g pyrazine/g $CHCl_3$) and 50 μL C_6F_6 were added. ^1H and ^2H NMR spectra were acquired with an 11.7 T Bruker Avance III HD system using a dedicated 5 mm ^2H-probe with ^{19}F lock and ^1H-decoupling coil as previously described [220]. ^1H spectra at 500.1 MHz were acquired with a 90-degree pulse, 10 kHz spectral width, 3 s of acquisition time and 5 s of pulse delay. Sixteen free-induction decays (fid) were collected for each spectrum. ^2H NMR spectra at 76.7 MHz were obtained with a 90-degree pulse, a 1230 Hz spectral width, an acquisition time of 0.37 s and a pulse delay of 0.1 s. Approximately 20,000 fid were acquired for each spectrum. Correction factors for partially-saturated ^2H signals were obtained from a set of seven samples where for each sample, a spectrum was acquired with the described parameters and immediately followed by a spectrum acquired under the same parameters with the exception of the acquisition time and pulse delay, which were set to 1 s and 8 s, respectively. For analysis of body water ^2H-enrichment, 10 μL of urine were mixed with 1 mL acetone and ~0.5 mL were loaded in a 5 mm NMR tube to which 50 μL C_6F_6 were added. ^2H NMR spectra of these samples were acquired with a 23° pulse angle, 922 Hz spectral width, 4 s acquisition time and 8 s pulse delay [223]. Sixteen fid were collected for each spectrum and water ^2H-enrichment was estimated from a calibration curve calculated from ^2H-enriched water standards [223].

For ^{13}C isotopomer analysis by ^{13}C NMR, dried TG samples were dissolved in 0.2 mL 99.96% enriched $CDCl_3$ (Sigma-Aldrich) and placed in 3 mm NMR tubes. ^{13}C NMR spectra were acquired at 150.8 MHz with an Agilent V600 spectrometer equipped with

a 3 mm broadband probe. Spectra were acquired with a 70° pulse, an acquisition time of 2.5 s, and a 0.5 s pulse delay. Between 4,000-12,000 fid were collected for each spectrum.

C.4.5 ^{13}C-Chemical shift assignments and quantification of FAs abundance

The ^{13}C chemical shifts of FA carbons are sensitive to their overall concentration in the NMR sample [224]. Therefore, ^{13}C-chemical shifts of individual FAs were verified with a mixture of five TG standards whose FAs collectively compromise 90-95% of TG FAs in mouse hepatic and adipose tissue [225, 226]. The mixture was based on the reported composition of TG FAs in mouse and human adipose tissues [226, 227] and consisted of glyceryl tripalmitate (16:0) (21 mol%), trioleate (18:1) (52 mol%), tristearate (18:0) (4 mol%), tripalmitoleate (16:1) (4 mol%) and trilinoleate (18:2) (19 mol%). The relative abundance of TG FAs was determined from the relative areas of their ω-2 ^{13}C signals. No corrections were made for differential longitudinal relaxation times or nuclear Overhauser effects.

C.4.6 Quantification of TG positional 2H-enrichments and estimates of FA and glycerol fractional synthetic rates

TG positional ^{2}H-enrichments in the glycerol and FA moieties were quantified by analysis of ^{1}H and ^{2}H NMR TG spectra as previously described [220, 228]. Fractional synthetic rates for the TG glycerol ($\mathbf{FSR_{Gly}}$) and FA moieties ($\mathbf{FSR_{FA}}$) over the overnight feeding period when $^{2}H_2O$ was administered were estimated from the ^{2}H-enrichments of

the 1,3-glycerol and FA ω-1 hydrogens and those of body water as previously described [220, 228].

C.4.7 Quantification of TG 13C-enrichment from [U-13C]glucose and [U-13C]fructose in the drinking water and the contribution of each sugar to TG glycerol and FA synthesis:

From the ω-1 singlet and doublet ^{13}C NMR signals, which are a composite of all saturated fatty acids (SFA) and monounsaturated fatty acids (MUFA) species, the weighted mean excess ^{13}C-enrichment of all SFA + MUFA species in the ω-1 position from [1,2-$^{13}C_2$]acetyl-CoA was calculated as follows:

$$\text{Weighted mean excess } ^{13}\text{C-enrichment of SFA + MUFA (\%)} = \boldsymbol{\omega\text{-}1\ D}/\boldsymbol{\omega\text{-}1\ S} \times 1.11 \quad (1)$$

Where **ω-1 D** and **ω-1 S** are the doublet and singlet components, respectively, of the ω-1 ^{13}C-resonance and 1.11 represents the background ^{13}C-enrichment (%).

Enrichments of individual FAs (oleate and palmitoleate) as well as that of SFA were estimated from their resolved ω-2 ^{13}C-resonances as follows:

$$\text{Excess } ^{13}\text{C-enrichment of FA } x\ (\%) = \boldsymbol{\omega\text{-}2\ D}_x/\boldsymbol{\omega\text{-}2\ S}_x \times 1.11 \quad (2)$$

Where $\boldsymbol{\omega\text{-}2\ D}_x$ and $\boldsymbol{\omega\text{-}2\ S}_x$ are the ω-2 doublet and singlet components of fatty acyl ***x***, and 1.11 represents the background ^{13}C-enrichment (%).

Enrichment of the glycerol moiety from ^{13}C-enriched Triose-P precursors was estimated as follows:

$$\text{Glycerol } ^{13}\text{C-enrichment (\%)} = \mathbf{GL^{13}C\text{-}Doublet}/\mathbf{GL^{13}C\text{-}Singlet} \times 1.11 \quad (3)$$

Where **$GL^{13}C$-Doublet** is the glycerol carbon 1 and carbon 3 (C1,C3) doublet signal originating from [U-^{13}C]Triose-P + [2,3-$^{13}C_2$]- or [1,2-$^{13}C_2$]Triose-P‡ incorporation into glycerol and **$GL^{13}C$-Singlet** is the singlet signal representing the 1.11% background ^{13}C-enrichment of C1,C3.

The fractional contribution of glucose or fructose in the drinking water to the TG FA and glycerol moieties was calculated as follows:

$$\text{Sugar contribution to FA (\%)} = \mathbf{^{13}C\text{-}FA}\ /\mathbf{^{13}C\text{-}Sugar} \times 100 \quad (4)$$

Where **^{13}C-FA** is the ^{13}C-excess enrichment of the ω-1, ω-2 FA moiety given by Equations 1 and 2, and **^{13}C-Sugar** is the enrichment of glucose or fructose in the drinking water.

$$\text{Sugar contribution to glycerol (\%)} = \mathbf{^{13}C\text{-}Glycerol}/\mathbf{^{13}C\text{-}Sugar} \times 100 \quad (5)$$

Where **^{13}C-Glycerol** is the enrichment of the glycerol moiety given by Equation (3) and **^{13}C-Sugar** is the enrichment of glucose or fructose in the drinking water.

‡ Triose-P isotopomers with 13C in carbons 1 and 2 and/or carbons 2 and 3 are generated by pentose pathway activity and/or carbon cycling between triose-P and the Krebs cycle. They have a minor contribution (10-15%) to the total Triose-P isotopomer population.

The contributions of glucose or fructose in the drinking water to newly-synthesized glyceryl and fatty acyl TG moieties (i.e. formed during the period when [U-^{13}C]glucose or fructose and $^{2}H_2O$ tracers were administered) were estimated as follows:

Sugar contribution to new glyceryl (%) = **^{13}C-Glyceryl**/**^{13}C-Sugar** × 100/**FSR_{Gly}** ×100% (6)

Sugar contribution to new fatty acyl (%) = **^{13}C-acyl**/**^{13}C-Sugar** × 100/**FSR_{FA}** × 100% (7)

C.4.8 Statistics

Data are represented as quartile distributions from the 25th to 75th percentiles under box and whisker plots. D'Agostino-Pearson omnibus analysis was applied to test for normality. According to the variables number different tests were applied. One-way ANOVA followed by Tukey's multiple comparison for single variables (with more than two groups) or two-way ANOVA with Tukey's multiple comparison for two variables. If in the presence of interaction between both variables, analysis proceeded separately for each one of them: two-tailed t-tests for variable pair comparison (two groups) or one-way ANOVA followed by Tukey's multiple comparisons (more than two groups). Statistical significance was defined by a *p* value < 0.05.

C.5 Results

C.5.1 ^{13}C NMR analysis of TG isotopomer enrichment from [U-^{13}C]fructose and [U-^{13}C]glucose

^{13}C NMR spectra of liver TGs revealed quantifiable ^{13}C-^{13}C-spin coupled isotopomer signals from mice that had fed on sugar enriched with [U-^{13}C]fructose as well as with [U-^{13}C]glucose. These signals were also detected in mesenteric (MAT) and subcutaneous adipose (SCAT) TGs of animals fed with the labeled sugars. However, they were generally less intense, or absent altogether in the case of SCAT of mice fed the sugar mixture enriched with [U-^{13}C]fructose (Figure C.2). Figure C.3 shows a ^{13}C NMR spectrum of liver TG from a female mouse following feeding with the exogenous sugar mixture enriched with [U-^{13}C]fructose. Signals from the FA ω–1 and ω–2 carbons, as well as those of glycerol 1 and 3, are shown in expanded view. The ω–1 natural-abundance resonances of the principal SFA and MUFA species (palmitate, stearate, oleate and palmitoleate) are almost isochronous at 14.1T, hence when the fid is processed with moderate line broadening (~1 Hz) they yield a composite singlet signal (**S**) that is resolved from that of linoleic acid (***S$_{LO}$***). The doublet components (**D**) originate from ^{13}C-^{13}C-spin-spin coupling of ω–1 carbons with their neighbors ($J_{C\text{-}C}$ = 34.8 Hz). Since **D** represents the sum of all ^{13}C-SFA and MUFA ω-1, ω-2 isotopomer abundances, its intensity relative to **S** represents the weighted average of excess SFA and MUFA enrichment from [1,2-^{13}C$_2$]acetyl-CoA (see Equation 1). The linoleate singlet did not have any associated doublet signals. This is consistent with the known capacity of mammalian liver to synthesize various SFA and MUFA species, but not linoleate.

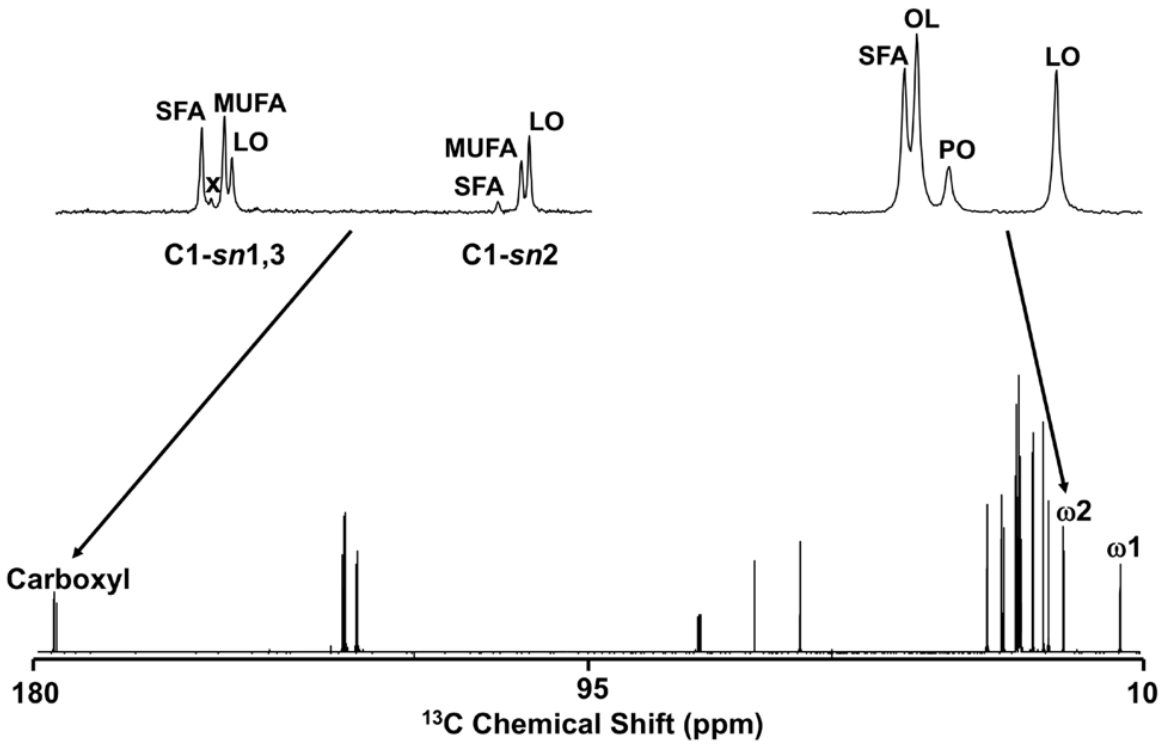

Figure C.2 - ^{13}C NMR spectrum of subcutaneous adipose tissue (SCAT) TG obtained from a mouse provided with a mixture of [U-^{13}C]fructose and unlabeled glucose. The ω-2 and carboxyl signals (C1-*sn*1,3 and C1-*sn*2) are shown in expanded form. **LO** = linoleate, **MUFA** = monounsaturated FAs, **OL** = oleate, **PO** = palmitoleate, **SFA** = saturated FAs, **X** = unknown.

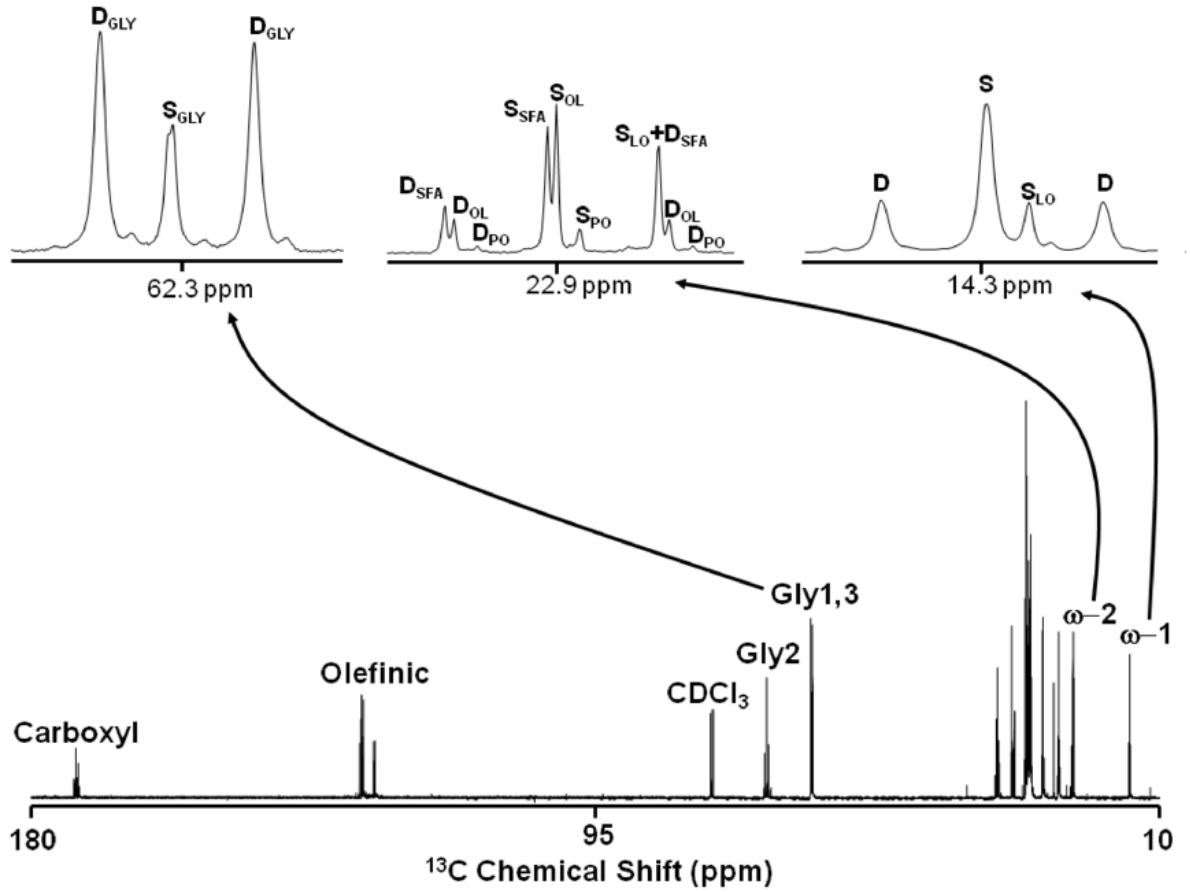

Figure C.3 – ^{13}C NMR spectrum of hepatic TG obtained from a mouse provided with a mixture of [U-^{13}C]fructose and unlabeled glucose – The FA ω-1 and ω-2 signals and the glyceryl signal corresponding to carbons 1 and 3 (Gly-*sn*1,3) are shown in expanded form. For the ω-1 resonances, **S** = composite natural abundance singlet from SFA and MUFA, **D** = composite ^{13}C-^{13}C spin-coupled doublet from SFA and MUFA, and $\mathbf{S_{LO}}$ = linoleate natural abundance singlet. For the ω-2 resonances, $\mathbf{S_{OL}}$ = oleate natural abundance singlet, $\mathbf{D_{OL}}$ = oleate ^{13}C-^{13}C spin-coupled doublet, $\mathbf{S_{PO}}$ = palmitoleate natural abundance singlet, $\mathbf{D_{PO}}$ = palmitoleate ^{13}C-^{13}C spin-coupled doublet, palmitoleate, $\mathbf{S_{SFA}}$ = saturated FAs natural abundance singlet, $\mathbf{D_{SFA}}$ = saturated FAs ^{13}C-^{13}C spin-coupled doublet. For the glyceryl 1,3 signals, $\mathbf{S_{GLY}}$ = natural abundance singlet, $\mathbf{D_{GLY}}$ = ^{13}C-^{13}C spin-coupled doublet.

An expanded view of the ω–2 cluster of resonances following fid processing with 0.1 Hz line broadening reveals resolved natural abundance ^{13}C singlet resonances of SFA, oleate, and palmitoleate. These are accompanied by flanking doublet signals representing their respective ω-1, ω-2 ^{13}C-isotopomers. At 14.1 T, the ^{13}C-chemical shift of the natural abundance linoleate singlet coincides with the upfield component of the SFA

doublet. In many liver spectra, the palmitoleate doublet signals had insufficient signal-to-noise ratios (snr) for reliable quantification therefore palmitoleate enrichment from [U-^{13}C]glucose and [U-^{13}C]fructose was not reported. ^{13}C-^{13}C-spin-coupled doublets of carboxyl carbons representing FA isotopomers enriched in both carboxyl and the neighboring α carbon were also observed ($J_{C\text{-}C}$ = 57.5 Hz) but their snr were also insufficient for reliable quantification (data not shown).

Finally, ^{13}C-^{13}C-spin-coupled doublet signals ($J_{C\text{-}C}$ = 43.7 Hz), were observed for the C1, C3 TG-glycerol resonance indicating enrichment of these carbons from ^{13}C-enriched Triose-P precursors. From the ratio of the ^{13}C-^{13}C-spin coupled signals to that of the natural abundance singlet signal, the fractional enrichments of SFA and oleate ω-1, ω-2 ^{13}C-isotopomers and those of glycerol carbons 1,3 were calculated (Equations 2 and 3 in the methods and Table C.1).

Table C.1 – Enrichment of TG ^{13}C-isotopomers at the FA ω-1 and ω-2 and the glyceryl 1,3 positions for liver, mesenteric adipose (MAT) tissue and subcutaneous adipose tissue (SCAT). Means and standard errors are shown.

^{13}C Liver TG isotopomer enrichments				
	Mean FA ω-1	**SFA ω-2**	**Oleate ω-2**	**1,3-Glyceryl**
Liver		*[U-^{13}C]glucose + unlabeled fructose (n=10)*		
	0.78 ± 0.40	0.7 ± 0.31	0.59 ± 0.27	1.3 ± 0.33
		[U-^{13}C]fructose + unlabeled glucose (n=9)		
	0.82 ± 0.31	1.01 ± 0.32	0.79 ± 0.33	3.69 ± 0.83
MAT		*[U-^{13}C]glucose + unlabeled fructose (n=10)*		
	0.62 ± 0.28	0.95 ± 0.37	0.56 ± 0.32	1.03 ± 0.47
		[U-^{13}C]fructose + unlabeled glucose (n=18)		
	0.09 ± 0.08	0.1 ± 0.13	0.02 ± 0.06	0.18 ± 0.14
SCAT		*[U-^{13}C]glucose + unlabeled fructose (n=12)*		
	0.11 ± 0.11	0.12 ± 0.14	0.02 ± 0.08	0.35 ± 0.23
		[U-^{13}C]fructose + unlabeled glucose (n=8)		
	0.02 ± 0.05	0.02 ± 0.06	0 ± 0	0.07 ± 0.11

C.5.2 ^{13}C NMR analysis of TG FA composition

The natural-abundance ^{13}C NMR signals inform the relative abundance of certain FA species as well as their distribution between the *sn*2 and *sn*1,3 sites of the glycerol moiety [216-219, 224, 229]. For the ω–2 sites, three ^{13}C signals arising from individual FAs (oleate, palmitoleate and linoleate) and a fourth signal representing SFA were well resolved (Table C.2 and Figure C.2). For the carbon 1 sites, there were resolved signals representing SFA, MUFA, and linoleate. These were distributed in two sets, an upfield cluster representing FAs attached to carbons 1 and 3 of glycerol (C1-*sn*1,3) and a downfield cluster representing FAs attached to glycerol carbon 2 (C1-*sn*2). Analysis of the natural-abundance (S) ω–2 signals allowed the relative proportions of SFA, oleate, palmitoleate and linoleate to be estimated while the C1 signals **(S)** provide information on the distribution of SFA, MUFA and linoleate between the *sn*2 and *sn*1,3 sites of glycerol.

Table C.2 – ^{13}C Chemical shift assignments for the ω1, ω2 and carbon 1 of individual FAs within TG as determined from a mixture of synthetic TGs approximating the FA composition of adipose tissue TG (see methods section). The FA carbon 1 resonances are split into two sets of signals: those attached to carbons 1 and 3 of glycerol (C1-*sn*1,3) and those attached to carbon 2 of glycerol (C1-*sn*2)**.** All chemical shifts are referenced to the center signal of the $CDCl_3$ triplet which was assigned a value of 77.23 ppm.

	SFA		**MUFA**		**PUFA**
	Palmitate	*Stearate*	*Oleate*	*Palmitoleate*	*Linoleate*
ω–1	14.321	14.321	14.315	14.308	14.274
ω–2	22.898	22.898	22.889	22.864	22.780
C1-*sn*2	173.081	173.081	173.046	173.046	173.034
C1-*sn*1,3	173.492	173.492	173.459	173.459	173.448

The natural abundance data **(S)** indicated that for all the tissues studied, SFA and oleate were the main FA constituents, followed by linoleate and palmitoleate (Figure C.4). Linoleate was more abundant in adipose tissue TG compared to liver. This is broadly consistent with previous GC-MS assays of mouse liver and adipose tissue FA distributions [226]. Analysis of the C1 signals **(S)** revealed a markedly non-uniform distribution of FA classes between *sn*1,3 and *sn*2 sites (Figure C.5 A, B, C). Linoleic acid and MUFA were more abundant in *sn*2 relative to *sn*1,3 sites while SFA were largely restricted to *sn*1,3 with only minor proportions at the *sn*2 site. The FA abundances and positional distributions in the liver, MAT and SCAT TGs did not differ significantly between male and female mice (data not shown).

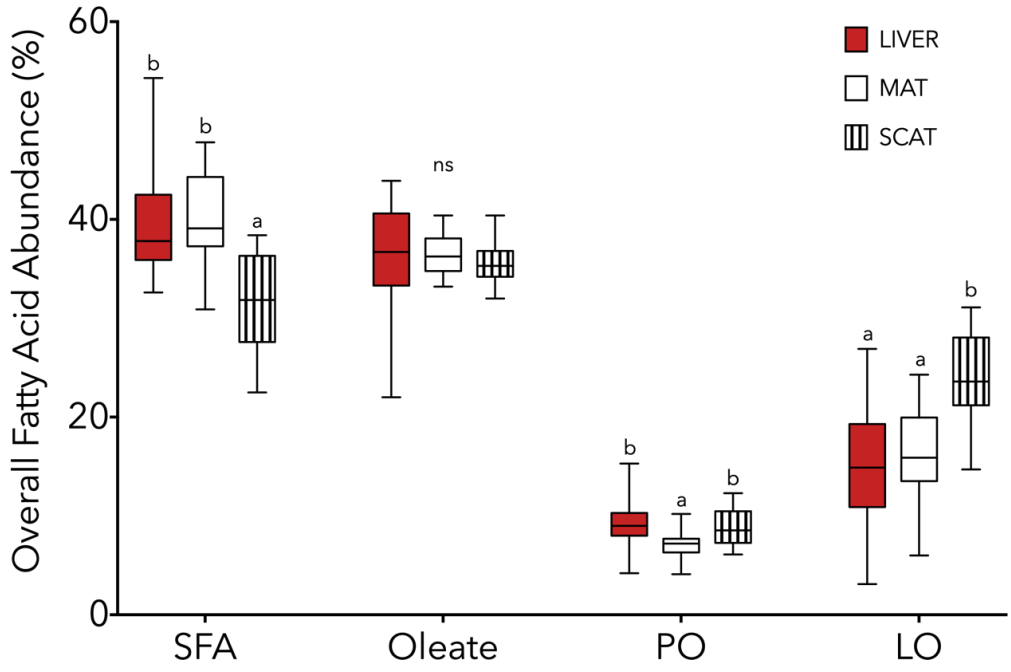

Figure C.4 – TG FA profiles of liver, mesenteric adipose tissue (MAT) and subcutaneous adipose tissues (SCAT)**.** The relative abundances of saturated fatty acids (SFA), oleate, palmitoleate (PO) and linoleate (LO) are shown for each tissue. Significant differences in the abundance of FA species between liver, MAT and SCAT were analyzed by one-way ANOVA and are represented by different letters. The p values are shown in Table C.3.

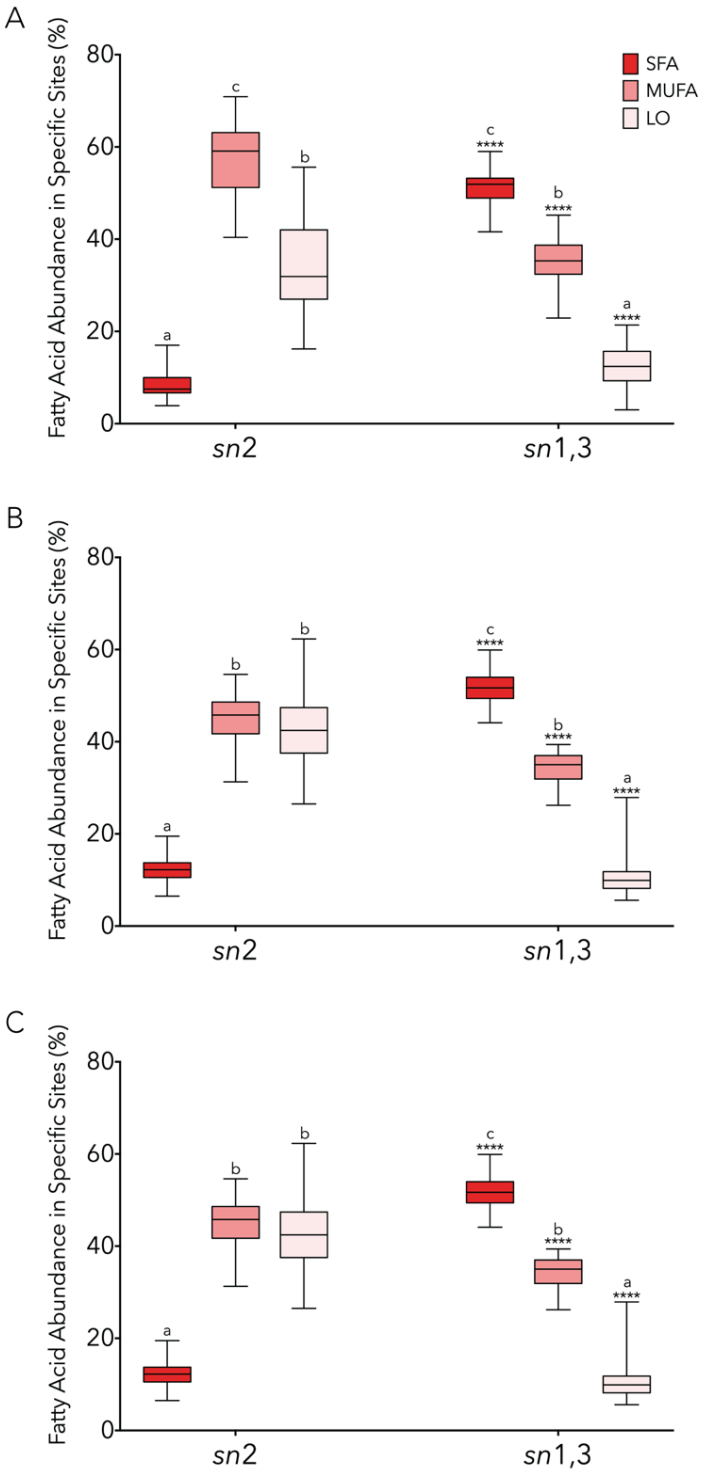

Figure C.5 – Distribution of saturated (SFA), monounsaturated (MUFA), and linoleic (LO) FAs between the glycerol *sn*1,3 and *sn*2 sites in A – liver; B – mesenteric adipose tissue (MAT), and C – subcutaneous adipose tissues (SCAT) (n = 28). Two-way ANOVA revealed interactions between variables, so the statistical analysis proceeded separately for each variable.

Fatty acid abundance differences within each *sn* site are represented by letters (one-way ANOVA; $p < 0.05$). For each FA, differences between *sn* positions are indicated by asterisks (t-test; * $p < 0.05$, ** $p < 0.01$ *** $p < 0.001$, **** $p < 0.0001$). Complete p values are shown in Table C.4.

Table C.3 – Results from one-way ANOVA (p values) applied to data on Figure C.4 representing FAs composition among different tissues: Liver, MAT and SCAT.

	One-way ANOVA (n=28)	*Tukey's multiple comparisons*		
		Liver vs MAT	**Liver vs SCAT**	**MAT vs SCAT**
SFA	*p < 0.0001*	*p = 0.7932*	*p < 0.0001*	*p < 0.0001*
Oleate	*p = 0.5406*	*p = 0.9854*	*p = 0.6869*	*p = 0.5346*
PO	*p = 0.0018*	*p = 0.0051*	*p = 0.9620*	*p = 0.0102*
LO	*p < 0.0001*	*p = 0.8526*	*p < 0.0001*	*p < 0.0001*

Table C.4 – Results from one-way ANOVA (p values) applied to data on Figure C.5 representing FAs distribution in each position – *sn*2 or *sn*1,3 – for the three different analyzed tissues: Liver, MAT and SCAT. Previous analysis under a two-way ANOVA for the two variables (FA; position) showed significant interactions for every tissue: Liver – Interaction ($p < 0.0001$), position ($p = 0.6220$), FA ($p < 0.0001$); MAT – Interaction ($p < 0.0001$), position ($p = 0.2001$), FA ($p < 0.0001$); SCAT – Interaction ($p < 0.0001$), position ($p = 0.1360$), FA ($p < 0.0001$). Due to interactions separate analysis were applied: one-way ANOVA for FA differences in each position; t-test for *sn*2 vs *sn*1,3 in each FA.

	One-way ANOVA (n=28)	*Tukey's multiple comparisons*		
		SFA vs MUFA	**SFA vs LO**	**MUFA vs LO**
			A (LIVER)	
sn2	*p < 0.0001*	*p < 0.0001*	*p < 0.0001*	*p < 0.0001*
			B (MAT)	
	p < 0.0001	*p < 0.0001*	*p < 0.0001*	*p = 0.2167*
			C (SCAT)	
	p < 0.0001	*p < 0.0001*	*p < 0.0001*	*p < 0.0001*
			A (LIVER)	
sn1,3	*p < 0.0001*	*p < 0.0001*	*p < 0.0001*	*p < 0.0001*
			B (MAT)	
	p < 0.0001	*p < 0.0001*	*p < 0.0001*	*p < 0.0001*
			C (SCAT)	
	p < 0.0001	*p = 0.3814*	*p < 0.0001*	*p < 0.0001*

	t-test (n=28)	***sn2 vs sn1,3***		
		SFA	**MUFA**	**LO**
Liver		*p < 0.0001*	*p < 0.0001*	*p < 0.0001*
MAT		*p < 0.0001*	*p < 0.0001*	*p < 0.0001*
SCAT		*p < 0.0001*	*p = 0.8847*	*p < 0.0001*

C.5.3 Integration of ^{13}C-isotopomer analysis and $^{2}H_2O$ measurement of DNL to estimate the contribution of [U-^{13}C]fructose and [U-^{13}C]glucose to newly-synthesized TG FAs and glycerol

By resolving the ^{13}C-enriched sugar contributions to newly synthesized TG, the proportion of acetyl-CoA and glycerol derived from the glucose and fructose provided in the drinking water relative to all other sources can be estimated. The fractions of newly synthesized TG-FAs and glycerol moieties for liver and adipose tissues (Figure C.6 A, B, C) were estimated from ^{2}H-enrichment of selected TG sites from $^{2}H_2O$ via analysis of TG $^{1}H/^{2}H$-NMR spectra (Figure C.7 and Table C.5). Enrichment of hepatic TG-FA and glycerol moieties were substantially higher than those of adipose tissues indicating a faster turnover of the hepatic TG pool compared to that of MAT or SCAT. Mesenteric adipose tissue showed a strong tendency towards higher fractional synthetic rates of TG-FAs and TG-glycerol compared to SCAT, see Table C.5. Integration of the ^{2}H- and ^{13}C-tracer data yields the contributions of fructose and glucose in the drinking water relative to all other substrates to TG-glycerol and TG-FA synthesis during the time that the mice were administered with the tracers. These data are shown in Figure C.6 D, E, F. For liver, this fructose contributed ~30% of the acetyl-CoA used for synthesis of all FAs whereas the contribution from the accompanying glucose was significantly lower, amounting to ~10% (Figure C.6D). Moreover, the fractional contribution of fructose to SFA synthesis was significantly higher compared to oleate while glucose contributions to *de novo* SFA and oleate synthesis were not significantly different. For both SFA and oleate, the majority of acetyl-CoA was derived from unlabeled substrates (~60 and 75%, respectively). For TG-glycerol, the fructose provided in the drinking water was highly

preferred over the accompanying glucose and accounted for about 60% of the newly synthesized TG-glycerol (Figure C.6A).

Mesenteric adipose tissue TG had low levels of ^{13}C-isotopomers from both [U-^{13}C]glucose and [U-^{13}C]fructose precursors, while SCAT had low enrichment from [U-^{13}C]glucose but negligible enrichment from [U-^{13}C]fructose (Table C.1). Estimates of [U-^{13}C]glucose and fructose contributions to FA and glycerol synthesis in MAT and SCAT presented relatively high variance (Figure C.6E, F), due in part to the much lower FSRs in these tissues compared to the liver (Figure C.6B, C). The higher coefficients of variation associated with these FSR estimates propagate larger variances in the estimates of sugar contributions to DNL and glycerol. These uncertainties notwithstanding, exogenous glucose contributed significantly more than fructose to TG-glycerol synthesis in both MAT and SCAT. In MAT, the contribution of glucose from the drinking water to TG-FAs tended to be higher than that of fructose. For SCAT, the contribution of fructose to those FAs that had been formed via DNL was negligible. Overall, unlabeled substrates either from endogenous sources or the chow diet accounted for the majority of DNL and glycerol synthesis in both MAT and SCAT TGs.

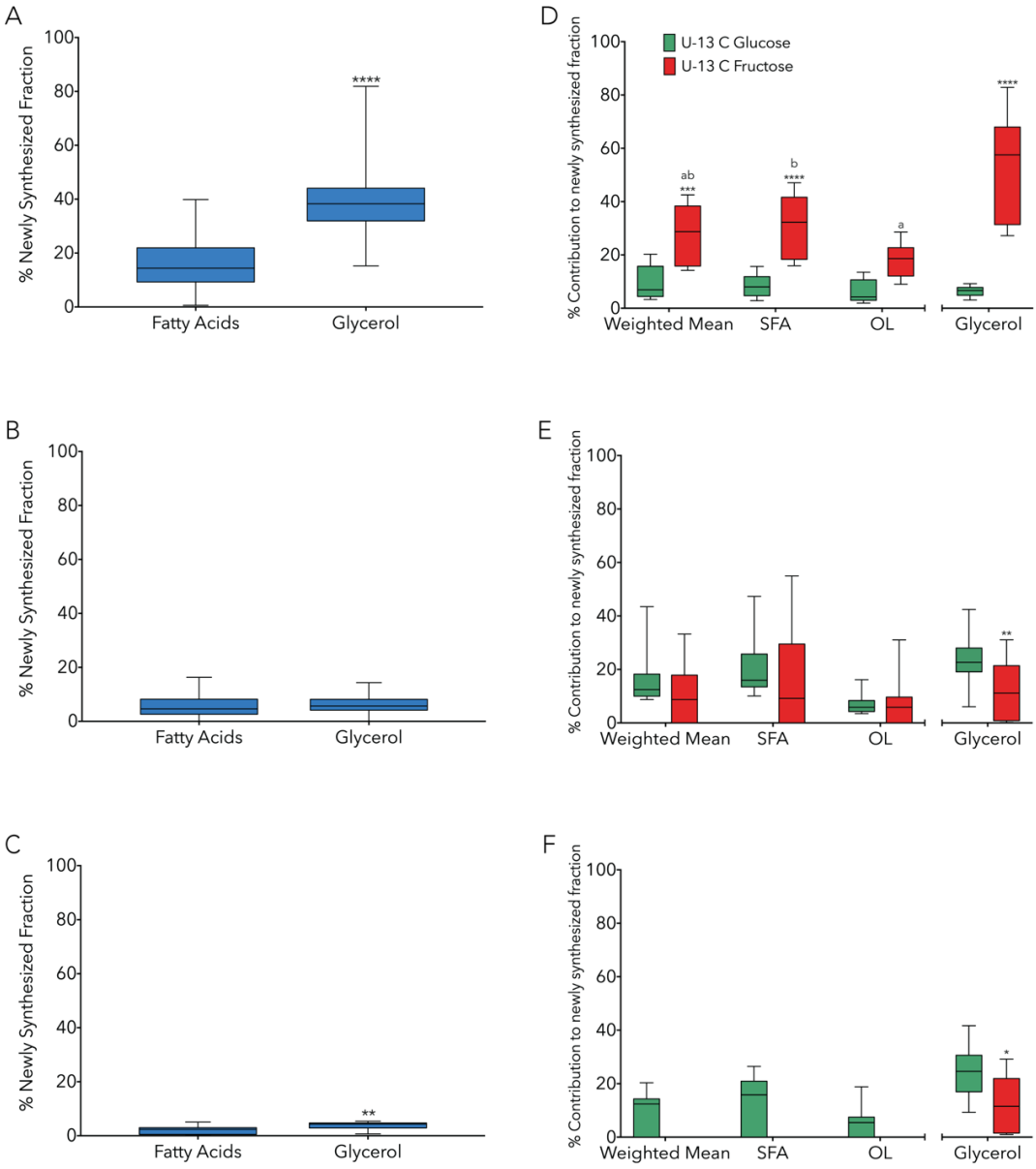

Figure C.6 – Fraction of newly formed TG FAs and glycerol in liver, mesenteric adipose tissue (MAT) and subcutaneous adipose tissues (SCAT) and the contributions of exogenous glucose and fructose to these newly formed TG components. Data for liver are shown in panels A and D, for MAT in panels B and E, and for SCAT in panels C and F. Data in blue represent those derived from $^{2}H_2O$ (n = 36), those in red from the combination of $^{2}H_2O$ and [U-^{13}C]fructose (n = 18) and those in green from the combination of $^{2}H_2O$ and [U-^{13}C]glucose (n = 18). Differences between newly formed TG FAs and glycerol for each tissue (A, B, C) are indicated by asterisks (t-test; * $p < 0.05$, ** $p < 0.01$ *** $p < 0.001$, **** $p < 0.0001$). Differences on the specific contribution for newly formed FAs (D, E, F) were analyzed under two variables – Tracer ([U-^{13}C]fructose or [U-^{13}C]glucose) & FA (Weighted Mean, SFA or OL) (two-way ANOVA). For each FA differences between tracers are indicated by asterisks (* $p < 0.05$, ** $p < 0.01$ *** $p < 0.001$, **** $p < 0.0001$); for each tracer, differences between FA are indicated by different letters. Differences on the specific contribution for newly formed glycerol are indicated by asterisks (t-test; * $p < 0.05$, ** $p < 0.01$ *** $p < 0.001$, **** $p < 0.0001$). Individual tissue results are described in Table C.6.

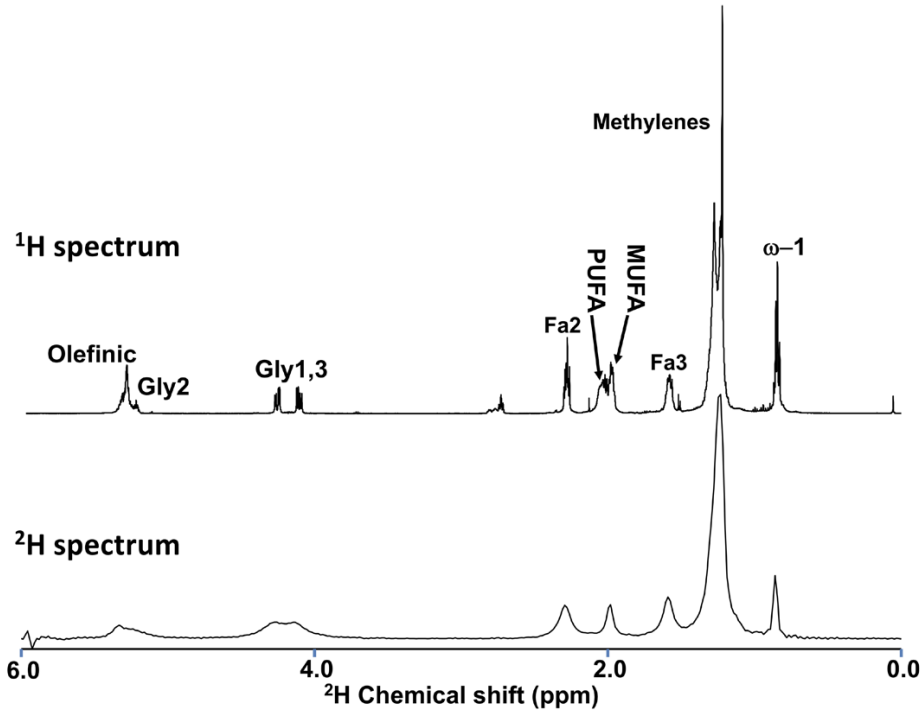

Figure C.7 – ^{1}H and ^{2}H NMR spectra of TG obtained from a mouse administered with ^2H_2O and provided with a mixture of [U-^{13}C]fructose and unlabeled glucose. **MUFA** = monounsaturated FAs, **PUFA** = polyunsaturated FAs, **ω-1** = terminal methyl hydrogens, **Fa2**, **Fa3** = FA position 2 and position 3 hydrogens, **Gly1,3** = hydrogens attached to carbons 1,3 of the glyceryl moiety, **Gly2** = hydrogens attached to carbon 2 of the glyceryl moiety, **Methylenes** = FA chain methylene hydrogens, **Olefinic** = hydrogens attached to olefinic carbons.

Table C.5 – ^{2}H Enrichment of the TG ω-1 and glycerol C1, C3 hydrogens in mice provided with ^2H_2O and combinations of [U-^{13}C]- and unlabeled glucose and fructose in their drinking water.

	^{2}H TG enrichment		
	FA ω-1	***sn1,3-Glyceryl***	***Body water***
Liver	*[U-^{13}C]glucose + unlabeled fructose (n=14)*		
	1.78 ± 1.03	3.74 ± 1.28	4.54 ± 1.56
	[U-^{13}C]fructose + unlabeled glucose (n=16)		
	1.49 ± 0.96	4.11 ± 1.30	4.09 ± 0.55
MAT	*[U-^{13}C]glucose + unlabeled fructose (n=14)*		
	0.7 ± 0.53	0.66 ± 0.44	4.59 ± 1.55
	[U-^{13}C]fructose + unlabeled glucose (n=21)		
	0.46 ± 0.28	0.68 ± 0.41	4.10 ± 0.51
SCAT	*[U-^{13}C]glucose + unlabeled fructose (n=16)*		
	0.12 ± 0.15	0.21 ± 0.17	4.97 ± 1.79
	[U-^{13}C]fructose + unlabeled glucose (n=13)		
	0.15 ± 0.13	0.29 ± 0.19	4.3 ± 0.35

Table C.6 – Results from two-way ANOVA applied on data from specific contributions of [U-^{13}C]glucose and [U-^{13}C]fructose to newly synthesized fractions of FA and two-tailed t-tests on specific contributions of [U-^{13}C]glucose and [U-^{13}C]fructose to newly synthesized fractions of glycerol for Liver, MAT and SCAT (represented on Figure C.6D, E, F).

	Two-way ANOVA			**Tukey's Multiple Comparisons**			**t-test (Glycerol)**
	Tracer	**FA**	**Interactions**	**Mean vs SFA**	**Mean vs OL**	**SFA vs OL**	**[U-^{13}C]Glucose vs [U-^{13}C]Fructose**
Liver	**** *p<0.0001*	* *p=0.0161*	*ns* *p = 0.1214*	*p > 0.9999*	[U^{13}C]Glucose *p = 0.9766*	*p = 0.9943*	**** *p < 0.0001*
				p = 0.9346	[U^{13}C]Fructose *p = 0.1619*	*p = 0.0167*	
MAT	*ns* *p=0.2368*	** *p=0.0034*	*ns* *p = 0.7214*	*p = 0.9740*	[U^{13}C]Glucose *p = 0.5144*	*p = 0.1402*	** *p = 0.0088*
				p = 0.6557	[U^{13}C]Fructose *p = 0.9216*	*p = 0.1369*	
SCAT	*ns* *p =0.1265*	*ns* *p =0.1295*	*ns* *p = 0.8691*	*p = 0.9873*	[U^{13}C]Glucose *p = 0.9633*	*p = 0.7091*	* *p = 0.0294*
				p = 0.7917	[U^{13}C]Fructose *p > 0.9999*	*p = 0.6971*	

C.6 Discussion

There is currently strong interest in the study of lipogenesis given its crucial role in the pathogenesis of major diseases such as NAFLD, Type 2 diabetes and cancer [230, 231]. Tracer methodologies based on either $^{2}H_2O$ or ^{13}C-acetate isotopes have been developed since the 1990´s for quantifying lipogenesis and TG-glycerol synthesis fluxes in humans, animal models and cell cultures [213, 232-236]. However, the sources of lipogenic acetyl-CoA and triose-Ps for FA and GLY synthesis remain largely undefined despite renewed interest in the role of specific substrates such as fructose in the pathogenesis of NAFLD, and glutamine in tumor lipid biosynthesis. Yoo et al. developed an isotopomer spectral

assay (ISA) method for quantifying contributions of specific [U-^{13}C]enriched precursors to DNL and glycerol synthesis in cultured pre-adipocytes [236]. With this approach, they quantified the fractional contributions of glutamine, acetate and ketone bodies to total DNL. More recently, ISA of fatty acid enrichment from [U-^{13}C]branched chain amino acids was applied to demonstrate the biosynthesis of monomethyl branched chain fatty acids (mmBCFA) by mammalian cells [237]. These data were integrated with parallel ISA studies of fatty acid enrichment from $^{2}H_2O$ and [3-^{2}H]glucose allowing the source of lipogenic NADPH, and therefore the probable intracellular sites of mmBCFA biosynthesis and elongation, to be determined.

Unlike ISA, our method is not dependent on having multiple [U-^{13}C]acetyl-CoA or ^{2}H incorporated into each fatty acid chain, therefore in principle it can function with the lower [U-^{13}C]precursor and ^{2}H-body water enrichments attained in animal models (the limitations are discussed in more detail subsequently). In addition to quantifying fractional substrate contributions to FA and glycerol synthesis, the ^{13}C NMR spectrum also provides lipidomic information that includes the distribution of SFA, MUFA and PUFA between the *sn*-1,3 and *sn*-2 positions of the glycerol unit. Lipidomic mass spectrometry approaches can provide the composition of the TG-FAs but do not provide positional information [238].

As proof-of-concept, we applied our approach to compare the contributions of glucose and fructose that were added to the drinking water of animals fed with standard chow to TG synthesis in liver, MAT and SCAT. A key objective of our work was to determine if this fructose supplied a greater fraction of carbon units for hepatic DNL compared to an equivalent amount of glucose. Elegant stable-isotope tracer studies have shown that ingestion of a fructose bolus acutely increases hepatic *de-novo* lipogenesis

(DNL) in humans [213, 239, 240]. Moreover, this increase is greater than that from an equivalent amount of glucose. Animal studies have shown a higher TG clearance with increased plasma circulating FAs and concomitantly higher hepatic DNL levels upon high fructose feeding [189, 241]. Lastly, for overweight and obese subjects, it was observed that DNL rates, postprandial TG levels and visceral adiposity were all significantly increased following sustained hypercaloric consumption of fructose-, but not glucose-sweetened beverages [242]. When these sugars were presented in the drinking water, our results indicate a higher recruitment of fructose over glucose from this source for hepatic DNL. Our data also indicate that fructose appears to be preferentially utilized for hepatic SFA synthesis over that of oleate, at least under the conditions of our study. Given that the SFA component is mainly palmitate [226, 227], then elongation activity could account for a lower ^{13}C-enrichment of oleate ω-1, ω-2 compared to that of SFA [243]. However, this does not explain the greater difference between SFA and oleate enrichment from [U-^{13}C]fructose compared to that from [U-^{13}C]glucose.

^{13}C NMR analysis of TG also provided new information on the arrangement of FAs in the TG molecule. While non-uniform distributions of FAs in the *sn*1,3 and *sn*2 positions have been previously reported in olive oil [219] and marine fish oils [217], to our knowledge this has not been previously described for mammalian TG pools. As was found in both fish and olive oils, SFA are mainly distributed in the *sn*1,3 positions while mono- and polyunsaturated FAs are mainly confined to the *sn*2 position. These observations are broadly consistent with biochemical studies of FA preference by each enzyme of the TG biosynthesis pathway. Glycerol-3-phosphate acyltransferase has a higher affinity for saturated over unsaturated FAs while acylglycerophosphate

acyltransferase has a preference for mono- and polyunsaturated FAs over SFA [244]. However diacylglycerol acyltransferase 2, which esterifies the final FA into the *sn*3 position, has been reported to have a high affinity for oleate *in vivo*, possibly due to co-localization with stearoyl-CoA desaturase [245]. Since the ^{13}C NMR method cannot resolve FAs in the *sn*1 and *sn*3 positions, we cannot confirm if MUFA is more prevalent in *sn*3 than *sn*1 or vice-versa.

Our method has several important limitations. Our estimates are limited to those substrate pools that can be reliably enriched with [U-^{13}C]tracers. In our experiment, this was comprised of glucose and fructose that were added to the drinking water. In addition to absorbed macronutrients, a diversity of endogenous substrates including endogenously-generated glucose, lactate, glycogen, amino acids and microbially-generated acetate can be recruited for lipogenesis and/or glyceroneogenesis. For the [U-^{13}C]glucose tracer, it is certain that it was diluted by unlabeled glucose originating from other dietary sources, for example digestion of the chow maltose. There could be further dilution from endogenously generated glucose, for example from intestinal and hepatic gluconeogenesis. To account for these glucose sources, enrichment of [U-^{13}C]glucose at its point of entry into glycolysis (i.e. in hepatocytes) would need to be measured. Estimates of the contribution of ^{13}C-enriched substrate to lipogenesis become highly uncertain when lipid FSRs are low and/or when the ^{13}C-enriched substrate is contributing a small fraction of acetyl-CoA precursors. Inspection of equations 6 and 7 indicate that when FSR_{FA} or FSR_{GLY} are low, they need to be quantified very precisely. This is because uncertainties are amplified by the (100/FSR) coefficient and propagated into estimates of ^{13}C-sugar contributions to newly synthesized lipids. Likewise, the minimum contribution of ^{13}C-enriched glycerol or FA that can be reliably quantified is

determined by the limit of quantification of the ^{13}C-isotopomer doublet signals according to their signal-to-noise ratios. For our data, we estimate this to be about 0.10% (i.e. a ^{13}C-doublet/singlet ratio of 1:10) for the more abundant fatty acids. The method cannot distinguish between ^{13}C-enriched FAs synthesized on site *versus* those made elsewhere and then imported into the tissue of interest. Thus, the ^{13}C-enriched FAs observed in adipose tissue could have been formed on site, or they could have been initially synthesized in the liver and then transferred to the adipose tissue via VLDL. With fructose, it is also possible that it was not directly utilized for lipogenesis but instead was converted beforehand to glucose by the liver and/or intestine [143]. These processes are likely to have substantially modified MAT enrichment from [U-^{13}C]fructose. On the one hand, immediately upon its conversion to glucose, there would be substantial dilution of the ^{13}C-label by unlabeled glucose. On the other hand, adipocyte glucose uptake is likely to be maximally stimulated by insulin under the study conditions. In terms of delivering the [U-^{13}C]fructose label into MAT TG, this would offset, at least in part, any prior dilution by glucose.

It should also be noted that while FSR of adipose tissues were lower compared to liver, their absolute rates of fatty acid synthesis and sugar utilization could well be higher on account of their much larger triglyceride mass. Finally, for the analysis of substrate contributions to TG-glycerol, estimates of FSR_{GLY} assume that the *sn*1 and *sn*3 hydrogens of GLY are fully exchanged with those of body water. During the synthesis of GLY from fructose via triose-P, exchange of GLY hydrogens, in particular the *sn*3 pair, may be incomplete. Chen et al showed that mice had equivalent enrichments of TG-glycerol and water hydrogens from $^{2}H_2O$ at baseline, but after infusion of a fructose load the TG-glycerol ^{2}H-enrichment dropped significantly below that of body water [246]. In our

study setting, this would result in an underestimate of FSR_{GLY} and a corresponding overestimate of the contributions of [U-^{13}C]glucose and [U-^{13}C]fructose to newly-synthesized TG-glycerol.

In conclusion, we describe the integration of $^{2}H_2O$ and ^{13}C-enriched substrates with ^{2}H and ^{13}C NMR spectroscopy for quantifying the contribution of a specific precursor to the synthesis of FAs and GLY of tissue TG. This approach revealed important differences in how the carbons of exogenous glucose and fructose are utilized for lipogenesis and GLY synthesis in the liver. Fructose contributed a greater share of carbons than glucose for GLY synthesis. It also contributed a higher share of acetyl-CoA to FA synthesis with an apparent preference for *de novo* synthesis of SFA over that of oleate.

Chapter D

General Discussion

A high intake of simple carbohydrates in general and fructose in particular promotes the development and progression of NAFLD. The longstanding view that the metabolic effects of fructose are mediated by changes in liver metabolism alone is now recognized as being incomplete. By providing evidence that diets high in simple sugars a) modify the intestinal microbiome and absorbable metabolites [138] and b) sustain *de novo* lipogenesis fluxes in visceral adipose tissues [210] the experimental studies of this thesis provides further evidence to reinforce this view.

D.1 High Fructose feeding results in an overflow of fructose into the lower intestine thereby providing a novel fermentable substrate for the intestinal microbiota

Mice that were fed a diet where 60% of total calories were from fructose, with no other carbohydrate components present, showed varying amounts of un-metabolized fructose in their faeces. This indicates that the intestinal capacity for fructose absorption had been exceeded, and that the entire intestinal microbiome had been exposed to fructose. Fructose malabsorption has been associated with decreased intestinal motility, gas production and pathologies such as inflammatory bowel disease [247]. Fructose

malabsorption has also been connected to disruption in the regulation of sugar metabolism by the host. Thus, mice that were unable to express ChREBP, a transcription factor that couples glucose and fructose metabolism to lipogenesis, showed gastrointestinal intolerance to high fructose feeding [248]. This suggests that the systemic regulation of fructose metabolism includes controlling the expression of the intestinal GLUT5 transporters. Lastly, exposure of the entire microbiome and intestinal tract to fructose could promote the establishment of fructophilic microorganisms such as the fructophilic Lactobacillus species [249]. The impact of such changes on the symbiotic relationship between host and microbiome remains unclear.

D.2 High fructose and high glucose feeding altered the intestinal short-chain fatty acids (SCFA) profile

SCFA are normally generated by microbial fermentation of complex carbohydrates and are absorbed alongside other nutrients through MCT-1 transporters [250]. In addition to being oxidized for energy by host tissues, SCFA also trigger intracellular signalling events in visceral tissues through a set of receptors that includes FFA2, FFA3 and GPR109a [251-253]. Activation of these receptors in intestinal tissues by SCFA is associated with anti-inflammatory processes as the modulation of cytokines, immune cells migration, differentiation and inflammasomes activation [254-257]. Effects also include intestinal permeability mediation [258] as well as cell proliferation control [259]. Intestinal metabolic signals are also influenced by SCFA that mediate GLP-1 release [260] for insulin secretion control and induce YY peptide synthesis that increases satiety through intestinal transit rates lowering [261]. Considering that FFA3 is expressed in tissues that

are innervated by the sympathetic nervous system, this implies a role of SCFA in gut-brain communication of nutrient sensing [262]. As we demonstrated in our study, alterations in the diet – in this case providing glucose or fructose as the sole dietary carbohydrate component, led to changes in intestinal SCFA levels, as measured by faecal acetate, propionate, and butyrate levels [138]. Changes in SCFA can mean alterations in the concentrations of the individual species as well as in the amount of one species relative to the other. Moreover, these changes may reflect a shift in the substrate profile that is being seen by the microbiome (for example fructose appearance in the lower intestine) as well as alterations in the microbiome species distribution. For example, we found that intestinal acetate levels were increased with glucose- and fructose-only carbohydrate diets that were correlated with an increased abundance of Lactobacillus. While lactate is the primary metabolite generated by this species, this can be metabolized to acetate through cross-feeding interactions with acetogenic species [263]. In women, increased faecal acetate levels were found to be positively correlated with risk factors for metabolic syndrome [264]. On the other hand, butyrate is considered to be important for colonocyte function since it is the main energy-providing substrate for these cells [265], hence increased levels of this SCFA species would be expected to be beneficial. In fact, we found that in comparison to normal chow and glucose-only carbohydrate diets, mice fed the fructose-only carbohydrate diet had a marked decrease in faecal butyrate levels. This could have a significant impact on intestinal barrier maintenance and inflammatory status.

Mice that were fed the glucose-only carbohydrate had lower faecal propionate levels compared to both normal chow and fructose-only carbohydrate diets. While propionate is efficiently extracted by the liver and is utilized as a gluconeogenic substrate, it also

suppresses hepatic lipogenesis [266]. Therefore, a decrease in propionate production could contribute to higher lipogenic activity and an increased potential for NAFLD development.

Considering lipogenesis, attention is normally drawn to hepatic mechanisms that lead to steatosis. However the influence can start even earlier and it has been proved that colonocytes are able to incur in lipid synthesis [267]. In this context, locally produced SCFA's serve as main lipogenic substrates with particular preference for butyrate and acetate [268]. To reinforce this role, it is also described that the carbon backbone sources for intestinal lipogenesis are not majorly derived from Krebs cycle so acetyl-coA primary precursors are most likely being derived by SCFA's. Generally, the intestinal lipid synthesis serves predominantly cell growth and membrane assembly but it also produces considerable amounts of free fatty acids [269]. Additionally to SCFA's, glucose is also a fuel for colonocytes lipid synthesis that was even demonstrated to potentiate lipogenesis in synergy with butyrate [267]. Under pathological conditions, on a colitis inflammatory phenotype it was observed an increase in glucose oxidation as opposed to a decrease in butyrate oxidation regarding lipid production [270]. The mechanisms involved are not clear and it deserves further investigation. Given this glucose role in disease conditions, the potential effect of high fructose conditions in colonocytes lipogenesis is worthwhile exploring considering as well this thesis results in which these diets promote a considerable lowering on intestinal butyrate availability [138].

D.3 Lipogenic metabolism of dietary sugar by mesenteric fat and liver

This dissertation reports results from studies integrating $^{2}H_2O$ and [U-^{13}C]sugar tracers that a) measured DNL rates in both liver and MAT, and b) allowed the contributions of exogenous fructose and glucose to these DNL activities to be determined for specific classes of fatty acids (saturated fatty acids, oleate and palmitoleate) [210]. Palmitoleate is a lipokine that among other things suppresses hepatic lipogenesis [271]. These data confirmed that for liver TG, exogenous fructose contributed a fraction of lipogenic acetyl-CoA that was about three times that of exogenous glucose. Moreover, fructose was utilized to an even greater extent that glucose for the synthesis of saturated fatty acids (SFA), which are considered to be the most lipotoxic in terms of macrophage activation, pro-inflammatory agents like IL-6 and TNF production [272].

Normally, there is a defence mechanism involving the activity of stearoyl-CoA desaturase-1 (SCD-1) that converts SFA (mainly palmitate and stearate) to mono-unsaturated fatty acids (MUFA) via desaturation. Gut microbiota and SCFA's are known to be involved in SCD-1 regulation including the activation of TLR's. Mice lacking TLR5 showed high expression levels of SCD-1 [273]. Thus, a relevant hypothesis can be proposed in which fructose, through changes in intestinal microbiota and SCFA production, leads to a decrease in hepatic SCD-1 levels. Concomitantly, the accumulation of lipotoxic SFA's will be favoured over the more beneficial MUFAs.

Generally, mesenteric adipose tissue (MAT), presented higher fractional rates of lipogenesis than subcutaneous adipose tissue (SCAT). It was clear that resultant lipid patterns were healthier in SCAT immediately by the observation that general SFA had

lower concentrations in this tissue when comparing to liver and MAT. Also, linoleate levels were exclusively higher in SCAT and considering that this lipid is the precursor for the synthesis of the essential fatty acids, docosahexaenoic (DHA) and eicosapentaenoic (EPA), that have beneficial effects on triglyceride levels control. It has even been demonstrated that gut microbiota derived polyunsaturated fatty acids can prevent obesity and metabolic syndrome [274]. Contrarily, MAT has demonstrated SFA levels similar to liver and an exclusive effect among all three different analysed tissues in which palmitoleate levels were decreased. This fatty acid is considered an important adipokine with its activity centralised on the mediation of the crosstalk between liver and adipose tissue [271] and normally improves systemic insulin sensitivity.

D.4 Future Perspectives

Our studies of lipogenic glucose and fructose metabolism involved giving a single overnight load of these sugars in healthy mice that had been previously fed a standard chow diet. Our results demonstrate a robust constitutive capacity for metabolizing both sugars into triglyceride fatty acid and glycerol moieties, with exogenous fructose being more extensively utilized than exogenous glucose [210]. How is this altered in mice that have been fed long term with a high sugar diet? It is known that in the case of prolonged feeding with a high fructose diet, there is upregulation of both intestinal GLUT5 and ketohexokinase expression [275, 276]. Therefore, the enterocyte capacity for absorption and conversion of fructose to triose-P is increased. This has to be balanced by an increased carbon efflux into the portal vein circulation. This can either be in the form of lactate via glycolysis or as glucose via intestinal gluconeogenesis [277, 278]. The extent of

these intestinal metabolic activities may have implications on hepatic lipid metabolism, in particular *de novo* lipogenesis.

Our study also demonstrated that mesenteric adipose tissue (MAT) had far higher DNL rates per unit mass compared to subcutaneous adipose tissues. Moreover, following a single night of glucose and fructose feeding, we found that a significant fraction of the acetyl-CoA sources were derived from exogenous fructose, as measured with ^{13}C-enriched fructose [210]. We do not know if fructose was directly metabolized by MAT - according to Varma et al. adipocytes have the capacity to uptake and metabolize fructose [279] - or if instead it was converted beforehand to glucose or lactate via intestinal metabolism. As a first step towards resolving these possibilities, it will be important to determine to what extent MAT are exposed to fructose during absorption. If exposure to fructose is limited, then the most likely explanation is that MAT utilize downstream products of intestinal fructose metabolism, i.e. lactate or glucose, as lipogenic precursors.

The combined contributions of glucose and fructose to hepatic DNL amounted to about 40% of the total lipogenic acetyl-CoA pool. This begs the question of where the remaining 60% of acetyl-CoA precursors had originated. Based on the analysis of fecal metabolites where acetate was found to be highly abundant [138], it is plausible that this metabolite could be a significant contributor to lipogenesis. This could be tested by labeling the colonic acetate pool with ^{13}C-enriched acetate and measuring its lipogenic incorporation into fatty acids. Metabolically, acetate lipogenesis bypasses the citrate shuttle and is primarily dependent on its uptake rate and the activity of cytosolic acetyl-CoA synthetase. Therefore, assessing these parameters could inform the capacity of liver and MAT for acetate lipogenesis.

Lastly, our long-term studies of mice that received either glucose or fructose as their sole dietary carbohydrate source revealed the effects of these diets on both the species and metabolic activities of lower intestine microbes [138]. In particular, there were significant changes in fecal SCFA levels, with a general shift towards increased abundance of acetate and decreased levels of butyrate. In the mice fed the fructose diet, the presence of un-metabolized fructose in the feces indicates that the lower intestine microbes must have had access to this sugar. By using ^{13}C-fructose and analyzing ^{13}C-enrichment of fecal metabolites by ^{13}C NMR, it should be feasible to determine the specific contribution of fructose to SCFA and other microbial fermentation products.

Chapter E

References

1. Bing, F.C., *The history of the word 'metabolism'.* J Hist Med Allied Sci, 1971. **26**(2): p. 158-80.

2. Goodpaster, B.H. and L.M. Sparks, *Metabolic Flexibility in Health and Disease.* Cell Metab, 2017. **25**(5): p. 1027-1036.

3. Kylin, E.S., *Hypertonie-Hyperglykamie-Hyperurikamiesyndrome.* Zentralblatt fur innere Medizin, 1923. **44**.

4. Rössner, S., *Eskil Kylin (1889–1975).* Obesity Reviews, 2009. **10**(3): p. 362-362.

5. Vague, J., *Sexual differentiation. A determinant factor of the forms of obesity. 1947.* Obes Res, 1996. **4**(2): p. 201-3.

6. Vague, J., *The degree of masculine differentiation of obesities: a factor determining predisposition to diabetes, atherosclerosis, gout, and uric calculous disease.* Am J Clin Nutr, 1956. **4**(1): p. 20-34.

7. Haller, H., *[Epidermiology and associated risk factors of hyperlipoproteinemia].* Z Gesamte Inn Med, 1977. **32**(8): p. 124-8.

8. Singer, P., *[Diagnosis of primary hyperlipoproteinemias].* Z Gesamte Inn Med, 1977. **32**(9): p. 129-33 concl.

9. Phillips, G.B., *Sex hormones, risk factors and cardiovascular disease.* Am J Med, 1978. **65**(1): p. 7-11.

10. Reaven, G.M., *Banting lecture 1988. Role of insulin resistance in human disease.* Diabetes, 1988. **37**(12): p. 1595-607.

11. Kaplan, N.M., *The deadly quartet. Upper-body obesity, glucose intolerance, hypertriglyceridemia, and hypertension.* Arch Intern Med, 1989. **149**(7): p. 1514-20.

12. DeFronzo, R.A. and E. Ferrannini, *Insulin resistance. A multifaceted syndrome responsible for NIDDM, obesity, hypertension, dyslipidemia, and atherosclerotic cardiovascular disease.* Diabetes Care, 1991. **14**(3): p. 173-94.

13. Alberti, K.G. and P.Z. Zimmet, *Definition, diagnosis and classification of diabetes mellitus and its complications. Part 1: diagnosis and classification of diabetes mellitus provisional report of a WHO consultation.* Diabet Med, 1998. **15**(7): p. 539-53.

14. Balkau, B. and M.A. Charles, *Comment on the provisional report from the WHO consultation. European Group for the Study of Insulin Resistance (EGIR).* Diabet Med, 1999. **16**(5): p. 442-3.

15. *Executive Summary of The Third Report of The National Cholesterol Education Program (NCEP) Expert Panel on Detection, Evaluation, And Treatment of High Blood Cholesterol In Adults (Adult Treatment Panel III).* Jama, 2001. **285**(19): p. 2486-97.

16. Einhorn, D., et al., *American College of Endocrinology position statement on the insulin resistance syndrome.* Endocr Pract, 2003. **9**(3): p. 237-52.

17. Grundy, S.M., et al., *Definition of metabolic syndrome: report of the National Heart, Lung, and Blood Institute/American Heart Association conference on scientific issues related to definition.* Arterioscler Thromb Vasc Biol, 2004. **24**(2): p. e13-8.

18. Alberti, K.G., P. Zimmet, and J. Shaw, *The metabolic syndrome--a new worldwide definition.* Lancet, 2005. **366**(9491): p. 1059-62.

19. Alberti, K.G., et al., *Harmonizing the metabolic syndrome: a joint interim statement of the International Diabetes Federation Task Force on Epidemiology and Prevention; National Heart, Lung, and Blood Institute; American Heart Association; World Heart Federation; International Atherosclerosis Society; and International Association for the Study of Obesity.* Circulation, 2009. **120**(16): p. 1640-5.

20. Ludwig, J., et al., *Nonalcoholic steatohepatitis: Mayo Clinic experiences with a hitherto unnamed disease.* Mayo Clin Proc, 1980. **55**(7): p. 434-8.

21. Younossi, Z., et al., *Global burden of NAFLD and NASH: trends, predictions, risk factors and prevention.* Nat Rev Gastroenterol Hepatol, 2018. **15**(1): p. 11-20.

22. Browning, J.D., et al., *Prevalence of hepatic steatosis in an urban population in the United States: impact of ethnicity.* Hepatology, 2004. **40**(6): p. 1387-95.

23. Marchesini, G., et al., *Nonalcoholic fatty liver, steatohepatitis, and the metabolic syndrome.* Hepatology, 2003. **37**(4): p. 917-23.

24. Chalasani, N., et al., *The diagnosis and management of non-alcoholic fatty liver disease: practice Guideline by the American Association for the Study of Liver Diseases, American College of Gastroenterology, and the American Gastroenterological Association.* Hepatology, 2012. **55**(6): p. 2005-23.

25. Day, C.P. and O.F. James, *Steatohepatitis: a tale of two "hits"?* Gastroenterology, 1998. **114**(4): p. 842-5.

26. Feldstein, A.E., et al., *Diet associated hepatic steatosis sensitizes to Fas mediated liver injury in mice.* J Hepatol, 2003. **39**(6): p. 978-83.

27. Malhi, H. and G.J. Gores, *Cellular and molecular mechanisms of liver injury.* Gastroenterology, 2008. **134**(6): p. 1641-54.

28. Stienstra, R., et al., *Kupffer cells promote hepatic steatosis via interleukin-1beta-dependent suppression of peroxisome proliferator-activated receptor alpha activity.* Hepatology, 2010. **51**(2): p. 511-22.

29. Tchkonia, T., et al., *Mechanisms and Metabolic Implications of Regional Differences among Fat Depots.* Cell Metabolism, 2013. **17**(5): p. 644-656.

30. Lee, M.-J., Y. Wu, and S.K. Fried, *Adipose tissue heterogeneity: implication of depot differences in adipose tissue for obesity complications.* Molecular aspects of medicine, 2013. **34**(1): p. 1-11.

31. Motamed, N., et al., *Fatty liver index vs waist circumference for predicting non-alcoholic fatty liver disease.* World journal of gastroenterology, 2016. **22**(10): p. 3023-3030.

32. Stern, J.H., J.M. Rutkowski, and P.E. Scherer, *Adiponectin, Leptin, and Fatty Acids in the Maintenance of Metabolic Homeostasis through Adipose Tissue Crosstalk.* Cell metabolism, 2016. **23**(5): p. 770-784.

33. Gaggini, M., et al., *Non-alcoholic fatty liver disease (NAFLD) and its connection with insulin resistance, dyslipidemia, atherosclerosis and coronary heart disease.* Nutrients, 2013. **5**(5): p. 1544-60.

34. Sonnenburg, J.L. and F. Backhed, *Diet-microbiota interactions as moderators of human metabolism.* Nature, 2016. **535**(7610): p. 56-64.

35. Ji, Y., et al., *Gut Microbiota-Derived Components and Metabolites in the Progression of Non-Alcoholic Fatty Liver Disease (NAFLD).* Nutrients, 2019. **11**(8).

36. Forslund, K., et al., *Disentangling type 2 diabetes and metformin treatment signatures in the human gut microbiota.* Nature, 2015. **528**(7581): p. 262-266.

37. Dabke, K., G. Hendrick, and S. Devkota, *The gut microbiome and metabolic syndrome.* J Clin Invest, 2019. **129**(10): p. 4050-4057.

38. Qin, J., et al., *A human gut microbial gene catalogue established by metagenomic sequencing.* Nature, 2010. **464**(7285): p. 59-65.

39. Li, J., et al., *An integrated catalog of reference genes in the human gut microbiome.* Nat Biotechnol, 2014. **32**(8): p. 834-41.

40. Sommer, F. and F. Backhed, *The gut microbiota--masters of host development and physiology.* Nat Rev Microbiol, 2013. **11**(4): p. 227-38.

41. Backhed, F., et al., *Host-bacterial mutualism in the human intestine.* Science, 2005. **307**(5717): p. 1915-20.

42. Ley, R.E., et al., *Microbial ecology: human gut microbes associated with obesity.* Nature, 2006. **444**(7122): p. 1022-3.

43. Turnbaugh, P.J., et al., *An obesity-associated gut microbiome with increased capacity for energy harvest.* Nature, 2006. **444**(7122): p. 1027-31.

44. Ridaura, V.K., et al., *Gut microbiota from twins discordant for obesity modulate metabolism in mice.* Science, 2013. **341**(6150): p. 1241214.

45. Backhed, F., et al., *Mechanisms underlying the resistance to diet-induced obesity in germ-free mice.* Proc Natl Acad Sci U S A, 2007. **104**(3): p. 979-84.

46. Rabot, S., et al., *Germ-free C57BL/6J mice are resistant to high-fat-diet-induced insulin resistance and have altered cholesterol metabolism.* Faseb j, 2010. **24**(12): p. 4948-59.

47. Ley, R.E., et al., *Obesity alters gut microbial ecology.* Proc Natl Acad Sci U S A, 2005. **102**(31): p. 11070-5.

48. Larsen, N., et al., *Gut Microbiota in Human Adults with Type 2 Diabetes Differs from Non-Diabetic Adults.* PLOS ONE, 2010. **5**(2): p. e9085.

49. Carroll, I.M., et al., *Luminal and mucosal-associated intestinal microbiota in patients with diarrhea-predominant irritable bowel syndrome.* Gut Pathog, 2010. **2**(1): p. 19.

50. Nadal, I., et al., *Imbalance in the composition of the duodenal microbiota of children with coeliac disease.* J Med Microbiol, 2007. **56**(Pt 12): p. 1669-74.

51. Krogius-Kurikka, L., et al., *Microbial community analysis reveals high level phylogenetic alterations in the overall gastrointestinal microbiota of diarrhoea-predominant irritable bowel syndrome sufferers.* BMC Gastroenterol, 2009. **9**: p. 95.

52. Rizzatti, G., et al., *Proteobacteria: A Common Factor in Human Diseases.* BioMed Research International, 2017. **2017**: p. 7.

53. Frank, D.N., et al., *Molecular-phylogenetic characterization of microbial community imbalances in human inflammatory bowel diseases.* Proceedings of the National Academy of Sciences, 2007. **104**(34): p. 13780-13785.

54. Machiels, K., et al., *A decrease of the butyrate-producing species Roseburia hominis and Faecalibacterium prausnitzii defines dysbiosis in patients with ulcerative colitis.* Gut, 2014. **63**(8): p. 1275-1283.

55. Wang, T., et al., *Structural segregation of gut microbiota between colorectal cancer patients and healthy volunteers.* The ISME Journal, 2012. **6**(2): p. 320-329.

56. Qin, J., et al., *A metagenome-wide association study of gut microbiota in type 2 diabetes.* Nature, 2012. **490**(7418): p. 55-60.

57. Joossens, M., et al., *Dysbiosis of the faecal microbiota in patients with Crohn's disease and their unaffected relatives.* Gut, 2011. **60**(5): p. 631-637.

58. Riva, A., et al., *Pediatric obesity is associated with an altered gut microbiota and discordant shifts in Firmicutes populations.* Environmental Microbiology, 2017. **19**(1): p. 95-105.

59. Geurts, L., et al., *Altered Gut Microbiota and Endocannabinoid System Tone in Obese and Diabetic Leptin-Resistant Mice: Impact on Apelin Regulation in Adipose Tissue.* Frontiers in Microbiology, 2011. **2**(149).

60. Sokol, H., et al., *Faecalibacterium prausnitzii is an anti-inflammatory commensal bacterium identified by gut microbiota analysis of Crohn disease patients.* Proc Natl Acad Sci U S A, 2008. **105**(43): p. 16731-6.

61. Collado, M.C., et al., *Specific duodenal and faecal bacterial groups associated with paediatric coeliac disease.* J Clin Pathol, 2009. **62**(3): p. 264-9.

62. Creely, S.J., et al., *Lipopolysaccharide activates an innate immune system response in human adipose tissue in obesity and type 2 diabetes.* Am J Physiol Endocrinol Metab, 2007. **292**(3): p. E740-7.

63. Caesar, R., et al., *Crosstalk between Gut Microbiota and Dietary Lipids Aggravates WAT Inflammation through TLR Signaling.* Cell Metab, 2015. **22**(4): p. 658-68.

64. Vrieze, A., et al., *Transfer of intestinal microbiota from lean donors increases insulin sensitivity in individuals with metabolic syndrome.* Gastroenterology, 2012. **143**(4): p. 913-6.e7.

65. Taoka, H., et al., *Role of bile acids in the regulation of the metabolic pathways.* World J Diabetes, 2016. **7**(13): p. 260-70.

66. Chow, M.D., Y.H. Lee, and G.L. Guo, *The role of bile acids in nonalcoholic fatty liver disease and nonalcoholic steatohepatitis.* Mol Aspects Med, 2017. **56**: p. 34-44.

67. Harte, A.L., et al., *Elevated endotoxin levels in non-alcoholic fatty liver disease.* Journal of Inflammation, 2010. **7**(1): p. 15.

68. Kim, K.-A., et al., *High Fat Diet-Induced Gut Microbiota Exacerbates Inflammation and Obesity in Mice via the TLR4 Signaling Pathway.* PLOS ONE, 2012. **7**(10): p. e47713.

69. Fukunishi, S., et al., *Lipopolysaccharides accelerate hepatic steatosis in the development of nonalcoholic fatty liver disease in Zucker rats.* J Clin Biochem Nutr, 2014. **54**(1): p. 39-44.

70. Ceccarelli, S., et al., *LPS-induced TNF-alpha factor mediates pro-inflammatory and pro-fibrogenic pattern in non-alcoholic fatty liver disease.* Oncotarget, 2015. **6**(39): p. 41434-52.

71. Pang, J., et al., *Significant positive association of endotoxemia with histological severity in 237 patients with non-alcoholic fatty liver disease.* Aliment Pharmacol Ther, 2017. **46**(2): p. 175-182.

72. Rau, M., et al., *Fecal SCFAs and SCFA-producing bacteria in gut microbiome of human NAFLD as a putative link to systemic T-cell activation and advanced disease.* United European Gastroenterology Journal, 2018. **6**(10): p. 1496-1507.

73. Tedelind, S., et al., *Anti-inflammatory properties of the short-chain fatty acids acetate and propionate: a study with relevance to inflammatory bowel disease.* World J Gastroenterol, 2007. **13**(20): p. 2826-32.

74. Sahuri-Arisoylu, M., et al., *Reprogramming of hepatic fat accumulation and 'browning' of adipose tissue by the short-chain fatty acid acetate.* Int J Obes (Lond), 2016. **40**(6): p. 955-63.

75. Zhou, D., et al., *Sodium butyrate attenuates high-fat diet-induced steatohepatitis in mice by improving gut microbiota and gastrointestinal barrier.* World J Gastroenterol, 2017. **23**(1): p. 60-75.

76. Ye, J., et al., *Butyrate Protects Mice Against Methionine–Choline-Deficient Diet-Induced Non-alcoholic Steatohepatitis by Improving Gut Barrier Function, Attenuating Inflammation and Reducing Endotoxin Levels.* Frontiers in Microbiology, 2018. **9**(1967).

77. Miura, K. and H. Ohnishi, *Role of gut microbiota and Toll-like receptors in nonalcoholic fatty liver disease.* World J Gastroenterol, 2014. **20**(23): p. 7381-91.

78. Cengiz, M., S. Ozenirler, and S. Elbeg, *Role of serum toll-like receptors 2 and 4 in non-alcoholic steatohepatitis and liver fibrosis.* J Gastroenterol Hepatol, 2015. **30**(7): p. 1190-6.

79. Himes, R.W. and C.W. Smith, *Tlr2 is critical for diet-induced metabolic syndrome in a murine model.* Faseb j, 2010. **24**(3): p. 731-9.

80. Sasaki-Imamura, T., et al., *Molecular basis of indole production catalyzed by tryptophanase in the genus Prevotella.* FEMS Microbiology Letters, 2011. **322**(1): p. 51-59.

81. Chu, W., et al., *Indole production promotes Escherichia coli mixed-culture growth with Pseudomonas aeruginosa by inhibiting quorum signaling.* Appl Environ Microbiol, 2012. **78**(2): p. 411-9.

82. Bansal, T., et al., *The bacterial signal indole increases epithelial-cell tight-junction resistance and attenuates indicators of inflammation.* Proc Natl Acad Sci U S A, 2010. **107**(1): p. 228-33.

83. Whitfield-Cargile, C.M., et al., *The microbiota-derived metabolite indole decreases mucosal inflammation and injury in a murine model of NSAID enteropathy*. Gut Microbes, 2016. **7**(3): p. 246-61.

84. Osawa, Y., et al., *Collaborative action of NF-kappaB and p38 MAPK is involved in CpG DNA-induced IFN-alpha and chemokine production in human plasmacytoid dendritic cells.* J Immunol, 2006. **177**(7): p. 4841-52.

85. Bauer, S., et al., *Human TLR9 confers responsiveness to bacterial DNA via species-specific CpG motif recognition.* Proc Natl Acad Sci U S A, 2001. **98**(16): p. 9237-42.

86. Minton, K., *LC3 anchors TLR9 signalling*. Nature Reviews Immunology, 2018. **18**(7): p. 418-419.

87. Garcia-Martinez, I., et al., *Hepatocyte mitochondrial DNA drives nonalcoholic steatohepatitis by activation of TLR9.* J Clin Invest, 2016. **126**(3): p. 859-64.

88. Christensen, K., T. Lawler, and J. Mares, *Dietary Carotenoids and Non-Alcoholic Fatty Liver Disease among US Adults, NHANES 2003(-)2014*. Nutrients, 2019. **11**(5).

89. Yilmaz, B., et al., *Carotenoids and non-alcoholic fatty liver disease.* Hepatobiliary Surg Nutr, 2015. **4**(3): p. 161-71.

90. Klassen, J.L., *Phylogenetic and Evolutionary Patterns in Microbial Carotenoid Biosynthesis Are Revealed by Comparative Genomics*. PLOS ONE, 2010. **5**(6): p. e11257.

91. Fennema, D., I.R. Phillips, and E.A. Shephard, *Trimethylamine and Trimethylamine N-Oxide, a Flavin-Containing Monooxygenase 3 (FMO3)-Mediated Host-Microbiome Metabolic Axis Implicated in Health and Disease*. Drug Metab Dispos, 2016. **44**(11): p. 1839-1850.

92. Barrea, L., et al., *Trimethylamine-N-oxide (TMAO) as Novel Potential Biomarker of Early Predictors of Metabolic Syndrome*. Nutrients, 2018. **10**(12).

93. Fon Tacer, K. and D. Rozman, *Nonalcoholic Fatty liver disease: focus on lipoprotein and lipid deregulation.* J Lipids, 2011. **2011**: p. 783976.

94. Xu, J. and J.I. Gordon, *Honor thy symbionts.* Proc Natl Acad Sci U S A, 2003. **100**(18): p. 10452-9.

95. McNeil, N.I., *The contribution of the large intestine to energy supplies in man.* Am J Clin Nutr, 1984. **39**(2): p. 338-42.

96. Aguirre, M., et al., *In vitro characterization of the impact of different substrates on metabolite production, energy extraction and composition of gut microbiota from lean and obese subjects.* PLoS One, 2014. **9**(11): p. e113864.

97. Cummings, J.H., et al., *Short chain fatty acids in human large intestine, portal, hepatic and venous blood.* Gut, 1987. **28**(10): p. 1221-7.

98. Walker, A.W., et al., *pH and peptide supply can radically alter bacterial populations and short-chain fatty acid ratios within microbial communities from the human colon.* Appl Environ Microbiol, 2005. **71**(7): p. 3692-700.

99. Gao, Z., et al., *Butyrate improves insulin sensitivity and increases energy expenditure in mice.* Diabetes, 2009. **58**(7): p. 1509-17.

100. De Vadder, F., et al., *Microbiota-generated metabolites promote metabolic benefits via gut-brain neural circuits.* Cell, 2014. **156**(1-2): p. 84-96.

101. Bloemen, J.G., et al., *Short chain fatty acids exchange across the gut and liver in humans measured at surgery.* Clin Nutr, 2009. **28**(6): p. 657-61.

102. Ang, Z. and J.L. Ding, *GPR41 and GPR43 in Obesity and Inflammation - Protective or Causative?* Front Immunol, 2016. **7**: p. 28.

103. Fellows, R., et al., *Microbiota derived short chain fatty acids promote histone crotonylation in the colon through histone deacetylases.* Nature Communications, 2018. **9**(1): p. 105.

104. Donohoe, D.R., et al., *The Warburg effect dictates the mechanism of butyrate-mediated histone acetylation and cell proliferation.* Mol Cell, 2012. **48**(4): p. 612-26.

105. Backhed, F., et al., *The gut microbiota as an environmental factor that regulates fat storage.* Proc Natl Acad Sci U S A, 2004. **101**(44): p. 15718-23.

106. Parseus, A., et al., *Microbiota-induced obesity requires farnesoid X receptor.* Gut, 2017. **66**(3): p. 429-437.

107. Harach, T., et al., *TGR5 potentiates GLP-1 secretion in response to anionic exchange resins.* Sci Rep, 2012. **2**: p. 430.

108. Malik, A.N., R. Shahni, and M.M. Iqbal, *Increased peripheral blood mitochondrial DNA in type 2 diabetic patients with nephropathy*. Diabetes Res Clin Pract, 2009. **86**(2): p. e22-4.

109. Vancamelbeke, M. and S. Vermeire, *The intestinal barrier: a fundamental role in health and disease*. Expert Rev Gastroenterol Hepatol, 2017. **11**(9): p. 821-834.

110. Nilaweera, K.N. and J.R. Speakman, *Regulation of intestinal growth in response to variations in energy supply and demand*. Obesity reviews : an official journal of the International Association for the Study of Obesity, 2018. **19 Suppl 1**(Suppl Suppl 1): p. 61-72.

111. Groschwitz, K.R. and S.P. Hogan, *Intestinal barrier function: molecular regulation and disease pathogenesis*. J Allergy Clin Immunol, 2009. **124**(1): p. 3-20; quiz 21-2.

112. Raleigh, D.R., et al., *Tight junction-associated MARVEL proteins marveld3, tricellulin, and occludin have distinct but overlapping functions*. Mol Biol Cell, 2010. **21**(7): p. 1200-13.

113. Fasano, A., et al., *Vibrio cholerae produces a second enterotoxin, which affects intestinal tight junctions*. Proc Natl Acad Sci U S A, 1991. **88**(12): p. 5242-6.

114. Wang, W., et al., *Human zonulin, a potential modulator of intestinal tight junctions*. J Cell Sci, 2000. **113 Pt 24**: p. 4435-40.

115. Tripathi, A., et al., *Identification of human zonulin, a physiological modulator of tight junctions, as prehaptoglobin-2*. Proc Natl Acad Sci U S A, 2009. **106**(39): p. 16799-804.

116. Fasano, A., *Regulation of intercellular tight junctions by zonula occludens toxin and its eukaryotic analogue zonulin*. Ann N Y Acad Sci, 2000. **915**: p. 214-22.

117. Goldblum, S.E., et al., *The active Zot domain (aa 288-293) increases ZO-1 and myosin 1C serine/threonine phosphorylation, alters interaction between ZO-1 and its binding partners, and induces tight junction disassembly through proteinase activated receptor 2 activation*. Faseb j, 2011. **25**(1): p. 144-58.

118. El Asmar, R., et al., *Host-dependent zonulin secretion causes the impairment of the small intestine barrier function after bacterial exposure*. Gastroenterology, 2002. **123**(5): p. 1607-15.

119. Zak-Golab, A., et al., *Gut microbiota, microinflammation, metabolic profile, and zonulin concentration in obese and normal weight subjects*. Int J Endocrinol, 2013. **2013**: p. 674106.

120. Jayashree, B., et al., *Increased circulatory levels of lipopolysaccharide (LPS) and zonulin signify novel biomarkers of proinflammation in patients with type 2 diabetes.* Mol Cell Biochem, 2014. **388**(1-2): p. 203-10.

121. Pacifico, L., et al., *Increased circulating zonulin in children with biopsy-proven nonalcoholic fatty liver disease.* World journal of gastroenterology, 2014. **20**(45): p. 17107-17114.

122. Yang, Q., et al., *Added sugar intake and cardiovascular diseases mortality among US adults.* JAMA Intern Med, 2014. **174**(4): p. 516-24.

123. Dolan, L.C., S.M. Potter, and G.A. Burdock, *Evidence-based review on the effect of normal dietary consumption of fructose on development of hyperlipidemia and obesity in healthy, normal weight individuals.* Crit Rev Food Sci Nutr, 2010. **50**(1): p. 53-84.

124. Walker, R.W., K.A. Dumke, and M.I. Goran, *Fructose content in popular beverages made with and without high-fructose corn syrup.* Nutrition, 2014. **30**(7-8): p. 928-35.

125. Lim, J.S., et al., *The role of fructose in the pathogenesis of NAFLD and the metabolic syndrome.* Nat Rev Gastroenterol Hepatol, 2010. **7**(5): p. 251-64.

126. Goran, M.I., S.J. Ulijaszek, and E.E. Ventura, *High fructose corn syrup and diabetes prevalence: a global perspective.* Glob Public Health, 2013. **8**(1): p. 55-64.

127. Williams, C.D., et al., *Prevalence of nonalcoholic fatty liver disease and nonalcoholic steatohepatitis among a largely middle-aged population utilizing ultrasound and liver biopsy: a prospective study.* Gastroenterology, 2011. **140**(1): p. 124-31.

128. Afshin, A., et al., *Health Effects of Overweight and Obesity in 195 Countries over 25 Years.* N Engl J Med, 2017. **377**(1): p. 13-27.

129. Menke, A., et al., *Prevalence of and Trends in Diabetes Among Adults in the United States, 1988-2012.* Jama, 2015. **314**(10): p. 1021-9.

130. Assy, N., et al., *Soft drink consumption linked with fatty liver in the absence of traditional risk factors.* Can J Gastroenterol, 2008. **22**(10): p. 811-6.

131. Abid, A., et al., *Soft drink consumption is associated with fatty liver disease independent of metabolic syndrome.* J Hepatol, 2009. **51**(5): p. 918-24.

132. Ouyang, X., et al., *Fructose consumption as a risk factor for non-alcoholic fatty liver disease.* J Hepatol, 2008. **48**(6): p. 993-9.

133. Barone, S., et al., *Slc2a5 (Glut5) is essential for the absorption of fructose in the intestine and generation of fructose-induced hypertension.* J Biol Chem, 2009. **284**(8): p. 5056-66.

134. Douard, V. and R.P. Ferraris, *Regulation of the fructose transporter GLUT5 in health and disease.* Am J Physiol Endocrinol Metab, 2008. **295**(2): p. E227-37.

135. Debosch, B.J., et al., *Glucose transporter 8 (GLUT8) mediates fructose-induced de novo lipogenesis and macrosteatosis.* J Biol Chem, 2014. **289**(16): p. 10989-98.

136. Mayes, P.A., *Intermediary metabolism of fructose.* Am J Clin Nutr, 1993. **58**(5 Suppl): p. 754s-765s.

137. Vos, M.B. and J.E. Lavine, *Dietary fructose in nonalcoholic fatty liver disease.* Hepatology, 2013. **57**(6): p. 2525-31.

138. Silva, J.C.P., et al., *Intestinal Microbial and Metabolic Profiling of Mice Fed with High-Glucose and High-Fructose Diets.* J Proteome Res, 2018. **17**(8): p. 2880-2891.

139. Steenson, S., et al., *Role of the Enterocyte in Fructose-Induced Hypertriglyceridaemia.* Nutrients, 2017. **9**(4).

140. Froesch, E.R. and J.L. Ginsberg, *Fructose metabolism of adipose tissue. I. Comparison of fructose and glucose metabolism in epididymal adipose tissue of normal rats.* J Biol Chem, 1962. **237**: p. 3317-24.

141. Kayano, T., et al., *Human facilitative glucose transporters. Isolation, functional characterization, and gene localization of cDNAs encoding an isoform (GLUT5) expressed in small intestine, kidney, muscle, and adipose tissue and an unusual glucose transporter pseudogene-like sequence (GLUT6).* J Biol Chem, 1990. **265**(22): p. 13276-82.

142. Jegatheesan, P. and J.P. De Bandt, *Fructose and NAFLD: The Multifaceted Aspects of Fructose Metabolism.* Nutrients, 2017. **9**(3).

143. Jang, C., et al., *The Small Intestine Converts Dietary Fructose into Glucose and Organic Acids.* Cell Metab, 2018. **27**(2): p. 351-361 e3.

144. Dushay, J.R., et al., *Fructose ingestion acutely stimulates circulating FGF21 levels in humans.* Mol Metab, 2015. **4**(1): p. 51-7.

145. Koo, H.Y., et al., *Dietary fructose induces a wide range of genes with distinct shift in carbohydrate and lipid metabolism in fed and fasted rat liver.* Biochim Biophys Acta, 2008. **1782**(5): p. 341-8.

146. Kim, M.S., et al., *ChREBP regulates fructose-induced glucose production independently of insulin signaling.* J Clin Invest, 2016. **126**(11): p. 4372-4386.

147. Lanaspa, M.A., et al., *Endogenous fructose production and metabolism in the liver contributes to the development of metabolic syndrome.* Nat Commun, 2013. **4**: p. 2434.

148. Patel, C., et al., *Fructose-induced increases in expression of intestinal fructolytic and gluconeogenic genes are regulated by GLUT5 and KHK.* Am J Physiol Regul Integr Comp Physiol, 2015. **309**(5): p. R499-509.

149. Kabashima, T., et al., *Xylulose 5-phosphate mediates glucose-induced lipogenesis by xylulose 5-phosphate-activated protein phosphatase in rat liver.* Proc Natl Acad Sci U S A, 2003. **100**(9): p. 5107-12.

150. Koo, H.Y., et al., *Replacing dietary glucose with fructose increases ChREBP activity and SREBP-1 protein in rat liver nucleus.* Biochem Biophys Res Commun, 2009. **390**(2): p. 285-9.

151. Matsuzaka, T., et al., *Insulin-independent induction of sterol regulatory element-binding protein-1c expression in the livers of streptozotocin-treated mice.* Diabetes, 2004. **53**(3): p. 560-9.

152. Nagai, Y., et al., *The role of peroxisome proliferator-activated receptor gamma coactivator-1 beta in the pathogenesis of fructose-induced insulin resistance.* Cell Metab, 2009. **9**(3): p. 252-64.

153. Jegatheesan, P., et al., *Citrulline and Nonessential Amino Acids Prevent Fructose-Induced Nonalcoholic Fatty Liver Disease in Rats.* J Nutr, 2015. **145**(10): p. 2273-9.

154. Lee, A.H., et al., *Regulation of hepatic lipogenesis by the transcription factor XBP1.* Science, 2008. **320**(5882): p. 1492-6.

155. Tappy, L. and K.A. Le, *Metabolic effects of fructose and the worldwide increase in obesity.* Physiol Rev, 2010. **90**(1): p. 23-46.

156. Johnson, R.J., et al., *Lessons from comparative physiology: could uric acid represent a physiologic alarm signal gone awry in western society?* J Comp Physiol B, 2009. **179**(1): p. 67-76.

157. Kang, D.H., et al., *Uric acid-induced C-reactive protein expression: implication on cell proliferation and nitric oxide production of human vascular cells.* J Am Soc Nephrol, 2005. **16**(12): p. 3553-62.

158. Wei, Y., et al., *Fructose-induced stress signaling in the liver involves methylglyoxal.* Nutr Metab (Lond), 2013. **10**: p. 32.

159. Volynets, V., et al., *Intestinal Barrier Function and the Gut Microbiome Are Differentially Affected in Mice Fed a Western-Style Diet or Drinking Water Supplemented with Fructose.* J Nutr, 2017. **147**(5): p. 770-780.

160. Zimmet, P. and J. Shaw, *Diabetes: Rising incidence of diabetes mellitus in youth in the USA.* Nat Rev Endocrinol, 2017. **13**(7): p. 379-380.

161. Younossi, Z.M., et al., *The economic and clinical burden of nonalcoholic fatty liver disease in the United States and Europe.* Hepatology, 2016. **64**(5): p. 1577-1586.

162. Jaacks, L.M., et al., *Type 2 diabetes: A 21st century epidemic.* Best Pract Res Clin Endocrinol Metab, 2016. **30**(3): p. 331-43.

163. Delzenne, N.M. and P.D. Cani, *Gut microbiota and the pathogenesis of insulin resistance.* Curr Diab Rep, 2011. **11**(3): p. 154-9.

164. Cani, P.D., et al., *Changes in gut microbiota control metabolic endotoxemia-induced inflammation in high-fat diet-induced obesity and diabetes in mice.* Diabetes, 2008. **57**(6): p. 1470-81.

165. Cani, P.D., et al., *Metabolic endotoxemia initiates obesity and insulin resistance.* Diabetes, 2007. **56**(7): p. 1761-72.

166. David, L.A., et al., *Diet rapidly and reproducibly alters the human gut microbiome.* Nature, 2014. **505**(7484): p. 559-63.

167. Heinritz, S.N., et al., *Impact of a High-Fat or High-Fiber Diet on Intestinal Microbiota and Metabolic Markers in a Pig Model.* Nutrients, 2016. **8**(5).

168. Kumari, M. and A.L. Kozyrskyj, *Gut microbial metabolism defines host metabolism: an emerging perspective in obesity and allergic inflammation.* Obes Rev, 2017. **18**(1): p. 18-31.

169. Francini, F., et al., *Changes induced by a fructose-rich diet on hepatic metabolism and the antioxidant system.* Life sciences, 2010. **86**(25-26): p. 965-971.

170. Dekker, M.J., et al., *Fructose: a highly lipogenic nutrient implicated in insulin resistance, hepatic steatosis, and the metabolic syndrome.* Am J Physiol Endocrinol Metab, 2010. **299**(5): p. E685-94.

171. Kawasaki, T., et al., *Rats fed fructose-enriched diets have characteristics of nonalcoholic hepatic steatosis.* J Nutr, 2009. **139**(11): p. 2067-71.

172. Rutledge, A.C. and K. Adeli, *Fructose and the metabolic syndrome: pathophysiology and molecular mechanisms.* Nutr Rev, 2007. **65**(6 Pt 2): p. S13-23.

173. Delgado, T.C., et al., *(2)H enrichment distribution of hepatic glycogen from (2)H(2)O reveals the contribution of dietary fructose to glycogen synthesis.* Am J Physiol Endocrinol Metab, 2013. **304**(4): p. E384-91.

174. Delgado, T.C., et al., *Sources of hepatic triglyceride accumulation during high-fat feeding in the healthy rat.* NMR Biomed, 2009. **22**(3): p. 310-7.

175. Zhao, Y., et al., *Gut microbiota composition modifies fecal metabolic profiles in mice.* J Proteome Res, 2013. **12**(6): p. 2987-99.

176. Yang, Y., et al., *An integrated metabonomic approach to studying metabolic profiles in rat models with insulin resistance induced by high fructose.* Mol Biosyst, 2014. **10**(7): p. 1803-11.

177. Hong, Y.S., et al., *1H NMR-based metabonomic assessment of probiotic effects in a colitis mouse model.* Arch Pharm Res, 2010. **33**(7): p. 1091-101.

178. Zhang, C., et al., *Structural modulation of gut microbiota in life-long calorie-restricted mice.* Nat Commun, 2013. **4**: p. 2163.

179. Wishart, D.S., et al., *HMDB: a knowledgebase for the human metabolome.* Nucleic Acids Res, 2009. **37**(Database issue): p. D603-10.

180. Veselkov, K.A., et al., *Recursive segment-wise peak alignment of biological (1)h NMR spectra for improved metabolic biomarker recovery.* Anal Chem, 2009. **81**(1): p. 56-66.

181. Dieterle, F., et al., *Probabilistic quotient normalization as robust method to account for dilution of complex biological mixtures. Application in 1H NMR metabonomics.* Anal Chem, 2006. **78**(13): p. 4281-90.

182. Berben, L., S.M. Sereika, and S. Engberg, *Effect size estimation: methods and examples.* Int J Nurs Stud, 2012. **49**(8): p. 1039-47.

183. Benjamini, Y. and Y. Hochberg, *Controlling the False Discovery Rate: A Practical and Powerful Approach to Multiple Testing.* Journal of the Royal Statistical Society. Series B (Methodological), 1995. **57**(1): p. 289-300.

184. Castillo, M., et al., *Quantification of total bacteria, enterobacteria and lactobacilli populations in pig digesta by real-time PCR.* Vet Microbiol, 2006. **114**(1-2): p. 165-70.

185. van Minnen, L.P., et al., *Modification of intestinal flora with multispecies probiotics reduces bacterial translocation and improves clinical course in a rat model of acute pancreatitis.* Surgery, 2007. **141**(4): p. 470-80.

186. Koh, A., et al., *From Dietary Fiber to Host Physiology: Short-Chain Fatty Acids as Key Bacterial Metabolites.* Cell, 2016. **165**(6): p. 1332-1345.

187. Arora, T. and F. Backhed, *The gut microbiota and metabolic disease: current understanding and future perspectives.* J Intern Med, 2016. **280**(4): p. 339-49.

188. Mellor, K., et al., *High-fructose diet elevates myocardial superoxide generation in mice in the absence of cardiac hypertrophy.* Nutrition, 2010. **26**(7-8): p. 842-8.

189. Nunes, P.M., et al., *Dietary lipids do not contribute to the higher hepatic triglyceride levels of fructose- compared to glucose-fed mice.* FASEB J, 2014. **28**(5): p. 1988-97.

190. van der Beek, C.M., et al., *Role of short-chain fatty acids in colonic inflammation, carcinogenesis, and mucosal protection and healing.* Nutr Rev, 2017. **75**(4): p. 286-305.

191. Jin, U.H., et al., *Short Chain Fatty Acids Enhance Aryl Hydrocarbon (Ah) Responsiveness in Mouse Colonocytes and Caco-2 Human Colon Cancer Cells.* Sci Rep, 2017. **7**(1): p. 10163.

192. Spruss, A., et al., *Metformin protects against the development of fructose-induced steatosis in mice: role of the intestinal barrier function.* Lab Invest, 2012. **92**(7): p. 1020-32.

193. Kumar, A., et al., *Lactobacillus acidophilus counteracts enteropathogenic E. coli-induced inhibition of butyrate uptake in intestinal epithelial cells.* Am J Physiol Gastrointest Liver Physiol, 2015. **309**(7): p. G602-7.

194. Chambers, E.S., D.J. Morrison, and G. Frost, *Control of appetite and energy intake by SCFA: what are the potential underlying mechanisms?* Proc Nutr Soc, 2015. **74**(3): p. 328-36.

195. Goffredo, M., et al., *Role of Gut Microbiota and Short Chain Fatty Acids in Modulating Energy Harvest and Fat Partitioning in Youth.* J Clin Endocrinol Metab, 2016. **101**(11): p. 4367-4376.

196. Arora, T., R. Sharma, and G. Frost, *Propionate. Anti-obesity and satiety enhancing factor?* Appetite, 2011. **56**(2): p. 511-5.

197. Dodd, D., et al., *A gut bacterial pathway metabolizes aromatic amino acids into nine circulating metabolites.* Nature, 2017. **551**(7682): p. 648-652.

198. Latulippe, M.E. and S.M. Skoog, *Fructose malabsorption and intolerance: effects of fructose with and without simultaneous glucose ingestion.* Crit Rev Food Sci Nutr, 2011. **51**(7): p. 583-92.

199. Jones, H.F., R.N. Butler, and D.A. Brooks, *Intestinal fructose transport and malabsorption in humans.* Am J Physiol Gastrointest Liver Physiol, 2011. **300**(2): p. G202-6.

200. Abd Elwahab, A.H., et al., *A Novel Role of SIRT1/ FGF-21 in Taurine Protection Against Cafeteria Diet-Induced Steatohepatitis in Rats.* Cell Physiol Biochem, 2017. **43**(2): p. 644-659.

201. Inam, U.L., et al., *Ameliorative effects of taurine against diabetes: a review.* Amino Acids, 2018. **50**(5): p. 487-502.

202. Choi, M.-J., *Effects of taurine supplementation on bone mineral density in ovariectomized rats fed calcium deficient diet.* Nutrition research and practice, 2009. **3**(2): p. 108-113.

203. Jiang, J., et al., *Diversity of bile salt hydrolase activities in different lactobacilli toward human bile salts.* Annals of Microbiology, 2010. **60**(1): p. 81-88.

204. Ruiz, L., A. Margolles, and B. Sánchez, *Bile resistance mechanisms in Lactobacillus and Bifidobacterium.* Frontiers in Microbiology, 2013. **4**(396).

205. Endo, A., *Fructophilic lactic acid bacteria inhabit fructose-rich niches in nature.* Microb Ecol Health Dis, 2012. **23**.

206. Stenman, L.K., et al., *A novel mechanism for gut barrier dysfunction by dietary fat: epithelial disruption by hydrophobic bile acids.* Am J Physiol Gastrointest Liver Physiol, 2013. **304**(3): p. G227-34.

207. Herrema, H., et al., *Bile salt sequestration induces hepatic de novo lipogenesis through farnesoid X receptor- and liver X receptor alpha-controlled metabolic pathways in mice.* Hepatology, 2010. **51**(3): p. 806-16.

208. Franklin, C.L. and A.C. Ericsson, *Microbiota and reproducibility of rodent models.* Lab Anim (NY), 2017. **46**(4): p. 114-122.

209. Lamichhane, S., et al., *Optimizing sampling strategies for NMR-based metabolomics of human feces: pooled vs. unpooled analyses.* Analytical Methods, 2017. **9**(30): p. 4476-4480.

210. Silva, J.C.P., et al., *Determining contributions of exogenous glucose and fructose to de novo fatty acid and glycerol synthesis in liver and adipose tissue.* Metab Eng, 2019. **56**: p. 69-76.

211. Stanhope, K.L., *Role of Fructose-Containing Sugars in the Epidemics of Obesity and Metabolic Syndrome*, in *Annual Review of Medicine, Vol 63*, C.T. Caskey, C.P. Austin, and J.A. Hoxie, Editors. 2012. p. 329-+.

212. Yki-Jarvinen, H., *Nutritional modulation of nonalcoholic fatty liver disease and insulin resistance: human data.* Current Opinion in Clinical Nutrition and Metabolic Care, 2010. **13**(6): p. 709-714.

213. Parks, E.J., et al., *Dietary sugars stimulate fatty acid synthesis in adults.* Journal of Nutrition, 2008. **138**(6): p. 1039-1046.

214. Uyeda, K., H. Yamashita, and T. Kawaguchi, *Carbohydrate responsive element-binding protein (ChREBP): a key regulator of glucose metabolism and fat storage.* Biochemical Pharmacology, 2002. **63**(12): p. 2075-2080.

215. McGarry, J.D., G.P. Mannaerts, and D.W. Foster, *Possible Role for Malonyl-Coa in Regulation of Hepatic Fatty- Acid Oxidation and Ketogenesis.* Journal of Clinical Investigation, 1977. **60**(1): p. 265-270.

216. Gouk, S.W., et al., *Rapid and direct quantitative analysis of positional fatty acids in triacylglycerols using 13C NMR.* European Journal of Lipid Science and Technology, 2012. **114**(5): p. 510-519.

217. Tengku-Rozaina, T.M. and E.J. Birch, *Positional distribution of fatty acids on hoki and tuna oil triglycerides by pancreatic lipase and 13C NMR analysis.* European Journal of Lipid Science and Technology, 2014. **116**(3): p. 272-281.

218. Siddiqui, N., et al., *Multicomponent analysis of encapsulated marine oil supplements using high-resolution H-1 and C-13 NMR techniques.* Journal of Lipid Research, 2003. **44**(12): p. 2406-2427.

219. Vlahov, G., A.A. Giuliani, and P. Del Re, *C-13 NMR spectroscopy for determining the acylglycerol positional composition of lampante olive oils. Chemical shift assignments and their dependence on sample concentration.* Analytical Methods, 2010. **2**(7): p. 916-923.

220. Viegas, I., et al., *Effects of dietary carbohydrate on hepatic de novo lipogenesis in European seabass (Dicentrarchus labrax L.).* Journal of Lipid Research, 2016. **57**(7): p. 1264-72.

221. Matyash, V., et al., *Lipid extraction by methyl-tert-butyl ether for high-throughput lipidomics.* J Lipid Res, 2008. **49**(5): p. 1137-46.

222. Hamilton, J.G. and K. Comai, *Rapid separation of neutral lipids, free fatty acids and polar lipids using prepacked silica Sep-Pak columns.* Lipids, 1988. **23**(12): p. 1146-9.

223. Jones, J.G., M. Merritt, and C. Malloy, *Quantifying tracer levels of $^{2}H_2O$ enrichment from microliter amounts of plasma and urine by ^{2}H NMR.* Magn Res Med, 2001. **45**(1): p. 156-158.

224. Mannina, L., et al., *Concentration dependence of C-13 NMR spectra of triglycerides: implications for the NMR analysis of olive oils.* Magnetic Resonance in Chemistry, 2000. **38**(10): p. 886-890.

225. Nelson, G.J., *LIPID COMPOSITION OF NORMAL MOUSE LIVER.* Journal of Lipid Research, 1962. **3**(2): p. 256-&.

226. Angrish, M.M., C.Y. Dominici, and T.R. Zacharewski, *TCDD-Elicited Effects on Liver, Serum, and Adipose Lipid Composition in C57BL/6 Mice.* Toxicological Sciences, 2013. **131**(1): p. 108-115.

227. Garaulet, M., et al., *Site-specific differences in the fatty acid composition of abdominal adipose tissue in an obese population from a Mediterranean area: relation with dietary fatty acids, plasma lipid profile, serum insulin, and central obesity.* American Journal of Clinical Nutrition, 2001. **74**(5): p. 585-591.

228. Duarte, J.A.G., et al., *A high-fat diet suppresses de novo lipogenesis and desaturation but not elongation and triglyceride synthesis in mice.* Journal of Lipid Research, 2014. **55**(12): p. 2541-2553.

229. Willker, W. and D. Leibfritz, *Assignment of mono- and polyunsaturated fatty acids in lipids of tissues and body fluids.* Magnetic Resonance in Chemistry, 1998. **36**: p. S79-S84.

230. Ameer, F., et al., *De novo lipogenesis in health and disease.* Metabolism, 2014. **63**(7): p. 895-902.

231. Schwarz, J.M., M. Clearfield, and K. Mulligan, *Conversion of Sugar to Fat: Is Hepatic de Novo Lipogenesis Leading to Metabolic Syndrome and Associated Chronic Diseases?* J Am Osteopath Assoc, 2017. **117**(8): p. 520-527.

232. Hellerstein, M.K. and R.A. Neese, *Mass isotopomer distribution analysis at eight years: theoretical, analytic, and experimental considerations.* American. Journal. of. Physiology., 1999. **39**(6): p. E1146-E1170.

233. Hudgins, L.C., et al., *Human fatty acid synthesis is stimulated by a eucaloric low fat, high carbohydrate diet.* Journal of Clinical Investigation, 1996. **97**(9): p. 2081-2091.

234. Diraison, F., C. Pachiaudi, and M. Beylot, *Measuring lipogenesis and cholesterol synthesis in humans with deuterated water: Use of simple gas chromatographic mass spectrometric techniques.* Journal of Mass Spectrometry, 1997. **32**(1): p. 81-86.

235. Timlin, M.T. and E.J. Parks, *Temporal pattern of de novo lipogenesis in the postprandial state in healthy men.* American Journal of Clinical Nutrition, 2005. **81**(1): p. 35-42.

236. Yoo, H., G. Stephanopoulos, and J.K. Kelleher, *Quantifying carbon sources for de novo lipogenesis in wild-type and IRS-1 knockout brown adipocytes.* J Lipid Res, 2004. **45**(7): p. 1324-32.

237. Wallace, M., et al., *Enzyme promiscuity drives branched-chain fatty acid synthesis in adipose tissues.* Nat Chem Biol, 2018. **14**(11): p. 1021-1031.

238. Bird, S.S., et al., *Serum Lipidomics Profiling Using LC-MS and High-Energy Collisional Dissociation Fragmentation: Focus on Triglyceride Detection and Characterization.* Analytical Chemistry, 2011. **83**(17): p. 6648-6657.

239. Faeh, D., et al., *Effect of fructose overfeeding and fish oil administration on hepatic de novo lipogenesis and insulin sensitivity in healthy men.* Diabetes, 2005. **54**(7): p. 1907-13.

240. Le, K.A., et al., *A 4-wk high-fructose diet alters lipid metabolism without affecting insulin sensitivity or ectopic lipids in healthy humans.* Am J Clin Nutr, 2006. **84**(6): p. 1374-9.

241. Janssens, S., et al., *An In Vivo Magnetic Resonance Spectroscopy Study of the Effects of Caloric and Non-Caloric Sweeteners on Liver Lipid Metabolism in Rats.* Nutrients, 2017. **9**(5).

242. Stanhope, K.L., et al., *Consuming fructose-sweetened, not glucose-sweetened, beverages increases visceral adiposity and lipids and decreases insulin sensitivity in overweight/obese humans.* J Clin Invest, 2009. **119**(5): p. 1322-34.

243. Oosterveer, M.H., et al., *High Fat Feeding Induces Hepatic Fatty Acid Elongation in Mice.* Plos One, 2009. **4**(6).

244. Yamashita, A., et al., *Acyltransferases and transacylases that determine the fatty acid composition of glycerolipids and the metabolism of bioactive lipid mediators in mammalian cells and model organisms.* Progress in Lipid Research, 2014. **53**: p. 18-81.

245. Man, W.C., et al., *Colocalization of SCD1 and DGAT2: implying preference for endogenous monounsaturated fatty acids in triglyceride synthesis.* Journal of Lipid Research, 2006. **47**(9): p. 1928-1939.

246. Chen, J.L., et al., *Physiologic and Pharmacologic factors influencing glyceroneogenic contribution to triacylglyceride glycerol measured by mass isotopomer distribution analysis.* Journal of Biological Chemistry, 2005. **280**(27): p. 25396-25402.

247. Biesiekierski, J.R., *Fructose-induced symptoms beyond malabsorption in FGID.* United European gastroenterology journal, 2014. **2**(1): p. 10-13.

248. Kato, T., et al., *ChREBP-Knockout Mice Show Sucrose Intolerance and Fructose Malabsorption.* Nutrients, 2018. **10**(3): p. 340.

249. Endo, A., et al., *Fructophilic Lactic Acid Bacteria, a Unique Group of Fructose-Fermenting Microbes.* Appl Environ Microbiol, 2018. **84**(19).

250. Borthakur, A., et al., *A novel nutrient sensing mechanism underlies substrate-induced regulation of monocarboxylate transporter-1.* Am J Physiol Gastrointest Liver Physiol, 2012. **303**(10): p. G1126-33.

251. Lu, Y., et al., *Short Chain Fatty Acids Prevent High-fat-diet-induced Obesity in Mice by Regulating G Protein-coupled Receptors and Gut Microbiota.* Sci Rep, 2016. **6**: p. 37589.

252. Priyadarshini, M., et al., *Role of Short Chain Fatty Acid Receptors in Intestinal Physiology and Pathophysiology.* Compr Physiol, 2018. **8**(3): p. 1091-1115.

253. Tough, I.R., S. Forbes, and H.M. Cox, *Signaling of free fatty acid receptors 2 and 3 differs in colonic mucosa following selective agonism or coagonism by luminal propionate.* Neurogastroenterol Motil, 2018. **30**(12): p. e13454.

254. Maslowski, K.M., et al., *Regulation of inflammatory responses by gut microbiota and chemoattractant receptor GPR43.* Nature, 2009. **461**(7268): p. 1282-6.

255. Smith, P.M., et al., *The microbial metabolites, short-chain fatty acids, regulate colonic Treg cell homeostasis.* Science, 2013. **341**(6145): p. 569-73.

256. Macia, L., et al., *Metabolite-sensing receptors GPR43 and GPR109A facilitate dietary fibre-induced gut homeostasis through regulation of the inflammasome.* Nat Commun, 2015. **6**: p. 6734.

257. Singh, N., et al., *Activation of Gpr109a, receptor for niacin and the commensal metabolite butyrate, suppresses colonic inflammation and carcinogenesis.* Immunity, 2014. **40**(1): p. 128-39.

258. Holota, Y., et al., *The long-term consequences of antibiotic therapy: Role of colonic short-chain fatty acids (SCFA) system and intestinal barrier integrity.* PLoS One, 2019. **14**(8): p. e0220642.

259. Bindels, L.B., et al., *Gut microbiota-derived propionate reduces cancer cell proliferation in the liver.* Br J Cancer, 2012. **107**(8): p. 1337-44.

260. Tolhurst, G., et al., *Short-chain fatty acids stimulate glucagon-like peptide-1 secretion via the G-protein-coupled receptor FFAR2.* Diabetes, 2012. **61**(2): p. 364-71.

261. Brooks, L., et al., *Fermentable carbohydrate stimulates FFAR2-dependent colonic PYY cell expansion to increase satiety.* Mol Metab, 2017. **6**(1): p. 48-60.

262. Kimura, I., et al., *Short-chain fatty acids and ketones directly regulate sympathetic nervous system via G protein-coupled receptor 41 (GPR41).* Proc Natl Acad Sci U S A, 2011. **108**(19): p. 8030-5.

263. Moens, F., M. Verce, and L. De Vuyst, *Lactate- and acetate-based cross-feeding interactions between selected strains of lactobacilli, bifidobacteria and colon bacteria in the presence of inulin-type fructans.* Int J Food Microbiol, 2017. **241**: p. 225-236.

264. Teixeira, T.F., et al., *Higher level of faecal SCFA in women correlates with metabolic syndrome risk factors.* Br J Nutr, 2013. **109**(5): p. 914-9.

265. Liu, H., et al., *Butyrate: A Double-Edged Sword for Health?* Adv Nutr, 2018. **9**(1): p. 21-29.

266. Weitkunat, K., et al., *Importance of propionate for the repression of hepatic lipogenesis and improvement of insulin sensitivity in high-fat diet-induced obesity.* Mol Nutr Food Res, 2016. **60**(12): p. 2611-2621.

267. Roediger, W.E., O. Kapaniris, and S. Millard, *Lipogenesis from n-butyrate in colonocytes. Action of reducing agent and 5-aminosalicylic acid with relevance to ulcerative colitis.* Mol Cell Biochem, 1992. **118**(2): p. 113-8.

268. Zambell, K.L., M.D. Fitch, and S.E. Fleming, *Acetate and butyrate are the major substrates for de novo lipogenesis in rat colonic epithelial cells.* J Nutr, 2003. **133**(11): p. 3509-15.

269. Awad, A.B., S.L. Ferger, and C.S. Fink, *Effect of dietary fat on the lipid composition and utilization of short-chain fatty acids by rat colonocytes.* Lipids, 1990. **25**(6): p. 316-20.

270. Ahmad, M.S., et al., *Butyrate and glucose metabolism by colonocytes in experimental colitis in mice.* Gut, 2000. **46**(4): p. 493-9.

271. Cao, H., et al., *Identification of a lipokine, a lipid hormone linking adipose tissue to systemic metabolism.* Cell, 2008. **134**(6): p. 933-44.

272. Chan, K.L., et al., *Palmitoleate Reverses High Fat-induced Proinflammatory Macrophage Polarization via AMP-activated Protein Kinase (AMPK).* J Biol Chem, 2015. **290**(27): p. 16979-88.

273. Singh, V., et al., *Microbiota-Dependent Hepatic Lipogenesis Mediated by Stearoyl CoA Desaturase 1 (SCD1) Promotes Metabolic Syndrome in TLR5-Deficient Mice.* Cell Metab, 2015. **22**(6): p. 983-96.

274. Bidu, C., et al., *The Transplantation of omega3 PUFA-Altered Gut Microbiota of fat-1 Mice to Wild-Type Littermates Prevents Obesity and Associated Metabolic Disorders.* Diabetes, 2018. **67**(8): p. 1512-1523.

275. Shu, R., E.S. David, and R.P. Ferraris, *Dietary fructose enhances intestinal fructose transport and GLUT5 expression in weaning rats.* Am J Physiol, 1997. **272**(3 Pt 1): p. G446-53.

276. Diggle, C.P., et al., *Ketohexokinase: Expression and Localization of the Principal Fructose-metabolizing Enzyme.* Journal of Histochemistry & Cytochemistry, 2009. **57**(8): p. 763-774.

277. Mithieux, G., F. Rajas, and A. Gautier-Stein, *A novel role for glucose 6-phosphatase in the small intestine in the control of glucose homeostasis.* J Biol Chem, 2004. **279**(43): p. 44231-4.

278. Mithieux, G., *A novel function of intestinal gluconeogenesis: Central signaling in glucose and energy homeostasis.* Nutrition, 2009. **25**(9): p. 881-884.

279. Varma, V., et al., *Metabolic fate of fructose in human adipocytes: a targeted 13C tracer fate association study.* Metabolomics, 2015. **11**(3): p. 529-544.